UCRL-19112

c.2

RECEIVED
LAWRENCE
RADIATION LABORATORY

JAN 9 1970

LIBRARY AND
DOCUMENTS SECTION

PHOTOCHEMISTRY OF IODINE

Joel B. Tellinghuisen
(Ph.D. Thesis)

November 1969

AEC Contract No. W-7405-eng-48

TWO-WEEK LOAN COPY

This is a Library Circulating Copy
which may be borrowed for two weeks.
For a personal retention copy, call
Tech. Info. Division, Ext. 5545

LAWRENCE RADIATION LABORATORY
UNIVERSITY of CALIFORNIA BERKELEY

UCRL-19112

DISCLAIMER

This document was prepared as an account of work sponsored by the United States Government. While this document is believed to contain correct information, neither the United States Government nor any agency thereof, nor the Regents of the University of California, nor any of their employees, makes any warranty, express or implied, or assumes any legal responsibility for the accuracy, completeness, or usefulness of any information, apparatus, product, or process disclosed, or represents that its use would not infringe privately owned rights. Reference herein to any specific commercial product, process, or service by its trade name, trademark, manufacturer, or otherwise, does not necessarily constitute or imply its endorsement, recommendation, or favoring by the United States Government or any agency thereof, or the Regents of the University of California. The views and opinions of authors expressed herein do not necessarily state or reflect those of the United States Government or any agency thereof or the Regents of the University of California.

TABLE OF CONTENTS

ABSTRACT---------- v

I. INTRODUCTION---------- 1

II. EXPERIMENTAL---------- 4

A. Photomultiplier---------- 5

B. Reaction Vessels---------- 6

C. Iodine Lamps---------- 13

D. Visible Excitation Sources and Filters---------- 14

E. Flashtube---------- 17

F. Experimental Arrangements and Signal Detection---------- 20

1. Ultraviolet Absorption Experiments---------- 20

2. Predissociation Experiments---------- 21

3. Iodine-Atom Recombination Studies---------- 25

G. Miscellaneous---------- 26

III. THE IODINE LAMP: ULTRAVIOLET ABSORPTION BY I and I_2---------- 30

A. Radiation Relationships---------- 30

B. Line Shapes and Absorption Relationships---------- 36

1. Line Shapes---------- 37

2. Absorption Measurements and Lifetimes---------- 39

C. Iodine Lamp Output---------- 41

1. Ultraviolet Radiation---------- 42

2. Visible Radiation---------- 48

D. Ultraviolet Absorption Experiments---------- 49

1. Measurements for I_2---------- 50

2. Absorption by Air---------- 58

3. Atomic Absorption---------- 60

IV. SPONTANEOUS PREDISSOCIATION IN I_2 ($B^3\Pi_{0^+u}$) ---------- 74

A. Detection of Resonance Fluorescence ---------- 74

B. Kinetics of I*Atom Production ---------- 80

1. Proposed Mechanism ---------- 80

2. Relaxation of Metastable Iodine Atoms ---------- 88

C. Collection and Treatment of Data ---------- 91

1. Procedures ---------- 91

2. Non-linearity Correction ---------- 93

D. Results and Discussion ---------- 98

1. Unimolecular Quantum Yield of Iodine Atoms ---------- 98

2. Possible Systematic Errors ---------- 120

3. Continuum Absorption in the Banded Region ---------- 130

4. Collisional Quenching of I_2^* (B) ---------- 144

5. I_2 Potential Diagram ---------- 151

6. Future Work ---------- 153

V. Heterogeneous Recombination of Iodine Atoms ---------- 155

A. Introduction ---------- 155

B. Kinetics ---------- 157

1. General Considerations ---------- 157

2. Diffusion Kinetics ---------- 160

C. Results and Discussion ---------- 161

APPENDIX I Absorption and Fluorescence Formulas ---------- 169

APPENDIX II Radiation Coefficients ---------- 174

APPENDIX III Computer Programs ---------- 177

A. Main Programs ---------- 177

B. Subroutines and Function Routines ---------- 193

ACKNOWLEDGMENTS ---------- 204

REFERENCES ---------- 205

PHOTOCHEMISTRY OF IODINE

Joel B. Tellinghuisen

Inorganic Materials Research Division, Lawrence Radiation Laboratory,
Department of Chemistry,
University of California, Berkeley, California

ABSTRACT

A method of atomic fluorescence spectroscopy has been developed and used to detect iodine atoms at concentrations as low as $1 \times 10^{10}/cm^3$ in several photochemical processes. The heart of the apparatus is a "solar-blind" photomultiplier having practically no sensitivity to radiation of wavelengths greater than 2500 A, but with good response in the region of the two strong iodine atomic resonance lines near 1800 A. Electrodeless discharge sources are employed to excite the fluorescence under optimum signal-to-noise conditions. The method is applied to the problem of predissociation in I_2, and used to study diffusion and wall reactions of iodine atoms.

Absorption measurements at 1783 A and 1830 A yield values of 3.6 nsec and 125 nsec, with uncertainties of 20%, for the lifetimes of the $6s\,^2P_{3/2}$ and $6s\,^4P_{5/2}$ states of atomic iodine. These results, together with relative emission strength measurements, indicate the coupling in the $5p^4 6s$ configuration is much closer to the Russell-Saunders case than has been presumed. Molecular iodine is found to absorb the λλ 1783, 1799, 1830, 1844, and 1876 atomic lines with approximately equal facility. The absorption data at 1830 A are used to calculate a rough lifetime of 10±5 nsec for the I_2 excited state. This value is an order of magnitude greater than estimates from extinction measurements, suggesting that several molecular transitions may be contributing to the total absorption in this region.

The quantum yield for unimolecular dissociation of I_2 ($B^3\Pi_{0^+u}$) has been determined for absorption at twelve wavelengths between 5000 A and 6240 A. The yield is found to increase to more than 90% at both ends of this region with an additional maximum of 72% at 5460 A (v' = 25-27) and a minimum of 33% at 5900 A (v' = 13-15). These results are further analyzed in terms of a 20% "parallel" contribution to the total absorption from the $^1\Pi_{1u} \leftarrow X$ transition, and a fluctuating predissociation rate for $B \rightarrow {}^1\Pi_{1u}$. The v'-dependent predissociation explains the previously reported erratic lifetime behavior of the B state. The high yield at long wavelengths is partly due to the onset of the $A^3\Pi_{1u} \leftarrow X$ continuum absorption, which accounts for 50% of the total absorption at 6240 A.

The recombination of iodine atoms at low I_2 pressures is found to be a first-order diffusion-controlled heterogeneous process. From the zero-pressure limiting rate, the "sticking" probability for iodine atoms colliding with "smooth" silica is .05-.075. The diffusion constant for I atoms in I_2 yields a cross section of 89 A^2 for the hard-sphere model. The reaction $I + I_2 \rightarrow I_3$ is seen to be of minor significance in this study; a rough estimate indicates that only one in 64,000 I-I_2 collisions leads to the formation of I_3.

I. INTRODUCTION

The well-known and oft-studied visible B $\longleftrightarrow$ X electronic transition in molecular iodine has received renewed attention in recent years, as several researchers have reported evidence that spontaneous predissociation competes with fluorescence and collisional predissociation in depopulating the B state. Chutjian, Link, and Brewer (1967) used the phase-shift method to measure collisional self-quenching cross sections and lifetimes over a range of values of v', the vibrational quantum number of the excited state. Their lifetime results displayed a rather erratic dependence on v', and they suggested that a weak spontaneous predissociation could be contributing to the total first-order decay rate and yielding anomalously short lifetimes in some vibrational regions. Later Chutjian and James (1969) measured the absorption strengths of a number of individual rotational lines in the dense B $\longleftrightarrow$ X absorption spectrum and used the results to calculate total radiative decay rates. A comparison of these rates with the lifetime results indicated that in the low-pressure limit two thirds of the excited molecules predissociate at v' = 25 and one third at v' = 14. Meanwhile Wassermann, et al. (1968a,b) had elaborated on some earlier work by Bowers and co-workers (1957) and Mayo (1964) and were using ERS techniques to follow iodine-atom concentrations under conditions of steady-state photolysis of I_2. Irradiating at several different wavelengths while varying the I_2 pressure from 10^{-4} to 10^{-1} torr, they observed parallel behavior above and below the dissociation limit of the B state (4995 A) and concluded that 30-60% of the excited molecules decay via predissociation. Steinfeld and co-workers (1969) studied the absorption spectrum at high resolution in the neighborhood of the dissociation limit and suggested

that an underlying continuum may be contributing strongly to the total intensity in that region. Most recently Wilson and collaborators (Busch, et al., 1969) have conducted a number of experiments with I_2 in a molecular beam crossed with a pulsed neodymium laser. Their observations indicate that excitation to the B state in the vicinity of v' = 33 produces atoms by at least two, possibly three different mechanisms.

Spontaneous predissociation in I_2 demands more than curious interest. Until recently the occurrence of spontaneous predissociation in a diatomic molecule has more or less implied the absence of fluorescence from the energy levels involved. Conversely, the observation of fluorescence has generally been accepted as prima-facie evidence for the non-existence of predissociation. Strongly allowed predissociations are predicted and found to have decay rates of 10^{10} to 10^{12} per second, hence the absence of fluorescence. However, the iodine B-state lifetimes run about 10^{-6} seconds, so spontaneous predissociation must be a million times weaker in this case. Furthermore the predissociation appears to occur to a greater or lesser degree throughout the B state, whereas strong predissociations are generally well defined in their energy dependence and are easily described in terms of non-crossing rules for zero-order Born-Oppenheimer states. The existence of weak predissociation in I_2 prompts one to suspect that many other diatomic molecules may be found to behave similarly on closer examination. It also illustrates the heuristic superiority of the scattering-well-resonance picture of predissociation put forth by Harris (1963) and others, in which all "discrete" states which exist in the continuum of at least one lower state are seen to have a finite probability for spontaneous predissociation.

Of the works mentioned earlier only the absorption study by Chutjian and James gives quantitative results for the predissociative yield of

atoms, and those results are indirect in that they derive from a comparison with the earlier lifetime data of Chutjian, et al. In addition the absorption work gives predissociation rates for only two vibrational levels of the B state. In order to more fully understand the nature of the spontaneous predissociation occurring in I_2 it is necessary to have more detailed quantitative information for the entire region of visible absorption, from 6300 A to 5000 A. Also, it would be desirable to obtain the results through a procedure which involves direct observation of iodine atoms, to further demonstrate that the discrepancy between phase-shift and absorption decay rates is in fact due to predissociation.

The steady-state photolysis experiment of Wassermann and colleagues should yield quantitative results, but the investigators didn't pursue the problem past the semi-quantitative stage. A careful consideration of the kinetics involved in steady-state irradiation of I_2 with visible light reveals that a direct comparison of atom production in the continuum ($\lambda < 5000$ A) with that in the banded portion of the B $\leftarrow$ X absorption determines the quantum yield of atoms in a simple, straightforward manner. Use of a comparison technique has one tremendous selling point: Only <u>relative</u> iodine atom concentrations are needed, so treatment of data is greatly simplified.

In the present study iodine atoms are detected by observing atomic resonance fluorescence. The development of the detection method has generated considerable experimental "fallout." The characterization of the iodine atomic excitation source inspired the measurement of absorption line strengths for ultraviolet resonance lines of both atomic and molecular iodine. And the ease of detection of iodine atoms under transient as well as steady-state conditions led quite naturally to a re-examination of the old iodine-atom recombination problem.

II. EXPERIMENTAL

Recent advances in photomultiplier technology have led to the commercial availability of a number of "solar-blind" photomultipliers, so designated because of their extreme insensitivity to visible radiation (Samson, 1967, Chpt. 7; Dunkelman et al., 1962). The photocathodes incorporated in these detectors are characterized by high work functions, making possible high gains with very low dark currents. The long-wavelength cutoffs fall between 2000 A and 3500 A, depending on cathode material; the short-wavelength cutoff is generally determined by window material. With commonly used LiF windows, these photomultipliers are sensitive down to 1050 A.

Solar-blind detectors make possible a relatively simple method of observing trace amounts of radicals formed in certain photochemical reactions. If the radical of interest has an absorption in the ultraviolet, then with an appropriate source of UV radiation it may be observed in absorption and/or fluorescence without interference from the visible or infrared radiation initiating the photochemical process under investigation. In particular the ability to observe ultraviolet fluorescence directly without the aid of a monochromator should enable one to detect quite small concentrations of radicals with good signal-to-noise ratios. And the fast response time of the photomultiplier makes it easy to observe radicals under transient as well as steady-state conditions.

The iodine atom is well suited for such experiments. Its resonance spectrum falls in the vacuum UV region, and the two strong lines at 1783 A and 1830 A can be produced readily in an electrodeless discharge. The transmissivity of fused silica is fair in this region, so with a properly designed quartz cell-and-lamp arrangement a solar-blind photo-

multiplier may be utilized to follow iodine atom concentrations in a number of interesting photochemical processes.

In this work we present the results of three loosely-related sets of experiments: ultraviolet line absorption measurements for I and I_2 (Section III), a study of predissociation in I_2 ($B^3\Pi_{0^+u}$) (Section IV), and an investigation of diffusion and wall reactions of I atoms produced in flash photolysis (Section V). Much of the experimental equipment found application in all of these studies; so to facilitate future discussions, we will describe the important apparatus here. Procedural details for the individual experiments are given in the appropriate sections.

A. Photomultiplier

The solar-blind photomultiplier used in these studies was an EMR[1] Model 541H-08-18, labeled "extreme solar blind" by the manufacturer. The tube is of the end-on type with a semi-transparent CuI photocathode on a 10-mm-diameter LiF window. The eighteen venetian-blind dynodes produce a gain of 10^7 at 3960 volts; the corresponding dark current is given as 5.6×10^{-11} amp. Maximum ratings are as follows: supply voltage -4000, anode current - 100μ amp, operating temperature - 100 C. The instrument is supplied as a potted assembly containing the tube and the dynode voltage divider in a metal housing, with three leads for high voltage and signal. The housing is fitted with an "O"-ring that provides a very effective vacuum seal.

Dunkelman (1962) has given spectral response curves for CuI. For the particular photomultiplier used here EMR quotes quantum yields of 1.7% and 1.4% at 1216 A and 1470 A, respectively, dropping off to less than 10^{-4}% at 2537 A. In addition the relative sensitivity of the instrument was determined in this lab by observing its response to six iodine

1. Electro-Mechanical Research, Inc., Princeton, New Jersey

atomic lines from a source previously calibrated with sodium salicylate and an RCA 1P21 photomultiplier. The latter arrangement is known to have a constant response over a wide range of frequencies in the ultraviolet. (Samson, 1967, Chpt. 7) Results are illustrated in Fig. 1a. Figure 1b shows the manufacturer's gain vs. voltage specifications.

EMR does not report a response time for the instrument, but typical values for multiplier phototubes are on the order of 10^{-8} seconds or less (RCA Photomultiplier Handbook). In flash experiments conducted in this lab, response time was limited by external circuitry.

The photomultiplier is afflicted with one serious operational drawback. Under conventional operating conditions of high negative cathode-to-ground voltages the tube is subject to destructive sparking from the LiF window to nearby grounded conductors if situated in a moderate vacuum where the electrical breakdown resistance of air is low. The vacuum developed by a good mechanical pump is sufficient for safe operation, but precautions must be taken to insure that leaks do not occur while the high voltage is on the cathode.

B. Reaction Vessels

All cells used in these studies were made of fused silica, Engelhard brand or equivalent. The cell used in the predissociation and recombination work is illustrated schematically in Fig. 2. The cylindrical cell body is about 35 mm in diameter and 115 mm long. The iodine lamp is affixed directly to the reaction cell at one end; evacuable ports are situated at the other end, and on the side about 40 mm from the lamp end, for observation of absorption and fluorescence, respectively. Windows at the observation ports and between lamp and cell are "Suprasil" silica about 13 mm in diameter. The cell body has two appendages: a "cold finger" near the absorption window and a connection to a right-

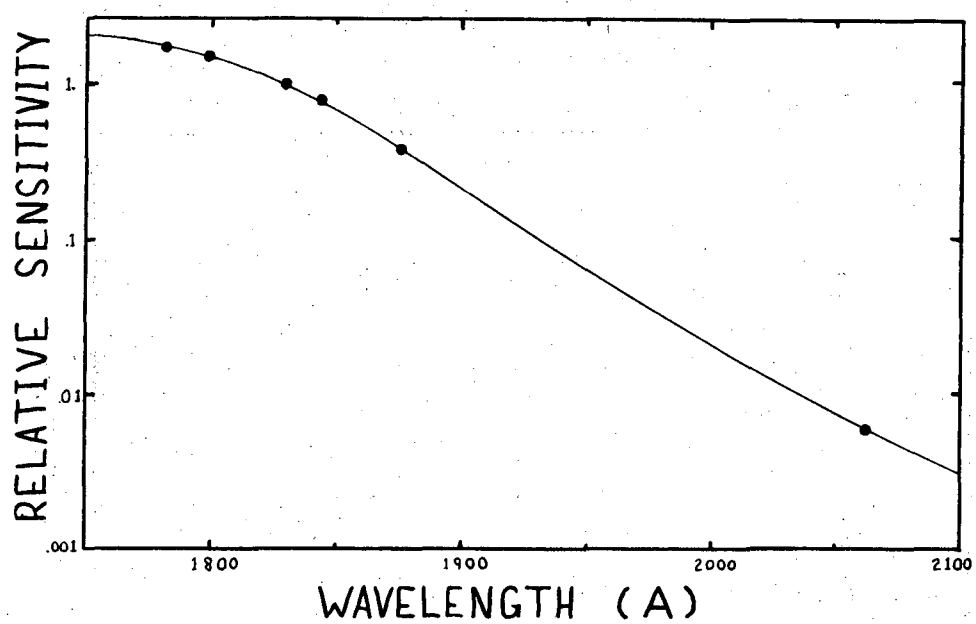

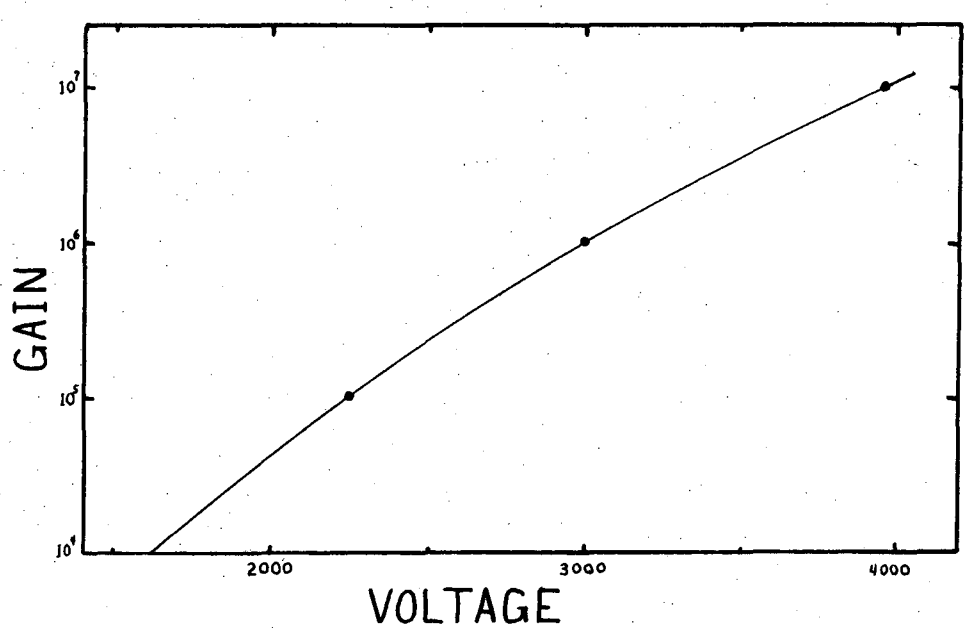

XBL 6910-5808

Fig. 1. Photomultiplier characteristics.

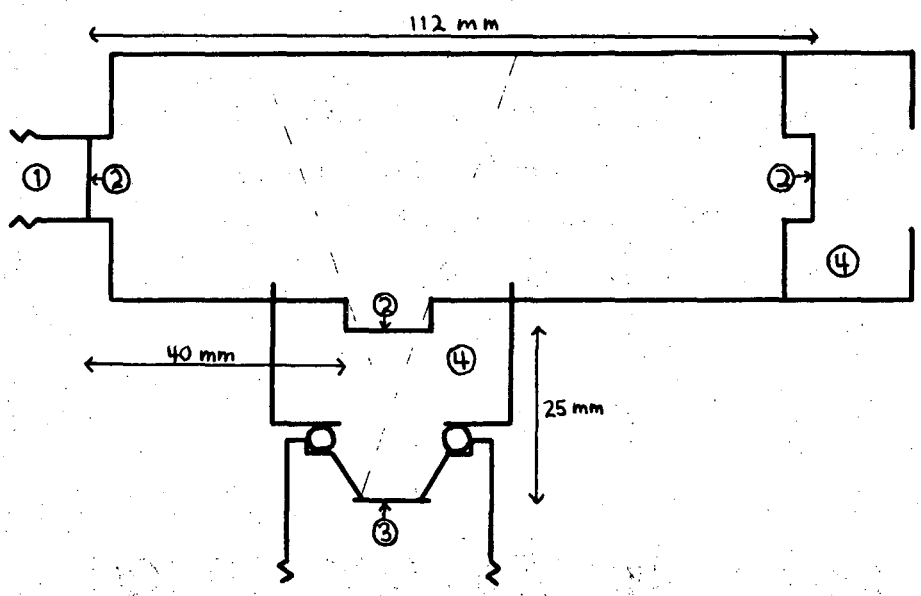

① Ultraviolet Atomic I Source
② Suprasil Windows
③ LiF Photomultiplier Window
④ Evacuable Observation Ports

PREDISSOCIATION CELL
(Top View — Actual Size)

XBL 6910-5841

Fig. 2

angle Westglass-brand greaseless stopcock directly above it. The stopcock is fitted with an "O"-ring-type taper for convenient connection to a vacuum distillation cell.

The Suprasil windows were used to insure good transmission in the 1800 A spectral region; however, the quality of commercial-grade fused silica has been improved greatly in recent years, so that it is possible to use the latter with only slight transmission losses. Several auxiliary sources and cells were constructed from commercial fused silica by Amersil[1] and were found to transmit down to 1700 A and slightly below quite satisfactorily.

The evacuable observation ports were designed to avoid absorption by oxygen in the air. The Schumann-Runge system of O_2 includes band heads at 1783 A and 1830 A, the positions of the two atomic iodine resonance lines of longest wavelength. Later studies indicated that absorption by air amounted to at most 15% at 1783 A and less at 1830 A for a 10-mm path length. However, traces of organic vapors from stopcocks and Tygon connecting tubes severely attenuated the ultraviolet radiation, especially that at 1783 A; so the vacuum served to maintain a "clean" space between cell and photomultiplier.

Wassermann et al. (1968a,b) report that treating cell walls with sulfuric acid reduces heterogeneous iodine atom recombination and dramatically increases the steady-state atom concentrations achievable in photolysis of I_2. The predissociation cell used here was treated in a manner similar to that detailed by the above workers (1968a) involving cleaning with hot alcoholic KOH solution, then hot chromic acid, and finally rinsing with 50% sulfuric acid. After several rinses with distilled water the cell was placed on a vacuum line and pumped on for about 20 hours at 10^{-5} torr with liquid nitrogen (LN) traps isolating the

1. Amersil, Inc., Hillside, New Jersey; distributed by Engelhard. This manufacturer quotes a lower transmission limit of 1650 A.

cell and the oil diffusion pump from the manifold of the vacuum line. The cell stopcock was then closed while the vacuum line was opened to air, so the distillation cell could be charged with resublimed iodine. The system was then evacuated to 10^{-4} torr before the cell stopcock was opened, and a portion of the iodine was condensed out on the cell walls with a piece of dry ice. When the amount of iodine collected was sufficient to leave crystalline iodine in equilibrium with vapor at room temperature, the greaseless stopcock was closed and the iodine was recondensed in the cold finger using liquid nitrogen, which gave a thin iodine film over a large area. Then the cold finger was immersed in alcohol at -30 to -40 C and the stopcock to the high vacuum was reopened for a few minutes, allowing part of the iodine and any volatile impurities to distill off. With the stopcock closed again, the iodine was sublimed and condensed again, and the distillation was repeated. This purification procedure was performed several times to compensate for solid entrapment of volatile impurities.

Successful acid treatment of the cell walls was fraught with frustrating complications, and, it seemed, a bit of witchcraft. Heating the cell above about 200 C seemed to destroy the prepared surface. Opening it to air after evacuation had a slightly detrimental but not disastrous effect. Too much washing after the final acid rinse gave poor results. These observations suggest that it is important to have a thin film of liquid H_2SO_4 on the silica surface.[1] The hydroxide and chromic acid treatments probably serve only to prepare a clean surface over which the dilute acid solution can spread evenly. Then under vacuum the dilute

---

1. These points were confirmed by W. E. Falconer of Bell Labs in a private communication. The acid-thin-film interpretation agrees with the findings of Ogryzlo (1961), which the author regrettably discovered only after completing the experimental work.

sulfuric acid dehyrates slowly until the vapor pressure is 10^{-4} torr or so, leaving a thin film of rather concentrated acid which keeps gaseous molecules out of direct contact with the silica surface.

Acid-treated surfaces continue to degass slowly for days, so it was important to re-evacuate the cell before each experimental run. During this operation the iodine was kept frozen in the cold finger with liquid nitrogen. After achievement of a good vacuum (5×10^{-5} torr) the liquid nitrogen was removed and the cold finger was allowed to warm up until the ion gage indicated rapid increase in iodine pressure. The stopcock was closed, the iodine was recondensed, and the stopcock was reopened for repetition of the warmup distillation. The procedure was repeated until the ion gage indicated that no volatile impurities were preceding the iodine in vaporization (usually three or four times). Then the stopcock was closed and the cell was removed for immediate collection of data.

Combination leak and degassing rates were determined by observing pressure increments with the ion gauge and multiplying by the volume ratio. (Volume of the cell was 120±5 ml; of the vacuum system below the diffusion pump, ~1.0 liter.) Results of numerous checks showed the cell was capable of holding vacuum below 10^{-2} torr for a day or more; cell degassing accounted for at least 75% of this "leak" rate, which appeared to be constant (.2-.4 mtorr per hour) with respect to time.

The cell used in the iodine atomic and molecular absorption studies is shown in Fig. 3. The lamp is attached at one end of the absorption cell; at the other is an evacuable window designed for direct "O"-ring sealing to the monochromator with some degree of thermal isolation. In use the cell was wrapped with insulating asbestos and heating tape and

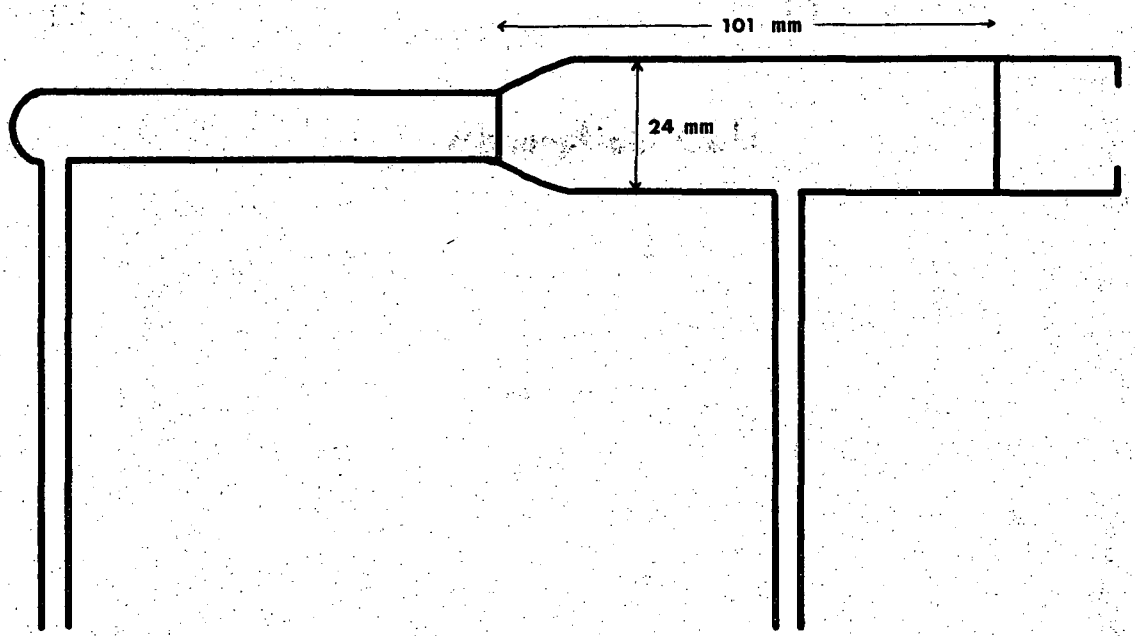

Absorption Cell

XBL 6910-5840

Fig. 3

warmed to several hundred degrees C, so it was important to insulate the cell from the monochromator to reduce thermal gradients.

The absorption cell was charged with I_2 on a high vacuum system. Acid treatment was unnecessary here and, in fact, undesirable, as atoms were to be produced by equilibrium thermal dissociation. Additional photolysis-produced atoms would only complicate the atomic absorption experiment. Before filling with I_2, the cell was baked out at ~500 C for about an hour. Then an excess of iodine was condensed in the cell by cooling with a piece of dry ice. A portion of the iodine was allowed to resublime before the cell was finally sealed off.

C. Iodine Lamps

Electrodeless discharge tubes of various designs were used as sources of atomic iodine radiation in these studies. They were powered by a high-frequency 100-watt microwave generator (2450-megacycle Burdick "Diathermy" MW/200), and were operated in open air under a Type A or Type C directional antenna. All sources were constructed from fused silica, with "cold fingers" for external thermal control of iodine pressures.

The lamps were prepared for use with the aid of a distillation cell which isolated the operations upstream from the vacuum manifold by means of an LN-cooled trap. Each lamp was charged with excess iodine and enough spectroscopic-grade argon (~1 torr) to maintain a stable, homogeneous discharge when the I_2 was frozen out at LN-temperatures. High vacuum was not necessary in the preparation of these sources: flushing the system once or twice with several torr argon accomplished the same purpose. The lamps were flamed several times with a gas-oxygen torch, with and without the discharge functioning; between flamings lamps were re-evacuated.

The visible output of each source was examined periodically through a hand spectrograph. The flaming-evacuating-refilling cycle was repeated until the discharge exhibited a pure line spectrum with the I_2 frozen out, and revealed no prominent molecular impurities when the cold finger was warmed. Then the lamp was sealed off and removed with the torch. Carefully prepared lamps had practically interminable working lifetimes.

Some effort was applied toward optimizing the ultraviolet output of one source by monitoring the 1830 A line through a monochromator while varying the argon pressure. At the high I_2 pressure (.03 torr) used in this test, the output was quite insensitive to variations in argon pressure.

The visible and UV output of these sources is discussed in detail in Section III-C. Qualitatively the discharge ranged from a pinkish-violet appearance at very low I_2 pressures to a bluish-white at I_2 pressures of .3-.5 torr and higher temperatures. The visible spectrum consisted almost entirely of Ar lines in the former case but was dominated by I_2 molecular features and a few strong atomic I lines in the latter.

D. Visible Excitation Sources and Filters

Visible excitation in the predissociation experiment was achieved with a tungsten strip lamp in combination with a number of narrow-band interference filters which spanned the spectrum from 4900 A to 6300 A. The lamp used was a 6-volt, 18-amp General Electric microscope illuminator bulb (18A/T10/2P-6V, SR6 filament); it was operated off a variac-controlled DC power supply at currents up to 22 amperes. The interference filters were purchased from Baird-Atomic; their optical characteristics are summarized later in this work in Table 4, which includes corresponding calculated excitation regions in the B state of I_2.

An optical pyrometer calibrated to the 1948 temperature scale was used to determine the brightness temperature at 6500 A of a lamp of the type used, as a function of current from 15 to 22 amperes. Thermodynamic filament temperatures were then determined with the aid of a nomogram given by Rutgers and deVos (1954). Results are displayed in Fig. 4.

Since the lamp was to be used intermittently, with an "on" time of 10-20 seconds, it was desirable to know the repeatability of the radiance at a given current under the experimental "on-off" conditions. Checks with a photodiode and with a monochromator-photomultiplier arrangement indicated this operation was replicable within 1%.

In some preliminary predissociation work a GE floodlamp of the tungsten-iodine type (V-line, DWY, 120V, 650W) was used for visible excitation. This source can be run directly off a Variac and produces more light than the tungsten strip lamp. However, the spiral-coiled filament was not as convenient to focus in the cell, and the presence of iodine in the lamp was of unknown consequence in the experiment. Hence the switch was made to the strip lamp. The tungsten-iodine lamp was retained as a general excitation source for producing large concentrations of atoms in investigating the efficiencies of various wall treatments.

Kodak Wratten neutral density filters were used to attenuate the visible exciting light in some experiments. They were calibrated singly and in combination with one another and with several interference filters on a Cary 14 scanning spectrophotometer. The optical densities appeared to be additive within 1%, which is the order of accuracy of the Cary instrument. A check with a monochromator and photomultiplier verified the Cary results.

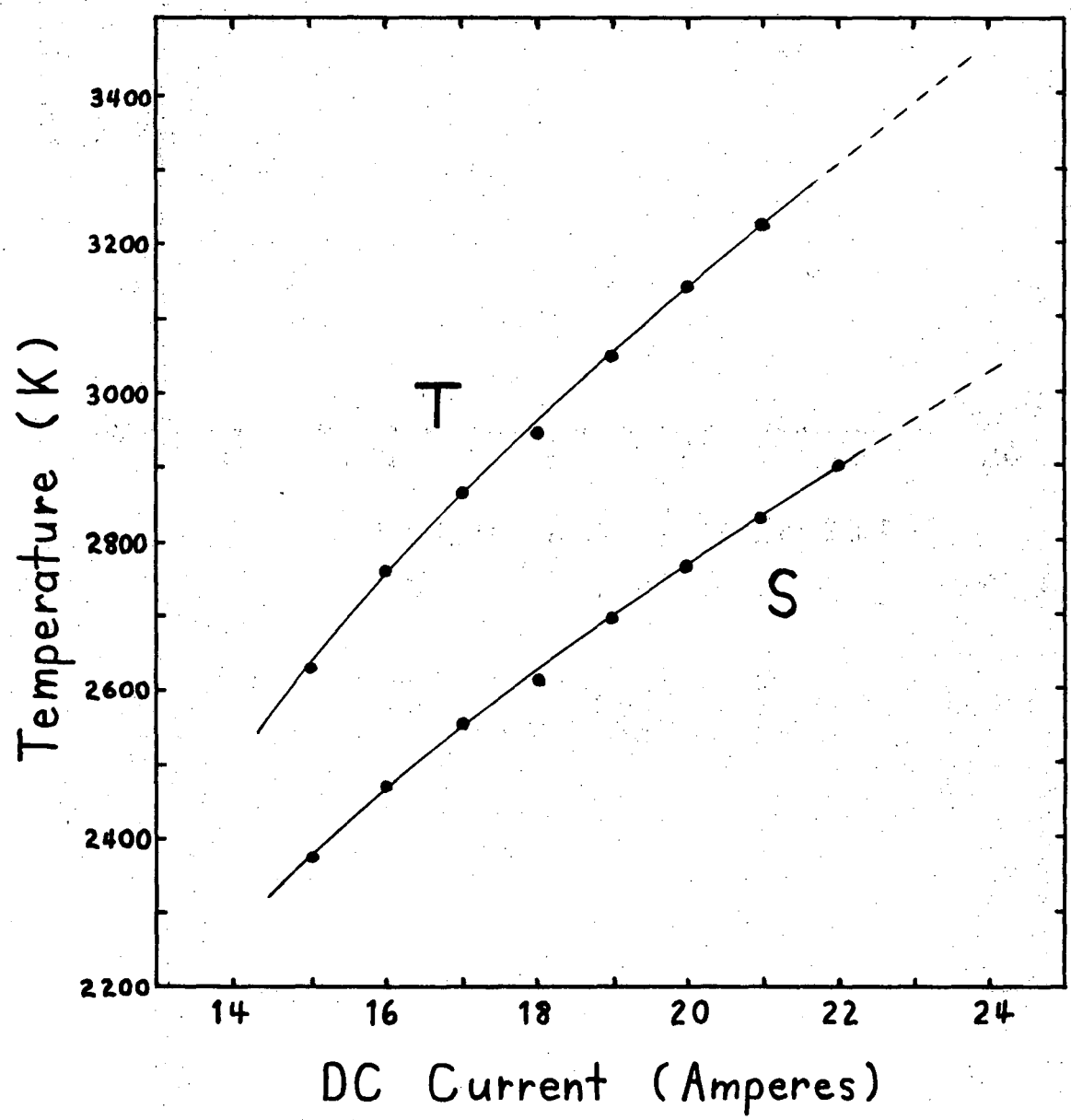

XBL 6910-5838

Fig. 4. Tungsten strip lamp performance. S is the brightness temperature at 6500 A; T is the thermodynamic filament temperature.

E. Flashtube

Xenon-filled flashtubes have been used in photochemical studies for more than twenty years. As early as 1946 Edgerton suggested their application in color photography, because their visible output was qualitatively quite similar to sunlight. At present they are widely employed in laser-pumping and kinetic spectroscopic work where their ability to produce a very short, extremely intense burst of light is of prime importance.

The flashtube used here was a model FP-5 xenon flashtube manufactured by Xenon Corporation.[1] The tube is of the simple linear design, about 1/4 meter long with an arc length of 125 mm. The envelope is clear fused quartz, with a 9-mm outer diameter. This flashtube is recommended for use at voltages up to 10 kilovolts and energies of 500 joules, and can be operated in a high hold-off manner with external triggering or in a thyratron-ignitron triggering circuit. With properly designed circuitry the flashtube pulse's 1/3-peak width can be less than 10 microseconds. The tube has a life expectancy of 10^4 to 10^5 flashes.

Because of the ease of detecting I atoms in UV fluorescence, powerful flashes were not required in these experiments and were in fact undesirable. (Too much light introduces thermal complications and nonlinearities in the detection system.) At the same time it was important to keep the flash as brief as possible, since I-atom recombination times were expected to be on the order of milliseconds. These demands were met by using a small charging capacitor at moderate voltage as shown in the circuit diagram, Fig. 5. The resistor was included to protect the power supply;

---

1. 39 Commercial Street, Medford, Massachusetts.

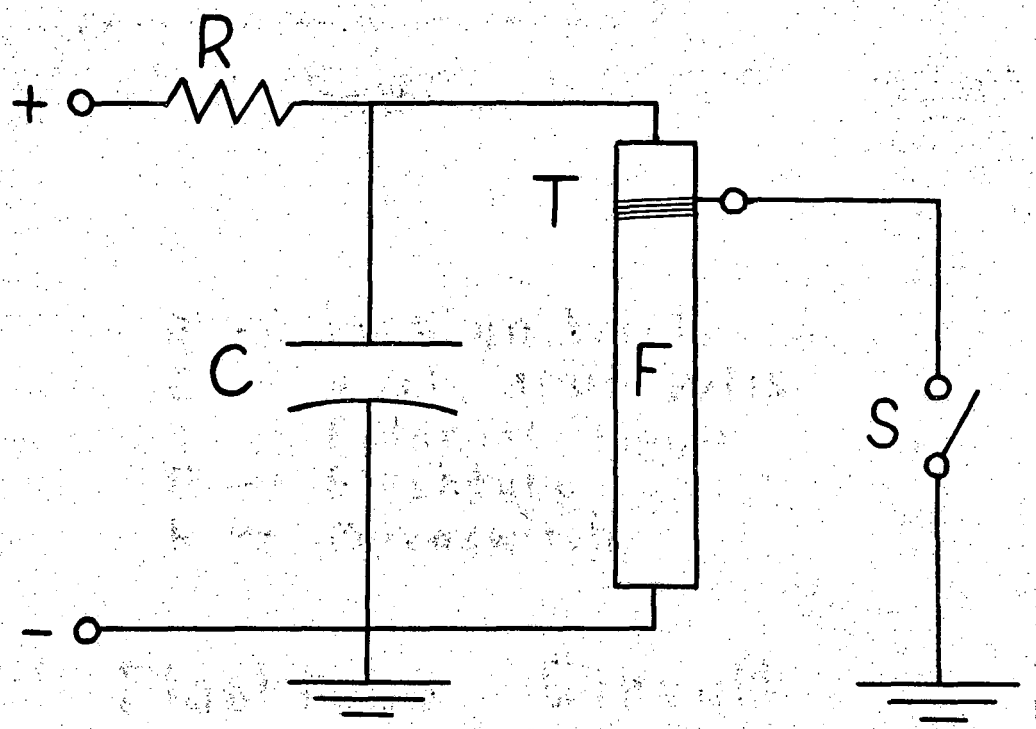

R — 270 K, 40 Watts
C — 4 μf, 3000 Volts
T — External Trigger
F — Flashtube
S — Microswitch

Flashtube Circuit

XBL 6910-5837

Fig. 5

the system required 8-10 seconds to recharge between flashes if uniform flashes were desired. The tube could be fired externally with a Tesla coil at voltages from 1500 up, and would hold off fairly well up to 3000 volts, the limiting rating for the capacitor. (At 2800-3000 volts, the tube was subject to occasional spontaneous flashes, which however, represented no real problem.) The system was customarily operated at 2500-2700 volts, where the flashes were found to be repeatable to better than 3% in maximum intensity. At these voltages the energy per flash ($CV^2/2$) was 12-15 joules.

The time dependence of the flash was investigated by displaying the signal from an RCA 935 phototube on the screen of a Tektronix 585 oscilloscope. The light reaching the phototube was attenuated with neutral density filters far below the saturation level of the tube, where further attenuation showed the response was linear. The tracings were photographed on Polaroid film. A cursory check was made on the time dependence at various wavelengths using Corning Glass filters to select desired spectral regions; the anticipated results showed the time character of the flash was constant with respect to wavelength. The characteristic rise-time of the flash was 5 μsec, and the 1/3-peak-height time was about 12 μsec. The area under the curves showed that about 90% of the total energy was dissipated in the first 12 μsec, with less than 2% of the emission coming after 25 μsec.

The Tesla coil external triggering mechanism produced a varying but uncontrollable amount of high frequency noise that proved a source of consternation in recording recombination tracings. It was eventually abandoned and replaced by a beautifully simple, absolutely noise-free alternative, discovered largely by accident. With the external trigger located near its anode, the flashtube could be fired by simply grounding

the trigger wire. The tube would flash almost without fail at voltages above 2500 if the lapse time between flashes was held to less than ~30 seconds. After longer periods the tube had to be "reconditioned" by firing once or twice with a Tesla coil. The performance of the flash-tube appeared to be affected negligibly by this change in the triggering method.

F. Experimental Arrangements and Signal Detection

1. Ultraviolet Absorption Experiments

In the investigation of the iodine lamp and subsequent ultraviolet absorption work, a Jarrell-Ash one-meter Seya-Namioka type Vacuum monochromator was employed with a grating blazed for 1500 A and having a dispersion of 10 A/mm in the first order. Slits could be opened to .4 mm providing a maximum bandwidth of ~8 A. A grating-drive mechanism offered twelve scan speeds from 5 to 2500 A per minute. The instrument was capable of evacuation to 10^{-6} torr using the oil diffusion pump, but for the spectral region of interest (1650 A to 1900 A) the mechanical pump produced a quite sufficient vacuum. All cells and sources were easily attached to the face of the entrance slit housing by means of "O"-ring seals.

The Jarrell-Ash instrument could be used as a spectrograph by replacing the exit slit housing with a vacuum camera attachment. The film holder took 35-mm films; Kodak SC-5 and 101-01 films served quite satisfactorily. Each exposure spanned about 500 A, and five exposures could be put on a film. Aberrations in the concave grating and minute vibrations from the mechanical pump both caused extensive blurring of sharp spectral features, so it was necessary to mask down the grating beforehand and turn off the pump for short periods when taking pictures. The latter procedure presented no difficulty as the system was capable

of maintaining a vacuum below ~.1 torr for thirty to forty-five minutes.

When the instrument was used as a monochromator, a sodium salicylate fluorescent window was used to convert the ultraviolet light to visible photons which could be detected with an RCA 1P21 photomultiplier. The fluorescent window was prepared in a manner similar to that described by Samson (1967, p. 212). A dilute aqueous sodium salicylate solution was prepared and several drops of it was spread over the window surface in a manner designed to produce a desired thickness of between 1 and 2 mg/cm^2 of the phosphor. The solution was dried rapidly with the aid of a heat gun in order to produce an even surface of small crystals.

The 1P21 photomultiplier tube was used at potentials as high as 1200 volts in a linear voltage-divider circuit as recommended by the manufacturer for maximum gain. The signal (anode current) was put through a 240 kilohm resistor to develop a potential, which was recorded on a ten-millivolt Varian G-10 chart recorder. The photomultiplier DC power supply was run off a Variac, and the chart recorder signal could be adjusted to scale by varying the AC input to the power supply. At maximum sensitivity, signal fluctuations were less than 5% of full scale; most experimental work was done under conditions where this noise level was less than 2%.

2. Predissociation Experiments

The experimental layout was very simple as can be seen in the schematic, Fig. 6. The tungsten strip lamp is contained in a cardboard box with an outlet for the light. The rest of the box is covered with black cloth to keep unwanted visible light from flooding the room. Light emerging from the hole in the box is gathered immediately by two 125-mm diameter condensing lenses, which focus the lamp filament in the predissociation cell about .3 meter away. The cell is covered with black paper in an effort to light-proof it against visible radiation from the iodine lamp.

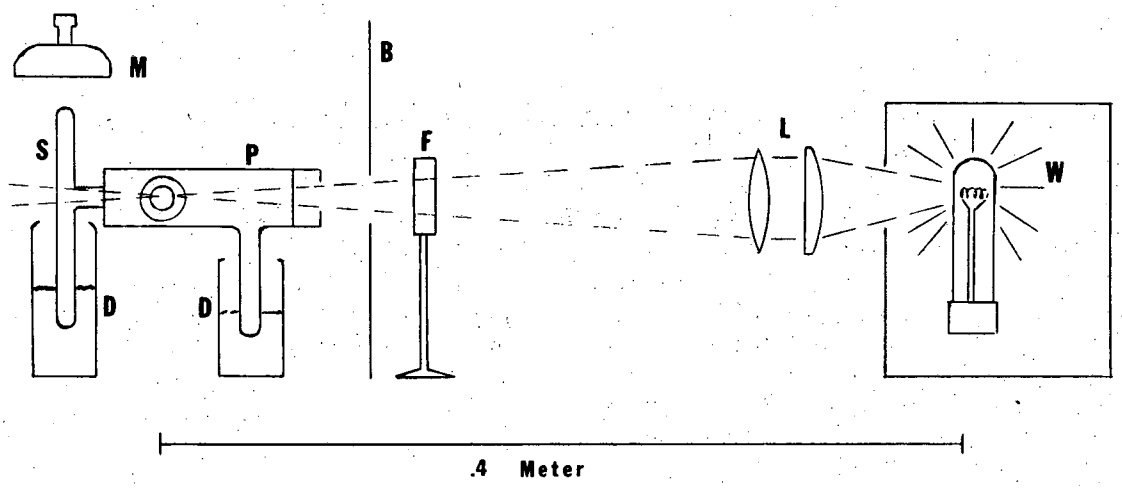

XBL 6910-5836

Fig. 6. Arrangement for predissociation experiments. M is the microwave antenna, which excites atomic emission in the source S. The latter is affixed directly to the predissociation cell P. The cold fingers are cooled by baths contained in the dewars D. Light from the tungsten lamp W is gathered by condensing lenses L and focused in the cell near the fluorescence window. The interference and neutral density filters are placed in the rigidly fixed filter holder F. Spurious visible light is reduced by means of the baffle B.

A rigidly fixed filter holder is located about 50 mm from the predissociation cell in the path of the light. A baffle is placed between the filter holder and cell to further eliminate spurious visible radiation from the tungsten source. With this arrangement the various 2"×2" interference and neutral density filters may be inserted into the light beam without affecting the geometry of the setup. The predissociation cell may be oriented perpendicular to the light beam in side-on excitation or coaxial with it for end-on excitation.

Fluorescence signals observed in the experiment were detected and recorded with the circuit shown in Fig. 7. The circuit consists primarily of two current dividers. The first is so designed that full scale on the 20-microampere current meter corresponds to a total anode current of 63 microamperes, well below the tolerance of the EMR photomultiplier. The second simply controls the size of the signal by bleeding off a variable fraction of the total current. Two chart recorders are used to record the data. The Varian G-10 records the total signal across a 5-kilohm resistor. A Leeds and Northrup Speedomax Type G (1-, 5-, 10-millivolt) measures the incremental signal, effectively multiplied by a factor of five, since it is taken across 25 kilohms of the load resistance. The loop containing the 6-volt battery is used to null the background so that the incremental signal may be observed full scale on the L and N recorder.

Photomultipliers are essentially low-noise current amplifiers and may be treated in circuits as current sources as long as the potential between the last dynode and the anode remains constant. Typically the dynode step potential is 100 volts or more. In passing through a 100 kilohm resistor, a current of 1 μamp develops a potential of .1 volt, an amount negligible with respect to the step potential. By keeping the

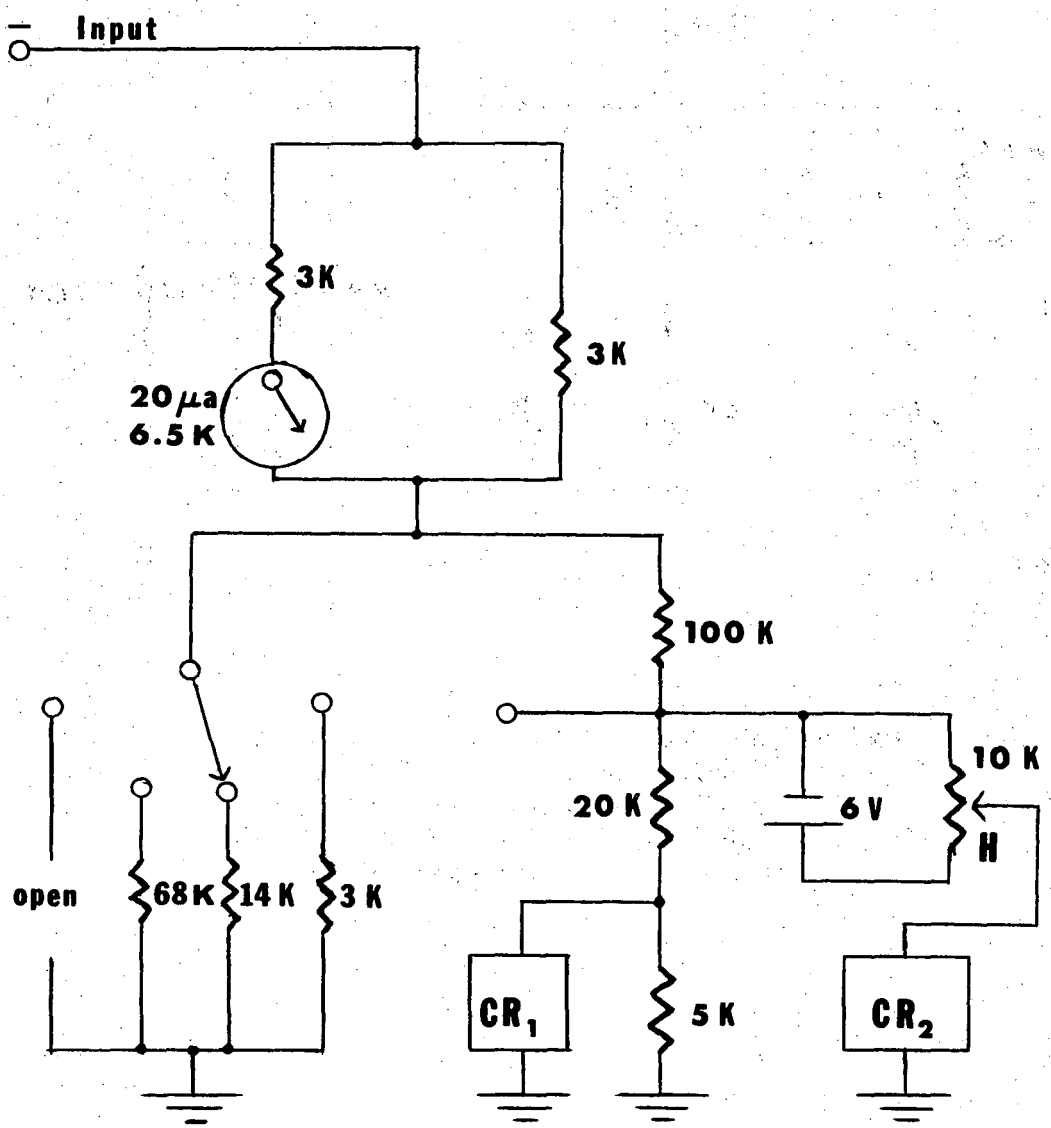

XBL 6910-5835

Fig. 7. Circuitry for recording signals in predissociation experiments. H is a 10-K "Helipot." CR_1 is the Varian chart recorder, which records the total signal. The L and N recorder CR_2 records the incremental signals.

load resistor and anode current low enough to maintain conditions such as these, one can insure that the photomultiplier current will be directly proportional to the photon intensity impingent upon the photocathode, over several orders of magnitude change in total irradiance. If the chart recorders in the circuit of Fig. 7 introduce no non-linearities, the recorded voltage signal will also be linearly dependent on photon intensity. Chart recorder impedances are about one megohm and are not found to vary noticeably with signal. In any case the relationship between chart recorder signal and microammeter current was checked for this circuit under operating conditions and found to be strictly linear.

The EMR photomultiplier was operated off a regulated power supply with cathode negative and anode near ground potential. Voltages as high as 3800 were required for the weakest signals encountered. Typically the total anode current was 1.5-2.0 μamp, yielding a signal of 4-6 mv on the Varian recorder. Noise and fluctuations were generally less than 3% of the total incremental signal recorded by the L and N recorder.

3. Iodine-Atom Recombination Studies

The physical setup for these experiments was similar to that described in preceding paragraphs, with less concern given to spurious visible light. The flashtube was placed in the cardboard box, where the unwanted UV component of the flash could be eliminated with a 3"×3" Wratten No. 16 filter. The I_2 cell was oriented for side-on excitation, with all "light-proofing" material removed. Iodine atoms could be observed in fluorescence or absorption.

The flashtube was operated off an unregulated 5-kV, 100-ma power supply at 2600-2800 volts, using the circuit described in Section II-E. Voltages as high as 3400 (regulated) were needed to run the EMR photomultiplier. The signal was developed across a 240K resistor and observed

and photographed on the screen of a Tektronix 585 oscilloscope operated in the single-trace mode. The horizontal sweep could be triggered by the signal itself. When the AC input mode was used, the oscilloscope signals exhibited some distortion, so tracings were photographed in the DC input mode. A Type W plug-in unit was used to null the DC background so that the transient signal could be observed full scale on the oscilloscope screen. Peak signals were 1-4 volts.

In experiments involving transient signals of complicated or unknown waveform, it is important to insure that the detection circuitry introduces no distorting effect. For a simple resistor circuit it suffices to keep the RC time constant much smaller than an appropriate time constant for the measured signal. In this work a large resistor was employed, so it was necessary to minimize stray capacitance. By using short lengths of coaxial cable it was possible to keep the time constant low enough that circuitry could be neglected in analyzing the tracings. Direct observation of the ultraviolet light from the flash through the EMR photomultiplier and 240K resistor yielded a decay time of 40-50 μsec. This value is about four times that observed with the RCA phototube, but still less than 1/20 of the exponential time constant for the fastest recombination tracing recorded. Additional small capacitors placed across the resistor proved effective in reducing shot noise, but increased the RC time constant in direct proportion to their smoothing effectiveness; hence they were removed.

G. Miscellaneous

A Spex[1] 3/4-meter Czerny-Turner spectrograph/monochromator was used to investigate in detail the visible output of the iodine sources. This instrument had an optical speed of f/6.8 and gave a dispersion of ~11 A/mm in the first order of a grating blazed for 5000 A. Spectra were recorded

1. Spex Industries Inc., Metuchen, New Jersey.

photographically on Polaroid 4"×5" Type 57 sheet film and on Type 47 roll film. With a narrow slit (.01 mm) exposures were generally about a minute when the lamp cold finger was cooled to -50 C or lower. When the instrument was employed as a scanning monochromator, signals were detected and recorded with the 1P21 photomultiplier and Varian G-10 chart recorder described previously.

A number of organic chemicals were used as coolants in the experiments. In the predissociation experiments the lamp seemed to perform best when cooled in an ethanol/dry-ice bath at ~-80 C. At various times liquid nitrogen (-196 C) and a 60% ethylene glycol and water solution (~-50C) were tried for this purpose; however, the lamp was weak in iodine atomic emission in the former bath and produced too much visible radiation in the latter. Temperatures in the range -30 C to 0 C were required to produce the desired molecular iodine pressures in the predissociation cell. Many data points were recorded using dry ice-cooled ethanol in a dewar to achieve these temperatures, which were read to the nearest tenth of a degree from a mercury thermometer calibrated in ice water. However, it was more desirable for much of the work to have constant temperature slushes available. The following materials were easy to obtain and convenient to use: (1) o-xylene (MP = -25.9 C), (2) benzyl alcohol (-15.3 C), (3) ethylene glycol (-13.2 C), (4) diethylene glycol (-10.5 C), (5) methyl salicylate (-8.6 C), (6) n-butyl silicylate (-5.9 C). Liquid nitrogen was generally used to cool the baths. In practice some of the above materials froze at temperatures 1/2-1 degree above their reported melting points; even so, it was easy to maintain a constant (within ~.1 degree) temperature for ~1 hour without refreezing the slush.

Temperatures above 100°C and below -30 C were determined with iron-constantan or chromel-alumel thermocouples. Potentials were measured with Leeds and Northrup potentiometers. The thermocouples were calibrated against accurate thermometers at several points between -30 C and 100 C. Temperatures were then obtained from the standard tables, corrected in accord with the calibration values.

An inexpensive phototransistor (Fairchild FPT 100, $ 1.20 each) proved useful in some experiments related to the predissociation and flash studies. This device has fair sensitivity with a rise-time of ~3 μs, and it responds linearily to light when the emitter lead is left unconnected. Furthermore this amazing gadget requires no external power supply, serving as a self-contained, light-actuated current source in a simple resistor loop circuit.

Finally, Plate 1 shows the author conducting some unrelated experiments; the results of these particular attempts were unpublishable.

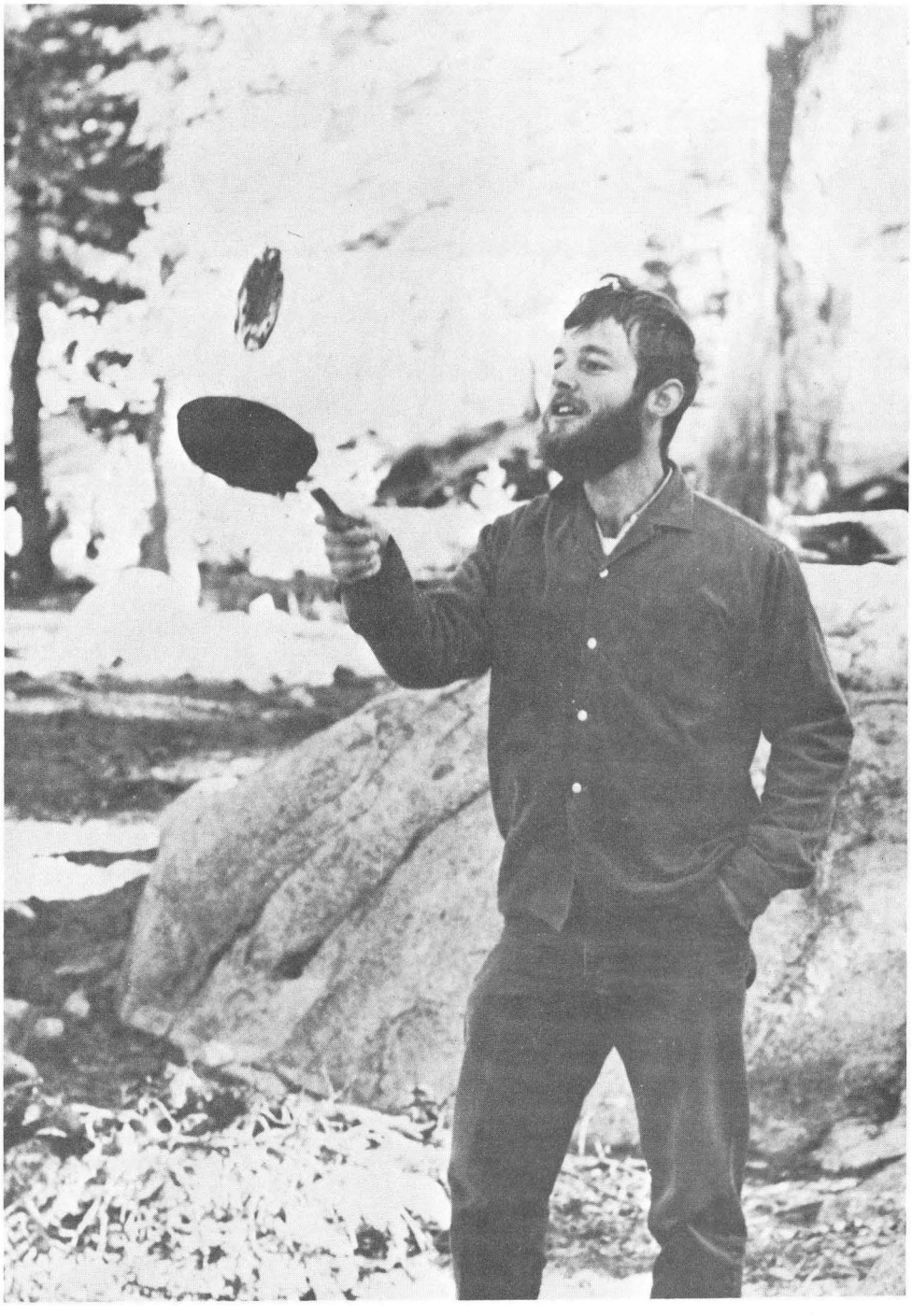

XBB 6910-6802

Plate 1. Unrelated research.

III. THE IODINE LAMP: ULTRAVIOLET ABSORPTION BY I AND I_2

A. Radiation Relationships

The important Einstein radiation relationships for dipole transitions are derived in most basic quantum mechanics texts and dealt with at length in works such as the classic treatises by Condon and Shortley (1951), Mitchell and Zeemansky (1934), and Herzberg (1950). Einstein derived his expressions from considerations of thermodynamic equilibrium applied to emitting and absorbing particles. Identical results are obtained using the approach of quantum electrodynamics. The important relationships will be summarized here for future reference.

The transition probability for spontaneous emission or "A value" is perhaps the easiest quantity to work with, because of simplicity of units ($time^{-1}$). For transitions between non-degenerate levels it is given by

$$A_{ab} = \frac{64\pi^4}{3h} \nu^3 |R^{ab}|^2 \qquad (1)$$

where h is Planck's constant, ν is the frequency in wave numbers, and R^{ab} is called the matrix element of the transition; for dipole transitions it is the vector of the dipole moment operator between the states involved. The power, or energy emitted by a source per second will be denoted the flux or radiant flux Φ[1]. For a transition between upper and lower states a and b, respectively,

---

1. The quantity called flux here is called intensity by many workers. However the latter term has been applied rather indiscriminately to several completely different quantities, resulting in some amount of confusion. The notation used here is in keeping with the recommendations of several commissions, published in the Journal of the Optical Society of America, 57, 854 (1967). Accordingly the radiant intensity I is defined as radiant flux leaving a point source per unit solid angle. Thus Φ for a point source will be $4\pi I$. The term "intensity" will also be used in a qualitative sense, where units are of no concern.

$$\Phi\,(a,b) = hc\,\nu\,N_a\,A_{ab} \qquad (2)$$

where N_a is the population of the excited state a and c is the speed of light. In photochemical work it is often more convenient to deal with the quantum flux, which differs from Eq. (2) in the absence of the energy factor $hc\nu$; it will be denoted Φ_q.

The probabilities for absorption and stimulated emission may be calculated using the Einstein "B values," which are related to the A value in a direct way but take a number of different forms, depending on the treatment of the radiation field. Considering non-degenerate levels only, the B value for absorption is equal to that for stimulated emission, and the transition rate in either direction is of the form

$$-\frac{dN_b}{dt} = \rho_\nu\,B\,N_b \qquad (3)$$

where N_b is the number of particles in state b and ρ_ν is descriptive of the radiation field. In Einstein's original treatment (1917), ρ_ν was in units of energy density, giving

$$B = \frac{1}{8\,\pi\,hc\,\nu^3}\,A \qquad (4)$$

In photochemical work it is often convenient to express ρ_ν as a quantum intensity. If ρ_ν is in units of quantum flux per unit solid angle, per unit surface area at normal incidence, we have

$$B = \frac{1}{8\,\pi\,c\,\nu^2}\,A \qquad (5)$$

A more practicable quantity for describing the absorption process for excitation from a beam is the absorption coefficient, to be dealt with in the next subsection. Other forms for B are discussed briefly in Appendix II.

---

1. It should be noted that ρ_ν is a distribution function of the frequency. Here the appropriate units are ergs/cm^3 per unit wave number interval, or ergs/cm^2. See Appendix II for further illumination on this point.

The presence of degeneracies in one or both levels introduces mild complications. If g_A and g_B are the degeneracies, the total A value for transitions from level A to level B becomes

$$A_{AB} = \frac{64\pi^4\nu^3}{3h} \frac{\sum_{a,b} |R^{ab}|^2}{g_A} \tag{6}$$

where the sum is taken over all degenerate sublevels a and b. The expression analogous to (4) is

$$B_{BA} = \frac{1}{8\pi hc\,\nu^3} \frac{g_A}{g_B} A_{AB} \tag{7}$$

and for the stimulated emission

$$B_{AB} = \frac{g_B}{g_A} B_{BA} \tag{8}$$

One additional quantity descriptive of radiative processes deserves mention here. The "f-value" or oscillator strength of a transition is a measure of the degree to which the strength of the transition approaches that calculated for a classical oscillating electron. f-value terminology is used widely by some workers, particularly astrophysicists; it has descriptive merit in that strong allowed transitions generally possess an f-value of the order of unity. The absorption f-value is related to the A value by

$$f_{BA} = \frac{mc}{8\pi^2 e^2} \frac{g_A}{g_B} \nu^{-2} A_{AB} \tag{9}$$

$$= 1.499 \frac{g_A}{g_B} \nu^{-2} A_{AB}$$

where m and e are the mass and charge of the electron. (In the second equation ν is in units of reciprocal centimeters.)

Condon and Shortley (1951, Chpt. 4) have defined a line strength S_{AB} for transitions between levels A and B, which has the advantage of being symmetric in the initial and final levels.

$$S_{Ab} = \sum_a |R^{ab}|^2 \tag{10a}$$

$$S_{aB} = \sum_b |R^{ab}|^2 \tag{10b}$$

$$S_{AB} = \sum_a S_{aB} = \sum_b S_{Ab} = \sum_{a,b} S_{ab} \tag{10c}$$

With these definitions (6) and (7) become

$$A_{AB} = \frac{64\,\pi^4\,\nu^3}{3h}\,\frac{S_{AB}}{g_A} \tag{11a}$$

$$B_{BA} = \frac{8\pi^3}{3h^2c}\,\frac{S_{AB}}{g_B} \tag{11b}$$

From these expressions it is clear that in situations where the emitting or absorbing populations are proportional to the degeneracies, the line intensities will be proportional to the S_{AB}'s. This point becomes particularly useful when we find that with certain assumptions about the nature of the coupling of the different angular momentum vectors in the atom or molecule, S_{AB} can be further expanded into a product of a reduced matrix element and a factor dependent on the angular momenta alone. For atoms obeying Russell-Saunders coupling, Condon and Shortley give (Chpt. 9)

$$S_{\chi\, SLJ,\, \chi'\, SL'J'} = s(SLJ;\, SL'J')\,|\langle \chi L|P|\chi' L'\rangle|^2 \tag{12}$$

Here the parameters S; L, and J are the conventional notations for spin, orbital, and total angular momenta, and χ represents all other quantum variables, particularly the position coordinates. Clearly, all the transitions in a given L, L' multiplet must have identical reduced matrix elements $\langle \chi L|P|\chi' L'\rangle$, so the relative intensities are given by the s factors. Furthermore the sum of all the s factors for a given level equals the degeneracy 2J+1 of that level, both for absorption and emission.

Entirely analogous expressions exist for diatomic molecules. S becomes

$$S = s_J \; |Re|^2 \tag{13a}$$

which, with the assumption that the dipole moment operator varies slowly with the internuclear distance, can be further expanded to

$$S = s_J \; \overline{Re}^2 \; |\langle v'|v''\rangle|^2 \tag{13b}$$

$\overline{Re}$ is the average electronic transition moment for the vibronic transition (v',v''). $\langle v'|v''\rangle$ is the overlap integral of the vibrational eigenfunctions in the upper and lower electronic states, and the absolute square of the overlap integral is the familiar Franck-Condon factor. s_J is the rotational line strength, for which expressions have been derived by Hönl and London and summarized by Herzberg (1950, Chpt. IV). Again the sum of the s_J values for all transitions to a given rotational level equals the degeneracy 2J+1, and the quantity $\overline{Re}^2 \; | \langle v'|v''\rangle|^2$ may be compared with the equivalent term for atoms, $|\langle XL|P|X'L'\rangle|^2$. Henceforth, the latter will also be referred to as $|Re|^2$.

Transition strengths may be determined three ways: (a) Theoretical calculations; (b) Absorption and emission strength measurements; (c) Lifetime measurements. The first of these will not be discussed here. In any case, results in this field of endeavor have generally fallen somewhat short of smashing success. Absorption methods will be discussed in more detail in the next subsection of this work. Lifetime techniques are a field in themselves; summaries of methods may be found in the works by Mitchell and Zemansky (1934, Chpt III) and Chutjian (1965). However several important considerations should be mentioned here.

The lifetime for excited state a is the reciprocal of the sum of all transition rates out of a. Symmetry arguments require that all degenerate states a_i of level A have the same lifetime. When level A combines with only one other level B, the lifetime is the reciprocal of

A_{AB} in (6). In the more general case, transitions may occur from A to several lower levels, so that

$$\frac{1}{\tau(A)} = \sum_i A_{AB_i} = \frac{64\pi^4}{3hg_A} \sum_i \nu_i^3 \, S_{AB_i} \qquad (14)$$

where the sum is over all lower levels B_i. If all the lines in an atomic Russell-Saunders multiplet have approximately the same ν_i, the sum over levels may be condensed to a sum over multiplets,

$$\frac{1}{\tau(A)} = \frac{64\pi^4}{3h} \sum_m \nu_m^3 \, |Re_{AB_m}|^2 \qquad (15)$$

where ν_m is the average frequency for the multiplet.

For diatomic molecules, the frequencies of the two or three rotational lines connecting with a given level (v',J) in a particular vibronic transition (v',v") are generally close enough to make the condensation analogous to (15) almost rigorous, and we have

$$\frac{1}{\tau(v',J)} = \frac{64\pi^4}{3h} \sum_i \nu_i^3 \, |\langle v'|v_i''\rangle|^2 \, \overline{Re}_i^2 \qquad (16)$$

$$= \frac{64\pi^4}{3h} \langle \overline{Re}^2 \rangle_{v'} \sum_i \nu_i^3 \, |\langle v'|v_i''\rangle|^2$$

The summation is over all vibrational levels of the lower electronic state, and ν_i represents the average frequency of the rotational lines involved in each vibronic transition. (If transitions can occur to more than one lower electronic state, the summation must be extended accordingly. Also, if electronic degeneracies exist, (16) must be altered as dictated by (6).) In the second expression the bracket denotes the average value of $\overline{Re}^2$. This is expected to vary much slower than the other quantities, hence is often taken out of the summation.[1] In general $\langle \overline{Re}^2 \rangle$ will be found to vary with v', which may complicate the comparison of lifetime results with

1. The validity of this and the earlier approximation which led to the definition of Re and the Franck-Condon factor have been questioned, tested, and in many cases found wanting, by a number of workers in recent years. See the study by Gabelnick (1969) for a discussion of this topic.

experimental absorption strengths.

So far the discussion of lifetime has been restricted to purely radiative decay. It should be noted that any additional process which can depopulate the excited state will affect the lifetime τ. First-order decay modes such as spontaneous predissociation and auto-ionization and second-order processes like collisional quenching contribute to make the lifetime shorter than would be the case if radiative processes were the only mode of decay.

B. Line Shapes and Absorption Relationships

The study of line shapes has received quite a bit of attention in recent years. The review by Breene in 1957 covers much of the work done in the field up to that time, and the literature is dotted with numerous investigations since then. However most of the important relationships governing absorption and emission of radiation in electronic transitions (spectral region ~1000-10000A) had been derived by the end of the first decade after the advent of modern quantum mechanics. Many of the expressions to be used here are given by Mitchell and Zemansky (1934). Although their work is directed toward the study of atomic transitions, most of the formulas they present are perfectly general. A more recent treatise in the field with emphasis on molecular applications is the book by Penner (1959). The author finds Penner's notation difficult to penetrate, so most of the notation used here will conform to that in the work of Mitchell and Zemansky (hereafter referred to as MZ), except that here ν is frequency in wave numbers instead of sec^{-1}, so the expressions below will differ from those in MZ by appropriate factors of c.

1. Line Shapes

The absorption coefficient k_ν of a gas is defined by the equation

$$I(\nu) = I_o(\nu) \; e^{-k_\nu \ell} \tag{1}$$

where $I_o(\nu)$ is the incident light intensity and $I(\nu)$ is the intensity transmitted through the absorbing layer of thickness ℓ. Since the exponential is dimensionless, k_ν has dimensions $(\text{length})^{-1}$. For a single isolated absorption line, k_ν will have a maximum value k_o and a full width $\Delta\nu$ at half maximum which will be called the half-width. The quantity $k_o \ell$ will be referred to as the optical depth.

The specific functional form for k_ν will be determined by one or several of the following: (a) Natural broadening, (b) Doppler broadening, (c) External fields, (d) Collisions with other particles. This work is concerned primarily with the first two of these, as experiments were conducted under conditions of low pressures and only incidental external fields. Under these conditions k_ν will be a symmetrical function about the center frequency ν_o.

The form of the absorption coefficient for natural broadening or "resonance damping" alone is

$$k_\nu = \frac{k_o}{1 + \left[\frac{2(\nu - \nu_o)}{\Delta\nu_N} \right]^2} \tag{2}$$

where the natural half-width is

$$\Delta\nu_N = \frac{1}{2\pi c \tau} \tag{3}$$

τ is the lifetime of the excited state, where <u>all</u> modes of decay must be included.[1] This result may be viewed as a direct consequence of the uncertainty principle. Analogously a simplified view of collisional

1. Strictly speaking, $1/\tau$ should be replaced by $(1/\tau(A) + 1/\tau(B))$, where A and B are the upper and lower levels involved in the transition. The correction is negligible when B is the ground level.

broadening gives

$$\Delta\nu_c = \frac{1}{2\pi c\,\tau_c} = \frac{Z}{2\pi c} \tag{4}$$

where Z is the collision rate and τ_c is the average time between collisions; k_ν will again have the Lorentzian form (2). Under conditions of moderate pressure ($\lesssim$ 1 atm) of foreign gas, inert with respect to the absorbing species, absorption coefficients are often found to exhibit a Lorentzian profile which conforms to (4); but higher pressures and stronger interactions produce shifts and distortions so that (4) is no longer valid.

Doppler broadening is produced by the random thermal motions of the absorbing particles and may be described as the result of a Maxwellian distribution of different frames of reference among the particles. The form of k_ν is Gaussian

$$k_\nu = k_o \exp\left[-\left(\frac{2(\nu - \nu_o)}{\Delta\nu_D}\sqrt{\ell n 2}\right)^2\right] \tag{5}$$

with

$$\Delta\nu_D = \frac{2\sqrt{2R\,\ell n 2}}{c}\,\nu_o\sqrt{T/M} \tag{6}$$

In general Doppler and natural broadening will both contribute to the form of k_ν. However, it is frequently the case that, in the absence of foreign gases, one of the two effects will dominate the other. M and Z define the natural damping ratio as

$$a = \frac{\Delta\nu_N}{\Delta\nu_D}\sqrt{\ell n 2} \tag{7}$$

and point out that for electronic transitions, a is often about .01. With a natural damping ratio of this magnitude k_ν will be determined almost entirely by the Doppler effect near the center of the line $(\pm\Delta\nu_D)$ and by natural broadening in the wings of the line $(|\Delta\nu| \gtrsim 3\,\Delta\nu_D)$. The complete expression for k_ν is a convolution of the forms (2) and (5), an integral representation which will not be used in this work, but can be found in MZ (p. 101).

In the often encountered situation where I_o in (1) is approximately constant in the region of absorption, and where spontaneous and stimulated emission are negligible, absorption lines have a simple profile. For low optical depth the shape is proportional to $k_\nu \ell$. In practice it may be difficult to achieve the instrumental resolution necessary to observe the true form. However, absorption measurements are usually aimed at obtaining the integrated absorption coefficient $\int k_\nu d\nu$, which can often be acquired without concern for instrumental broadening. (This point is explicated below.)

Emission-line profiles can be quite complex for "turbulent" sources. However, for a homogeneous source of low optical depth the radiation may be represented (MZ, p. 108)[1]

$$E_\nu = C(1 - e^{-k_\nu' \ell'}) \tag{8}$$

where C is a scaling factor, k_ν' is the absorption coefficient in the source, and ℓ' is the length of the source. In the limit of low optical depth (8) becomes

$$E_\nu = C \; k_\nu' \; \ell' \tag{9}$$

Eq. (9) with a one-parameter Gaussian form for k_ν' is often used to describe a source for which detailed information is lacking.

2. Absorption Measurements and Lifetimes

Regardless of what processes contribute to the form of k_ν, the following relationship must hold when spontaneous and stimulated emission are negligible:

$$\int k_\nu \, d\nu = \frac{1}{8\pi c \; \nu^2} \; \frac{g_A}{g_B} \; N \; A_{AB} \tag{10}$$

Here N is the concentration of absorbers. If k_ν is given by (5) we have

1. M and Z present this expression for the case of an "ideal resonance lamp," but the same functional form should apply to any homogeneous source where emission and absorption along the optical path in the source are taken into account, but where diffusion of radiation may be neglected.

$$\int k_\nu \, d\nu = k_o \frac{\Delta\nu_D}{2} \left(\frac{\pi}{\ell n 2}\right)^{1/2} \tag{11}$$

When absorption measurements are carried out using a line source, it is convenient to define a quantity Ab, called the absorption and given by

$$Ab = \frac{\int E_\nu \, d\nu \, (1-e^{-k_\nu \ell}) \, d\nu}{\int E_\nu \, d\nu} \tag{12}$$

E_ν is the frequency distribution of the incident radiation. The absorption is simply the fraction of source radiation that is absorbed. With certain choices for E_ν, Ab can be expressed as a power series expansion; for some cases it must be calculated numerically. Expressions for Ab are given in Appendix I for several different E_ν's of the former type. For a Gaussian source line having the same center frequency ν_o as the absorption line, the result is

$$Ab = -\sum_{n=1}^{\infty} \frac{(-k_o \ell)^n}{n!} (1 + n\gamma)^{-1/2} \tag{13a}$$

with

$$\gamma = \left(\frac{\Delta\nu_{D,source}}{\Delta\nu_{D,cell}}\right)^2 \tag{13b}$$

The general procedure for determining a lifetime from line-absorption measurements[1] is to use a theoretically plausible k_ν [such as (5)] and a form for E_ν containing one or more adjustable parameters. The absorption is measured at a number of different concentrations N, and the area under the absorption coefficient is calculated for each point using (12) with fixed values for the parameters in E_ν. The results for $\int k_\nu d\nu$ should yield a straight line when plotted against N. If they do not, the parameters in E_ν are adjusted until they do. The A value is then calculated from the slope of the line.

Frequently the absorption and emission lines consist of several separate but unresolved components. (hyperfine structure, for example) In that case (12) becomes

1. Absorption measurements employing sharp-line sources will hereafter be called line-absorption measurements.

$$\overline{Ab} = \frac{\sum_i \int E_{\nu i}(1-e^{-k_{\nu i}\ell})\, d\nu_i}{\sum_i E_{\nu i}\, d\nu_i} \tag{14}$$

This expression is still practicable as long as one has experimental or theoretical knowledge of the various $E_{\nu i}$ and $k_{\nu i}$. If the components overlap badly, the only valid procedure is to use (12) and do all the integrations numerically.

An alternate procedure for obtaining $\int k_\nu d\nu$ involves using a continuous source and scanning the absorption line with a monochromator. Although the line profile will in general be broadened instrumentally, the area,

$$\int (1 - e^{-k_\nu \ell})\, d\nu = EW \tag{15}$$

will remain the same, the only requirement being that the monochromator adequately isolate the absorption line from other absorption features. This technique is called the equivalent width method (EW), as the integral in (15) is the width of an equivalent rectangular line that is 100% absorbed. The key to success with this method is the use of the complete expression for k_ν, including all broadening phenomena, as measurements often fall in the region of optical depth where the simpler forms (2) and (5) cannot be applied. In many situations a moderate pressure of foreign gas can be used to broaden the lines and insure the suitability of the Lorentzian form (2). When the Doppler absorption coefficient (5) is appropriate, EW becomes

$$EW = -1.065\, \Delta\nu_D \sum_{n=1}^{\infty} \frac{(-k_o \ell)^n}{n!\sqrt{n}} \tag{16}$$

as is shown in Appendix I.

C. Iodine Lamp Output

Spectral features of atomic and molecular iodine were observed in various types of discharge sources at least seventy years ago.[1] Wood

1. Wood and Kimura (1917) mention a study by Konen in Annalen der Physik, 65, (?) 257, 1898. The author was unable to see the latter work.

and Kimura (1917) pioneered the study of the visible molecular bands and observed the Zeeman effect in several atomic lines, using a source with external electrodes. Tolansky (1935) and Schmidt (1939) used hollow cathode sources to study hyperfine structure in several visible atomic lines. More recently Harteck and co-workers (1964) reported the development of a powerful iodine lamp, useful as a photochemical source at 2062 A. The present work utilized low-power electrodeless discharge lamps operated by a 2450-megacycle microwave power supply. The nature of the experiments called for a fairly detailed characterization of the lamps in both the ultraviolet and visible spectral regions.

1. Ultraviolet Radiation

The ultraviolet output of the iodine electrodeless discharge was investigated photographically and photoelectrically. The equipment used has been described in Section II. Although the strengths of the observed lines varied radically with changes in the discharge conditions, the same lines could be detected at all times. No molecular bands were seen in the region 1600-2200 A; however, some members of Verma's (1960) molecular resonance fluorescence series were barely discernable in several films exposed with the discharge operating at an iodine pressure of ~30 mtorr.

The atomic transitions can be described in terms of the energy level diagram, Fig. 8.[1] All lines shown were seen. In addition two lines at 1657 and 1930 A were detected but could not be readily assigned to either iodine or argon.

---

1. The energy levels were taken from the tables of Moore (1962). A more complete diagram is given by Harteck, et al. (1964).

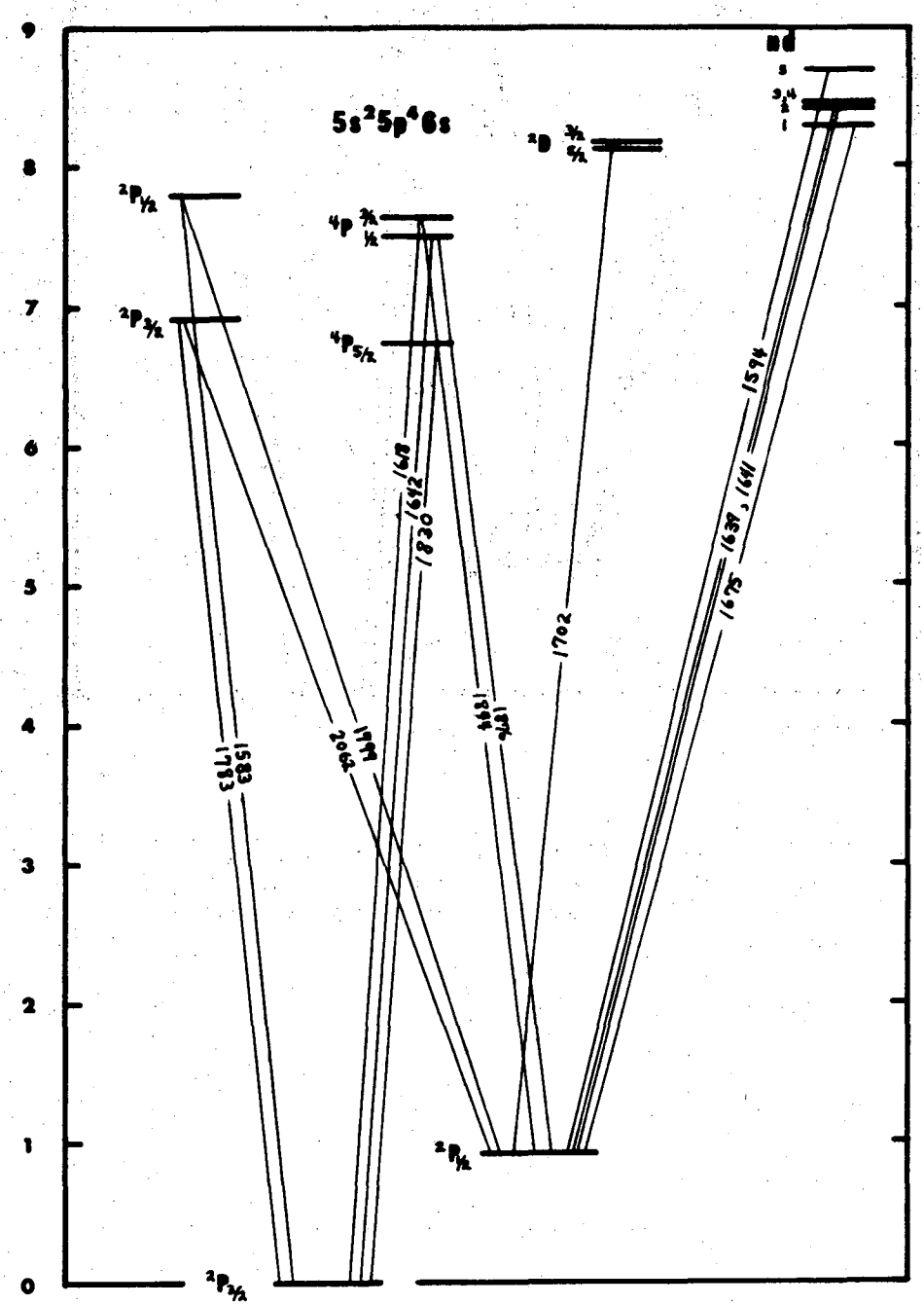

XBL 6910-5834

Fig. 8. Energy level diagram for atomic iodine. Energies are given in electron volts; wavelengths for the transitions are given in angstroms.

Although the intensities of the lines at wavelengths shorter than 1783 A seemed to be relatively insensitive to variations in the lamp's iodine pressure, the six lines at longer wavelengths -- λλ 1783, 1799, 1830 1844, 1876, 2062-- varied substantially in strength as the cold-finger temperature was decreased from 20 C to -196 C. The relative as well as the absolute intensities changed, as can be seen in Table 1.[1] This behavior is a familiar manifestation of radiation entrapment phenomena, which results in a redistribution of the energy out of the resonance lines and into the excited-excited state transitions. In addition the strong molecular absorption of the 1783-1876 lines undoubtedly plays an important role . (See III-D.) Note that the $\Phi_{q1783}:\Phi_{q2062}$ ratio goes from .1 to 10 in the extreme cases. The latter value was measured in a very low-concentration source of short length, where the observed strengths should approach the theoretical values. From the tables given by Condon and Shortly (1951, p. 241) for LS coupling, the relative line strengths for $^2P_{3/2} \leftrightarrow {}^2P_{3/2}$ and $^2P_{3/2} \leftrightarrow {}^2P_{1/2}$ are 5 and 1, respectively. Including the ν^3 dependence gives a ratio 7.7/1 in good agreement with the observed value.

The stability of the lamps was difficult to control, which is understandable when one realizes that at the low cold-finger temperatures (~80°) a change of one degree represents a 15-20% change in the I_2 pressure. Drifts of 10-15% in a minute were commonly encountered but could be minimized by applying considerable effort toward maintaining a constant cold bath and a fixed geometry of lamp, dewar, and microwave antenna.

---

1. Here intensities are given relative to that at 1830 A, as determined by scanning the spectrum using the sodium salicylate detection setup. Values in parentheses are for the lamp on the predissociation cell. The actual intensities may differ slightly from these reported numbers because of small wavelength dependences in the grating function and the transmission of the quartz windows. The sodium salicylate screen is, however, reported to be a linear quantum detector, as was noted in Section II.

TABLE 1. Relative quantum intensities of ultraviolet iodine lines.

Wavelength (A)	Cold-Finger Temperature			
	20 C	0 C	-80 C	-196 C
1782.8	2.0	.40	.35 (.60)	.25 (.80)
1799.1	.8	.15	.06 (.10)	.05 (.10)
1830.4	1.0	1.00	1.00	1.00
1844.5	1.4	.20	.06	.04
1876.4	1.4	.15	.01	.01
2062.3	20.0	2.20	.04 (.35)	.25 (.08)

The temperature of one discharge tube was measured in a rough way by attaching an iron-constantan thermocouple to the source with asbestos tape. The temperature varied from about 90° at low power and low iodine pressure to around 150 C with high microwave power and an iodine pressure of ~200 mtorr. As long as the thermal gradients in the source are not very steep (which should be the case for these low-pressure lamps), the jacket temperature will be descriptive of the plasma temperature. Then the Doppler profile of the lines is fixed by (B-6), and with T = 400 K, $\Delta\nu_D$ = .07 cm^{-1}. Of course the electron temperature in such a source is probably one to two orders of magnitude greater than the gas temperature, so that excited state populations are likely determined by degeneracies (Herzberg, 1944, p. 159) and electron impact cross sections, a subject which will not be dealt with here.

Natural iodine is 100% I^{127}. Since the iodine-127 atom has a nuclear spin of 5/2, all of the lines in the diagram, Fig. 8, must display hyperfine structure. From the general rules for adding angular momenta, we can see immediately that the $^2P_{1/2}$ levels have two hyperfine levels; the $^2P_{3/2}$, four; and the $^4P_{5/2}$, six. This means, for example, that the prominent lines at λλ 1783, 1830, and 2062 must have ten, twelve, and six hyperfine components, respectively. Although the hyperfine splitting has not been studied in these lines, it has been worked out for several lines in the visible, some of which connect with the $6s\,^4P_{5/2}$ level, the upper level in the 1830 A transition. With Schmidt's (1939) results for $^4P_{5/2}$ and the values of Jaccarino and co-workers (1954) for the zero-field splitting in the ground state, it was easy to produce the hyperfine structure diagram, Fig. 9.[1]

---

1. The intensities are drawn as they would be for simple coupling of the angular momenta ($\vec{F} = \vec{J} + \vec{I}$) with no perturbations, and with emitting populations proportional to degeneracies. In that case the intensities are proportional to the line strengths given by Condon and Shortly. See Section III-D for further discussion.

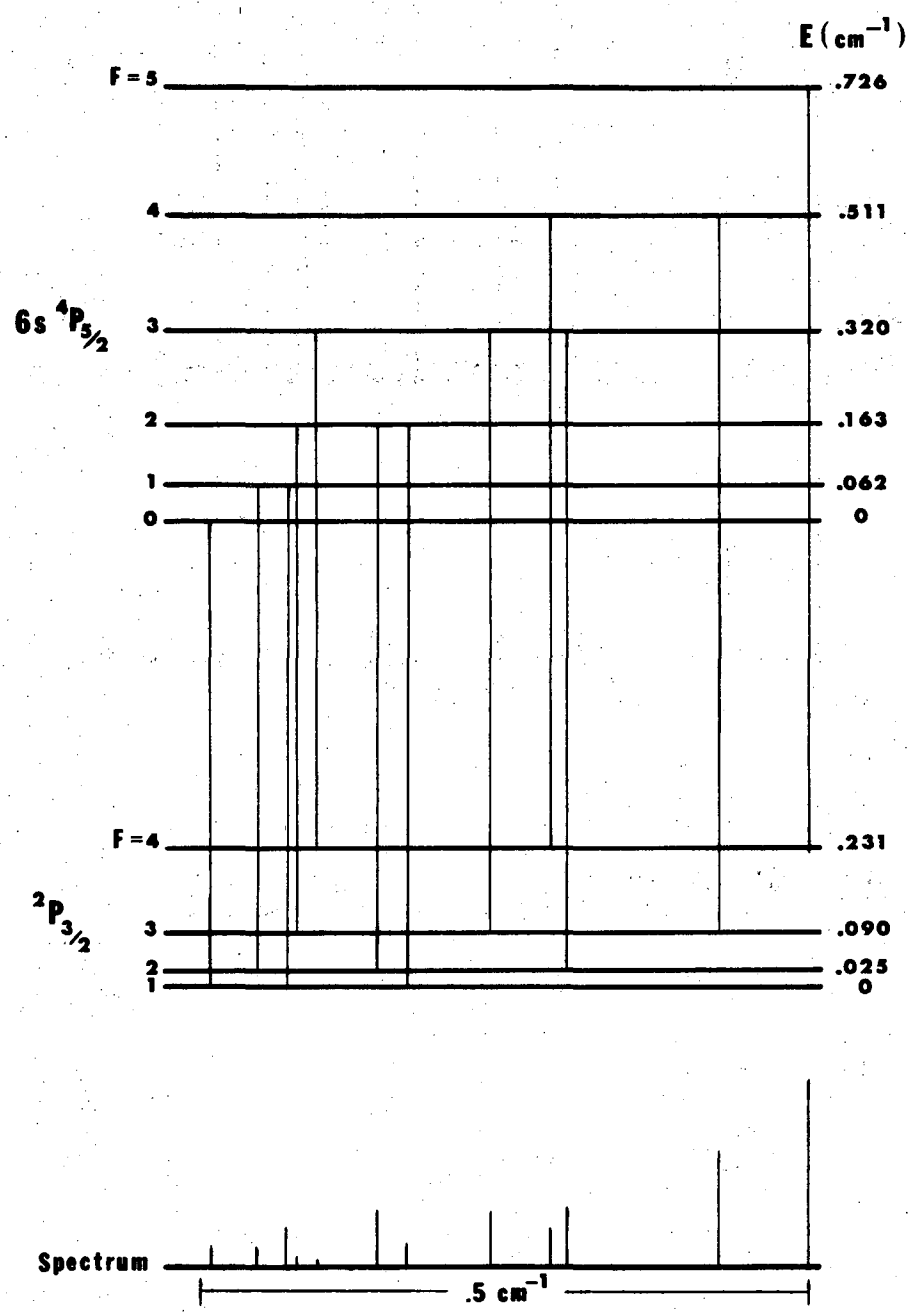

XBL 6910-5833

Fig. 9. Hyperfine structure diagram for the 1830.4 A resonance line of atomic iodine.

The splitting of the $6s^2P_{3/2}$ level has not been worked out, so it is not possible to calculate accurately the structure in the 1783-A resonance line.

2. Visible Radiation

Since the B state of I_2 absorbs strongly in the region 4800-6000 A, it is necessary to have some knowledge of the iodine lamp's visible output. A cursory investigation was made of the emission from 4250 A to 6400 A under various conditions of the discharge. For this purpose the Spex instrument was used both as a spectrograph and as a monochromator.

At iodine pressures below ~10 mtorr the spectrum consisted almost entirely of I and Ar atomic lines. The former increased in strength gradually as the iodine pressure was raised, until at a pressure of ~200 mtorr several lines around 5000 A became very strong, and the discharge assumed a bluish hue. The molecule $B \rightarrow X$ emission seemed strong around $P(I_2)$ = 10-50 mtorr, but weakened again (relatively) as the pressure and temperature were raised. This relative weakening is consistent with the known large cross section for collisional self-quenching in $I_2(B^3\Pi_{0^+u})$ (Chutjian, et al., 1967).

Nearly all the lines recorded on Polaroid film were readily assigned to Ar or I, indicating the sources were essentially free of atomic impurities. However some very weak molecular features persisted in the discharge even at lowest iodine concentrations. The majority of these occurred in the green, and were eventually assigned to C_2.

The possibility of strong absorption of the visible atomic lines by I_2 was checked by recording Polaroid spectra of the source on the cell in Fig. 2 through various concentrations of I_2 in the cell. None of the lines exhibited noticeable attenuation, although some must certainly show at least small absorption by the dense $B \leftarrow X$ molecular system.

At very low cold-finger temperatures the visible output of the lamp was quite weak, and it changed much more slowly with temperature than the UV output. For example, a monochromator scan of the 5000-A region showed about 50% increase in intensity as the cold-finger temperature was raised from -196 to -80 C; similar scans in the ultraviolet showed a three- or four-fold increase. (This behavior is expected, since the UV output was almost entirely atomic iodine emission, where the visible output for these conditions was dominated by Ar spectra. The Ar emission should not vary much as the cold-finger temperature is changed from -196 to -80 C.)

D. Ultraviolet Absorption Experiments

The iodine lamp provides a convenient source for ultraviolet line-absorption experiments. The discharge is of the low-pressure type, where line shape is generally determined by Doppler broadening.[1] The nature of the discharge may be varied drastically by simply altering the cold-finger temperature and hence the I_2 pressure in the source, so in principle absorption measurements can be made for different source conditions and extrapolated to an "ideal" limit of zero concentration. Furthermore, line intensities are high enough that measurements can be obtained easily for even the lowest practical iodine concentrations (LN-cooled cold finger). The hyperfine structure in the atomic lines is both an asset and a liability. It effectively broadens the lines to ~.5 cm^{-1}, increasing the likelihood of some coincidence with molecular absorption lines and decreasing the chance of severe self-reversal problems in the source. On the other hand accurate quantitative work would require precise knowledge

---

1. The Doppler half-width was given earlier as .07 cm^{-1} for the atomic resonance lines, assuming a source temperature of 400 K. With a lifetime of 3.6 nsec for the $6s^2P_{3/2}$ state (Lawrence, 1967), (B-3) gives $\Delta\nu_{N,1783} = .0015$ cm^{-1}; $\Delta\nu_{N,1830}$ is much narrower. The collision rate of I atoms with Ar atoms for P(Ar) = 2 torr is ~10^8 per second for a collision cross section of 100 A^2 (about 10 times the gas-kinetic value), so $\Delta\nu_c$ from (B-4) is less than $\Delta\nu_N$.

of the source and absorption lines and the use of numerical integration to obtain A values from the measured absorption.

With these points in mind it was felt that UV absorption measurements for both molecular and atomic iodine would prove instructive and worthwhile. Also, as a matter of interest for the predissociation experiments (Section IV) the absorption by air was determined.

1. Measurements for I_2

It has been known for a number of years that I_2 has a strong absorption band system in the region 1700-2000 A, but the analysis of this system or systems has not yet been worked out conclusively (Nobs and Wieland, 1966; Wieland, private communications). Oldenberg (1923) noted that several iodine atomic lines excite I_2 fluorescence lines, and Kinura and Tonomura (1935) published several short fluorescence series with excitation attributed to the 1783, 1799, 1830, 1844, and 1876 atomic lines. Verma (1960) studied the resonance fluorescence series produced by the 1830 line in a microwave discharge; according to his analysis all observed features were ascribed to 1830 excitation. It appears that no one has studied the line absorption quantitatively, although several disparate values for the molar extinction coefficient have been reported. The present study indicates that all five atomic lines, 1783 through 1876 A, are absorbed to a comparable degree by I_2, so Verma's results imply that his discharge was dominated by the 1830 line. From the absorption data at 1830 A and Verma's assignment of the rotational levels excited, we can calculate a rough lifetime for the excited state.

Measurements were obtained using the absorption cell (Fig. 3) and the Jarrell-Ash monochromator described earlier; the latter was fitted with the sodium salicylate fluorescent screen and 1P21 photomultiplier.

Slits were opened to .4 mm. Signals were recorded on the Varian chart recorder. The procedure for collecting the data was as follows.

First the I_2 in the absorption cell was frozen out in the cold finger using LN, until the grating angle could be optimized and a fairly constant lamp output was observed. Then the cell's cold finger was immersed in a thermal bath contained in a dewar, and the bath was stirred until the signal leveled off at the new reading,[1] at which time the bath temperature was recorded and the cold finger was re-cooled with LN. The procedure was repeated for 10-15 different bath temperatures between -30 and +20 C; ethanol and water were used as baths and were cooled as necessary with dry ice and LN. As long as the lamp remained stable, points could be recorded at the rate of one every four or five minutes.

Data were obtained for all six I lines, 1783-2062 A, with the source cold finger cooled in ice water and the microwave power 20-25% of capacity. In addition a complete run was made at 1830 A with the lamp cold finger at ~-50 C in an ethylene glycol-water bath. For the latter "cool" source a few points were checked at the other wavelengths and found to agree with those recorded with the "hot" lamp.

I_2 vapor pressures were calculated from the free-energy functions given by Shirley and Giaugue (1959) for solid I_2 and the JANAF Tables (1961) for I_2 vapor. The required free-energy function interpolations were done with a computer routine using a four-point Newton interpolation formula. A table of vapor pressures between -80 C and 30 C at .1 degree intervals was prepared for convenient reference in this and other experiments.

Figure 10 is exemplary of the data recorded for all lines. It is a logarithmic plot of the 1830 A transmittance for the two source conditions used. The curvature is typical of line-absorption; a straight line would

---

1. Approaching the vapor pressure equilibrium from above and below gave equivalent results.

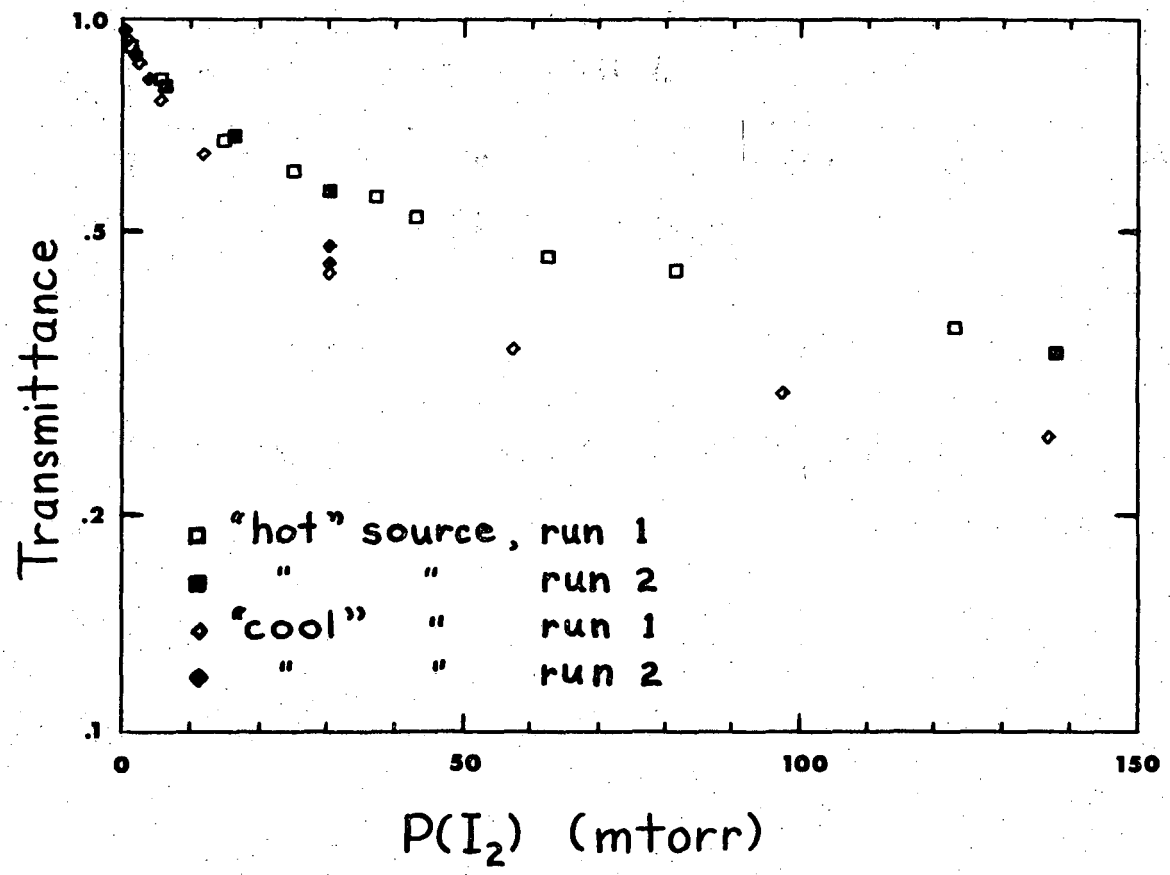

XBL 6910-5832

Fig. 10. I_2 absorption of 1830-A atomic line.

result if the absorption were by a continuum or a semi-continuum of overlapped rotational lines.[1]

It seems strange that only the 1830 absorption exhibited separate curves for the two source conditions. If atomic self-reversal occurs, it should affect the 1783 line more than the 1830 line.[2] Of course the actual absorption must be very complicated, involving, at each wavelength, several I_2 rotational lines overlapping to various degrees one or more partially concurrent hyperfine components of each atomic line. In the "hot" source the I_2 pressure was about 30 mtorr, so the atomic source lines should be distorted by molecular self-reversal. One would expect under these circumstances that the absorption curves at <u>all</u> wavelengths might display even greater dependence on source conditions than that shown at 1830 A.

The approximately equal absorption of the five lines from 1783 to 1876 A is surprising, but not unbelievable when we realize that the I_2 spectrum is particularly dense in this region. Since the hyperfine structure spreads the source lines to an effective width of ~.5 cm^{-1}, it would be unreasonable <u>not</u> to find I_2 absorption of all atomic lines.

The absorption data for the several source lines could be made to give approximate straight line dependences of $\int k_\nu d\nu$ on concentration, by using (B-13) and adjusting T_{source}, which, with T_{cell} = 300 K, determines the relative line-width parameter γ. However, the resulting values for

---

1. For continuum absorption of a Gaussian line, γ in (B-13) becomes 0, and we can apply Beer's Law in the simple form usually encountered in quantitative analysis textbooks.

2. The 1783 transition has an oscillator strength ~15 times that of the 1830 line. See Part 3.

T_{source} varied from 300 to 700 K (corresponding to different degrees of curvature in the log plots). In view of the complicated nature of the absorption it is doubtful that these numbers have any real significance.

For all results except those at 1830 A, a simple presentation of the transmittances is probably as useful as any quantity computed from the line-absorption. Relative to the "hot" source 1830 absorption, the transmittances for $P(I_2)$ = 30 mtorr at 1783, 1799, 1844, and 1876 were 1.02, 0.95, 0.88, and 1.07, in order. The 2062 line displayed only 10% attenuation at I_2 pressures greater than 200 mtorr.

We can use the results at 1830 A along with Verma's analysis of the excitation process to calculate an approximate value for the lifetime of the upper state. From Eqs. (B-6, 13) we have

$$\gamma = \frac{T_s}{T_c} \times \frac{M_c}{M_s} \qquad (1)$$

where T_s and T_c are the source and cell temperatures, and M_s and M_c are the molecular weights of the emitting and absorbing gases. For our case, taking T_s to be 400 K and T_c = 300 K, $\gamma = 2.67$. We use (B-13) to calculate the optical depth $k_o \ell$ for each measured point. The integrated absorption coefficient $\int k_\nu d\nu$ is given by (B-11) for this case, and we need the value of ℓ = 101 mm to calculate $\int k_\nu d\nu$ for each point. From (B-10) we see that the slope of a plot of $\int k_\nu d\nu$ versus N contains the desired A value. Taking $g_A = g_B$ for the large J values of the rotational lines involved, we obtain from the "cool" source data measured at I_2 pressures lower than ~15 mtorr.

$$A_{app} = 3.0 \times 10^4/\text{sec} \qquad (2)$$

where A_{app} indicates the apparent A value, calculated assuming all the I_2 molecules participate in the absorption. (i.e. N was taken as the total I_2 concentration.)

To convert A_{app} to an actual A value we need to know the fraction of iodine molecules capable of absorbing the 1830 radiation. Verma assigned the absorption to J" = 23, 24, 47, 48, and 86 from v" = 0 to three upper vibrational levels v' = n, n+1, n+4. The fraction fr of the total I_2 population in the five given rotational levels is

$$fr = \frac{\Sigma N_{Ji}}{N} = \frac{1}{q_r} \times \frac{1}{q_v} \sum_{i=1}^{5} (2J_i+1)\, e^{-\epsilon_{Ji}/kT} \qquad (3)$$

with[1]

$$q_r = \frac{kT}{hcB} = \frac{T}{\theta r} \qquad (4)$$

$$q_v = \frac{1}{1-e^{-hc\nu/kT}} = \frac{1}{1 - e^{-\theta_\nu/T}} \qquad (5)$$

q_r is the rotational partition function (without symmetry number), and q_v is the vibrational partition function with zero-point energy removed. B is the rotational constant and ν is the vibrational frequency (taken from the energy difference for the lowest vibrational levels, G" (1) - G"(0)). θ_r and θ_v are called characteristic temperatures for rotation and vibration. Hill (1960, p. 153) has tabulated values of these parameters for a few diatomic molecules including I_2, from which we obtain $q_r = 5.55 \times 10^3$, $q_v = 1.55$. Equation (3) then yields fr = 0.030, or 3.0% of the total I_2 molecules participate in the absorption. The corrected A value is

$$A = A_{app}/fr = 1.0 \times 10^6/\text{sec} \qquad (6)$$

Now we can manipulate Eqs. (A-11a,13b) to calculate a value for $|Re|^2$ and then compute a value for τ using (A-16). Of course we don't know the Franck-Condon factors, since the upper state hasn't been analyzed; but we can make some reasonable guesses. From completeness relationships for

1. Actually, since I_2 is homonuclear with atomic spin 5/2, the even and odd rotational levels have different nuclear spin degeneracies. As a result, for the ground state of I_2, NJ must be multiplied by 5/6 for even levels and 7/6 for odd. The overall correction here was a negligible 3%.

orthonormal sets of functions we have the sum rules

$$\sum_{v''} |\langle v'|v''\rangle|^2 = \sum_{v'} |\langle v'|v''\rangle|^2 = 1 \qquad (7)$$

so the sum of all F-C factors for transitions out of v" = 0 is unity. In the I_2 visible (B-X) system, maximum F-C factor $|\langle v'|0\rangle|^2$ occurs for v' = 30 and is only .0314[1], because the absorption out of v" = 0 is spread out broadly over v' levels ~15-50. In the ultraviolet system the absorption appears to be distributed at least as much, perhaps more,[2] with the maximum falling near 1850 A. Consequently a good guess for the average F-C factor involved in the absorption might be .025. There appears to be no Q-branch in this system, so s_J/g_A is roughly 1/2 for all absorption lines, giving a value for $|Re|^2$ of ~1.6 (debye)^2. The fluorescence out of the upper states was observed by Verma right out to the dissociation limit of the ground state, with a few transitions missing or very weak because of low F-C factors. Therefore a reasonable estimate for the average value of ν^3 in (A-16) might be (48000 cm^{-1})^3. This number yields

$$A_T = 5.4 \times 10^7/\text{sec} \qquad (8)$$

$$\tau = 1.8 \times 10^{-8} \text{ sec}$$

The above results may easily be off by a factor of 3 or 4 because of the crude approximations that were made. However these were taken in such a way that the 18-nsec value should serve as an upper limit to the true radiative lifetime. The estimates for the absorption F-C factor and ν^3 should be within 50% and 10%, respectively of the true values. The most error-prone part of the calculation was probably the determination of the apparent A value, where the absorption was treated in terms of a single

---

1. This value was calculated by P. Cunningham using Zare's (1963) program.

2. The absorption is more broadly distributed with respect to v' if the upper state potential curve is steeper in the vicinity of vertical transitions (r=2.67 A). In both the B state and the UV state, transitions are to the "left hand" branch of the potential curve.

Doppler-profile source line, and overlapping rotational absorption lines of the same frequency. Actually the different rotational lines may be excited by different hyperfine components of the source line; some or all may fall at frequencies as much as $\Delta\nu_D/2$ off the center of the source line (or lines). Any detailed consideration of these possibilities must give an upward correction to the A value; as a result τ is more likely 10±5 nsec.

The corrected value of 3 (Debye)^2 for $|Re|^2$ may be compared with the value ~1.0 measured by Chutjian and James (1969) for the B-X transition. Evidently, because of the ν^3 dependence the lifetime of the UV state is more than an order of magnitude smaller than that for the B state.

A comparison of these results with those calculated from broad-band absorption measurements is rather disappointing: the latter give lifetimes an order of magnitude lower than the 10-nsec value. Unfortunately there appears to be no reliable value for the molar extinction coefficient of I_2 in this system. The maximum occurs about 1850 A and is 1.0×10^4 (liter mole^{-1} cm^{-1}) according to Huebert and Martin (1968), 2.4×10^4 from Julien and Person (1968), or 1.0×10^5 if we accept the results of Bayliss and Sullivan (1954). It is possible to derive the relationship

$$f = 4.32 \times 10^{-9} \int \epsilon_\nu \, d\nu \tag{9a}$$

from Eqs.(A-9) and (B-10) by using the conversion

$$k_\nu = N \left(\frac{2.3\times10^3 \epsilon_\nu}{N_o} \right) \tag{9b}$$

where N is again the particle density, N_o is Avagadro's number, and ϵ_ν is the decadic molar extinction coefficient. The f-values calculated from (9a) and reported in the second and third references above are .43 and 2.29. Assuming an average fluorescence energy of 48000 cm^{-1}, we can calculate from (A-9) approximate lifetimes of 3.5, 1.5 and 0.3 nsec.

The source of the great disagreement among the several works is not clear. In this study the assumed value of .025 for the F-C factor could be drastically wrong if the absorption maximum occurred near or above the dissociation limit[1]; however, 1850 A appears to be well within the banded region of the transition so (7) should hold, as it does in the B-X system.[2] Another possibility is that the absorption consists of two or more overlapping systems; however, the electronic absorption band profile has the appearance expected for a single system. Curve-of-growth problems are often encountered in medium-pressure absorption measurements, but such effects are in the wrong direction to explain the disparities here. Perhaps with the inevitable proliferation of new measurements of ϵ_ν in the near future (as double-beam scanning vacuum spectrophotometers become standard laboratory equipment), and the eventual analysis of the spectrum, the discrepancies can be explained.

2. Absorption by Air

The Schumann-Runge system of O_2 occurs at wavelengths shorter than ~1900 A, delimiting "vacuum ultraviolet" spectroscopy from "air" spectroscopy. Since the 1830 and 1783 I resonance lines fall on or near strong (9,0; 13,0) bandheads of this system, it was of interest to know the absorption coefficient of air for these lines so that vacuum procedures for

---

1. In that case the sum rule (7) must be extended to include continuum transitions, with the continuum wave functions normalized in some convenient manner. See the results of Halmann and Laulicht (1966) and Harris, et al. (1969) for an apparent example of this situation in the Schumann-Runge system of O_2.

2. F-C factors for the B-X system were calculated for v' = 0-47. (See Section IV). The corresponding sum (7) for v" = 0 was ~.75. Including the remaining v' levels up to the dissociation limit would probably raise the sum to >.9, leaving < .1 for the continuum absorption. (The recent results of Steinfeld and co-workers (1969) seem to indicate practically no continuum contribution from v" = 0. This point will be discussed at length in Section IV.)

other experiments could be conducted accordingly. Absorption strength measurements and Franck-Condon factors for this system have been published recently (Halmann and Laulicht, 1966; Harris, et al., 1969). However it was easier to measure the line-absorption directly than to carry out the calculations necessary to use the published data. With some additional computational effort the results obtained here can perhaps be compared with those given by Halmann (1966); but that will not be done at the present time.

The procedure was simple. The predissociation cell (Fig. 2) was employed in the same monochromator setup used in the I_2 absorption work. Upon establishment of a steady lamp output, air was admitted to the cell via an LN trap, included to minimize absorption by organic impurities in the vacuum system (mechanical pump, no diffusion pump). The pressure was read from a mercury manometer and the cell was re-evacuated, establishing the reference level between points.

Logarithmic plots of the transmittance versus pressure gave reasonably straight lines. This may be understood qualitatively in terms of the low γ value, which from Eq. (D-1) is .34 for the light O_2 molecule. Observations at greater optical depths would probably reveal curvature of the type shown by the I_2 data. The absorption coefficients for air, from the linear semi-log plots were .021, .0096, .0086, and .0036 $torr^{-1}$ $meter^{-1}$ for the 1783, 1799, 1830, and 1844 lines, in order. Values at 1876 and 2062 A were much lower -- .0009 and .0005, respectively.

The absorption by air was weak enough to justify use of "low-vacuum" techniques in the predissociation and atom recombination experiments, to be discussed in Section IV and V. However, before inclusion of the LN trap, incidental concentrations of organic vapors (and possibly I_2) were seen to absorb strongly (especially at 1783 A), indicating the importance of maintaining "clean", preferably short gaps between cells and photomultipliers.

3. Atomic Absorption

Lawrence (1967) has reported the results of phase-shift determinations for the lifetimes of the $6s^2P_{3/2}$ and $6s^4P_{5/2}$ states of atomic iodine. He measured 3.6 nsec (± 15%) for $^2P_{3/2}$ and 90±30 nsec for $4P_{5/2}$. (The uncertainty in the latter value was high because of cascading complications). He also calculated relative line strengths for the intermediate coupling case (Condon and Shortley, Chpt. 11) and used the above lifetime values to scale his relative strengths to absolute values. His calulated A values yield resultant lifetimes of 3.66 nsec and 63 nsec. Furthermore, they indicate that the 1783 line is ~100 times stronger than the 2062 line, which is an order of magnitude in disagreement with the relative intensities in the iodine lamp reported in III-C. Absorption measurements on the resonance lines should provide independent A values for comparison with Lawrence's results.

Two methods were used to measure atomic absorption. The first involved dissociating I_2 thermally; the second used photolytic production of atoms in a steady-state situation. In the first case atomic concentrations were known accurately from thermodynamic data. The second method yielded only relative absorption strengths for the two resonance lines.

a. Thermal Dissociation Method

For the method of thermal production of atoms, the experimental setup and procedures were essentially the same as those used in the I_2 work. The one important difference was the inclusion of a heating element necessary to achieve temperatures high enough to give workable concentrations of I atoms. Since I_2 absorbs strongly at pressures greater than 1 mtorr, it was necessary to work at very low I_2 concentrations and correspondingly high cell temperatures of 300-450 C. At these tempera-

tures small thermal gradients in the cell can give large uncertainties in the dissociation constant, so good insulation was essential. Best result were achieved with a two piece aluminum tube about 6 mm thick, which could be clamped together snugly around the absorption cell. Three chromel-alumel thermocouples, insulated by asbestos, were implanted in the aluminum tube in such a way that the junctions lay in contact with the cell at points near both ends and the middle. Then the tube was wrapped with electrical heating tape and asbestos cloth. With this design temperatures at three points agreed with 4-10 degrees at the highest cell temperatures employed.[1]

Measurements on both resonance lines were conducted using a "cool" source with cold finger immersed in a slush of ethylene glycol and water at ~-50 C. Cell temperatures were read to the nearest degree.[1] An ethanol bath was used to cool the cell's cold finger to temperatures of -30 to -80C, which were read to the nearest .1 degree with an iron-constantan thermocouple.[2] The resulting low I_2 pressures were required for two reasons: to minimize absorption by I_2, mentioned above; and to insure that the I_2 pressure in the heated cell was related to that in the cold finger by the transpiration equation[3]

---

1. The middle thermocouple always gave the highest reading; the junction nearest the monochromator gave the lowest. This was as expected, because the ends of the tube were difficult to insulate, so greatest heat losses occurred there. Losses at the source end were offset somewhat by heating by the microwaves. An average of the three temperatures was recorded and used in calculating the dissociation constant.

2. The chromel-alumel thermocouples were calibrated in boiling water and found to conform to the standard tables within the accuracy of the particular potentiometer used (±.5 degree). Likewise the iron-constantan thermocouple agreed with the tables, but the potentiometer used in the cold bath measurements was much more sensitive, with a precision of better than .1 degree.

3. In general for (10) to hold, the mean free path in the gas must be large relative to the cell dimensions. Otherwise viscous flow occurs and the pressures are equal throughout the cell. At P=1 mtorr, T=300 K. I_2 has a mean free path of ~40 mm, substantially greater than the stem diameter for the cell.

$$\frac{P_1}{P_2} = \sqrt{\frac{T_1}{T_2}} \qquad (10)$$

Measurements were recorded as in the I_2 work. The 100% transmittance level was established between points by freezing the I_2 out with LN; the baseline was zeroed by closing the exit slit.

Iodine atom concentrations were calculated from the I_2 vapor pressure tables prepared earlier, the relationship (10), and the dissociation constant K_p. Required values for the latter were calculated from the free-energy functions tabulated in the JANAF Tables using the same interpolation routine utilized in the I_2 vapor pressure computations. The iodine atom concentration N_I is

$$N_I = \frac{\left(K_p \quad P_{I_2}\right)^{1/2}}{kT} \qquad (11)$$

It was hoped that the data would be good enough to allow the use of Eq. (8) in App. I, with two variable parameters for the source line shape, in calculating the optical depths $k_o \ell$ from the measured absorptions. However, early calcuations using the one-parameter expression (B-13) indicated something was wrong with the experiment: As the cell temperature was raised, the measured absorption did not keep pace with the increasing atom concentration. Worse still, identical concentrations at cell temperatures 100° apart differed in absorption by factors of two or more. Such behavior is difficult to account for in terms of the absorption line shape but was finally attributed to problems in the source. The latter was not sufficiently isolated thermally from the hot absorption cell (Fig. 3), as the junction was located inside the heated aluminum tube several cm from the end. Although the discharge appeared to operate properly within the Al tube, heating undoubtedly produced a higher concentration of atoms near the junction. Under these conditions the source line shape should still follow approximately the form (B-8), but the parameters T_s and k_o' change with T_c in a complicated manner. The effect is to produce a broader and flatter source line at the higher cell

temperatures, resulting in an apparent decrease in the absorption.[1] Figures 11 and 12 illustrate this behavior. Here all points were calculated assuming a Doppler-profile source line of T_s = 400 K. Curiously the 1830 results at different T_c values seem to fall on roughly parallel straight lines, while the 1783 results show some curvature at all but the lowest temperature. There is also some evidence that the lamp behavior at 1783 A changed in a gross manner from Run 1 to Run 2. The only ready explanation for the parallel lines at 1830 A is the possibility that absorption by I_2 or some impurity sets in strongly at the higher temperatures.[2]

The points recorded at the lower cell temperatures should not suffer from the above problems, because the I_2 concentrations in the source were too low to allow for appreciable atomic concentrations from thermal dissociation.[3] However, at lower cell temperatures higher I_2 concentrations were needed to get measureable absorption. Without a wide range of absorption values, the source parameter adjustment method (SPAM) cannot be utilized, so the low-T_c points in Figs. 11 and 12 were used directly (in the naive assumption of a Doppler source line having T_s = 400 K) to calculate approximate A values. The straight lines illustrated are the results of linear fits

---

1. If in addition a "dead" layer of unexcited atoms exists near the cell junction, the source lines may be self-reversed and the absorption may decrease quite dramatically.

2. The impurity hypothesis was tentatively ruled out when the same behavior resulted after the cell was baked out and charged with I_2 a second time, and in a slightly different way. From the I_2 absorption results, the molecular absorption here should have been no more than 1-2%, unless the higher temperatures led to an increased population or a more favorable overlap for an otherwise weak rotational line absorption.

3. On the other hand the electron attachment dissociation

$$I_2 + e^- \rightarrow I^- + I$$

is known to be quite efficient (Dose, 1968; Truby, 1968). This process may account for most of the atomic concentration at low I_2 pressures.

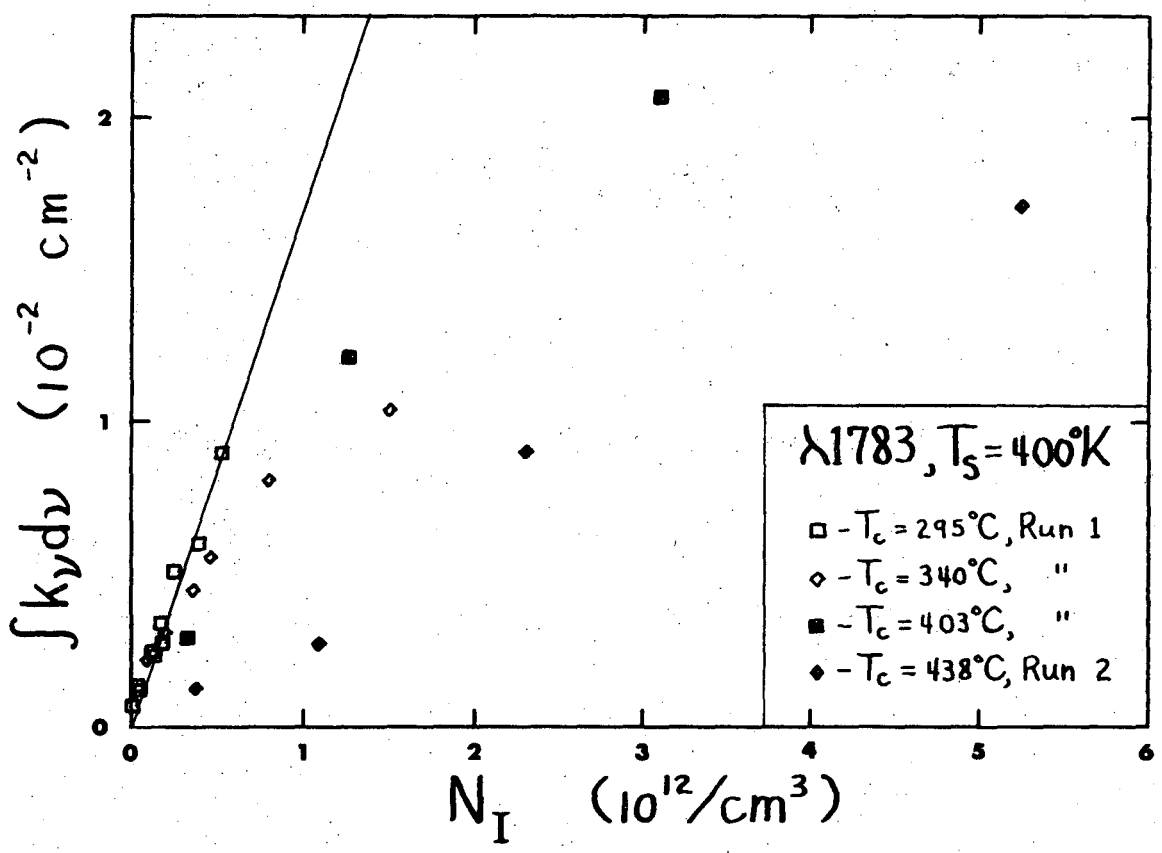

XBL 6910-5843

Fig. 11. Iodine atomic absorption of 1783-A resonance line.

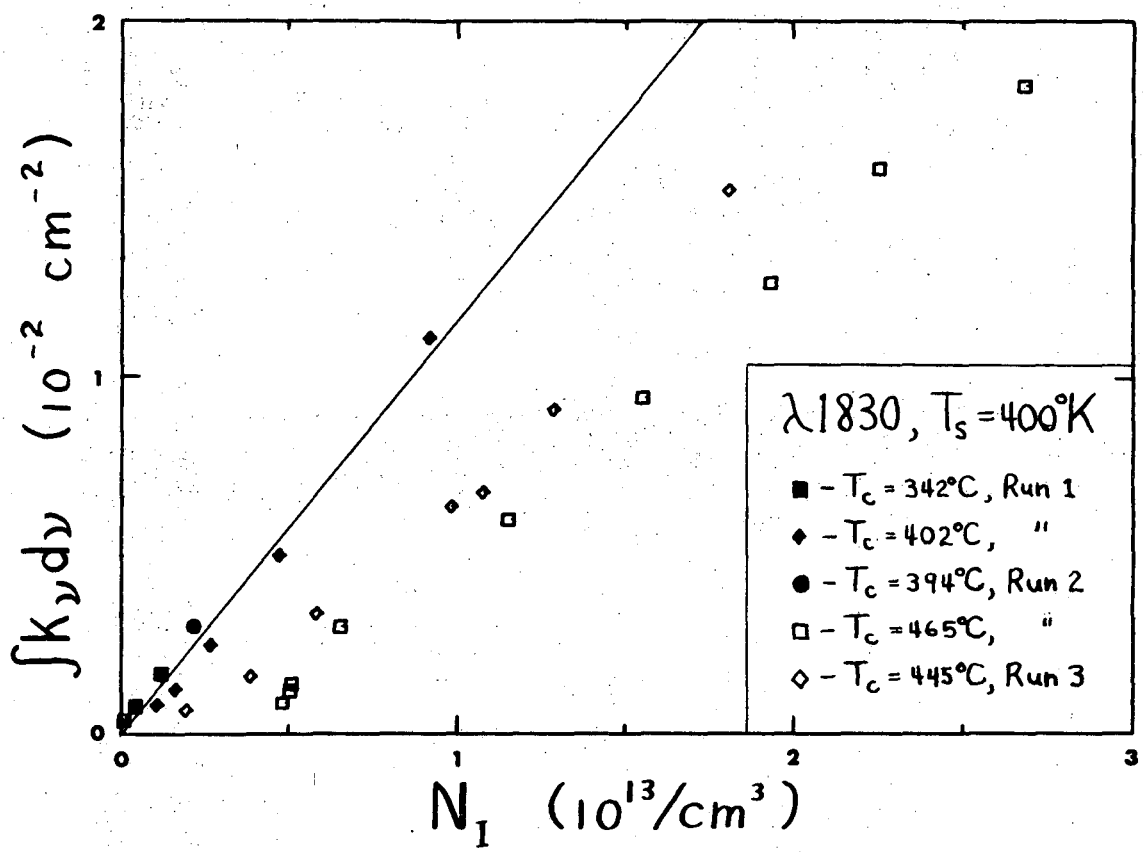

XBL 6910-5842

Fig. 12. Iodine atomic absorption of 1830-A resonance line.

$\int k_\nu d\nu$ = const. $\times N_I$. From the slopes of these lines one calculates $A_{1830} = 1.74\times10^6$/sec and $A_{1783} = 4.01\times10^7$/sec.[1] In obtaining these values, we have neglected one very important aspect of the absorption -- the existence of hyperfine structure. A hyperfine correction factor will be derived below. Anticipating the form of the correction we may write

$$A_{1783} = 4.01 \times 10^7/\text{sec} \times C_{Hf,1783} \tag{12a}$$

$$A_{1830} = 1.74 \times 10^6/\text{sec} \times C_{Hf,1830} \tag{12b}$$

b. Line Strength Comparison - Photodissociation Method

It was easy to observe atomic absorption of both resonance lines in the predissociation cell (Fig. 2), using the "sun-gun" to photolyze the I_2 in the cell. Where such absorption was barely detectable in the absorption cell, it was substantial in the predissociation cell, with its "poisoned" walls, even at I_2 pressures as low as 1 mtorr. The calculation of atomic concentrations in this steady-state photodissociation is rather complicated, but relative absorption strengths for the two lines can be measured quite readily.

The procedure used here involved recording the absorption of both lines under identical conditions of pressure and irradiance, for several different I_2 pressures and different sun-gun powers. Steady-state euqilibrium obtained in the cell almost as rapidly as the sun-gun could be turned on with the Variac, so problems arising from heating by this visible source were minimal. The iodine lamp was cooled in the -50° bath used previously.

The optical depth $k_o\ell$ for each measured point was again calculated on the assumption of a Doppler source line at T_s = 400 K. If, as expected, the absorption by I_2 interferes with the measurements, an extrapolation of the relative $k_o\ell$ values to $P_{I_2} = 0$ should eliminate the problem. Then we

---

1. Both data sets gave good straight lines with relative standard deviations of ~4%. The fits resulted from nine points at T_c=345 and 400C for λ 1830, ten points at 295 C for λ 1783. Changing the assumed source temperature by 100° altered the results by only 6%.

can see from (B-6, 10 and 11) that

$$\frac{(k_o\ell)_{1830}}{(k_o\ell)_{1783}} = \left(\frac{1830}{1783}\right)^3 \times \frac{6}{4} \times \frac{A_{1830}}{A_{1783}} \times \frac{C_{Hf,1783}}{C_{Hf,1830}} \tag{13}$$

where we have again included the hyperfine correction factor introduced above.

The results are illustrated in Figs. 13a and b. There appears to be no specific dependence on the I_2 pressure, which may be reasonable in view of the nearly equal absorption of both lines by I_2. The two points at greatest $k_o\ell$ seemed in disagreement with the others, probably because the absorption at 1783 A for these points was quite large (~90%), where the deviations from the assumed Doppler source line become important. The experimental value for the ratio on the left-hand side of (13) was taken from the plot of $(k_o\ell)_{1830}$ vs $(k_o\ell)_{1783}$ in Fig. 13b. The least-squares slope obtained from the seven lower points was .0591 ± .0018.

c. Correction for Hyperfine Structure

The existence of hyperfine structure leads to an apparent weakening of the line absorption since it spreads the absorption out over the several components of the line. For example, if there are n equal, separate components and we calculate $k_o\ell$ assuming a single line, our corresponding values for $\int k_\nu d\nu$ and A will be a factor of n too low. In general the correction will not be this simple, because the components may have different strengths and may overlap; but with a few approximations we may derive an expression for the correction which should be good enough for our purposes.

The equation relating the measured absorption to the $\{k_{\nu i}, E_{\nu i}\}$ when two or more separate components are involved in the emission-absorption

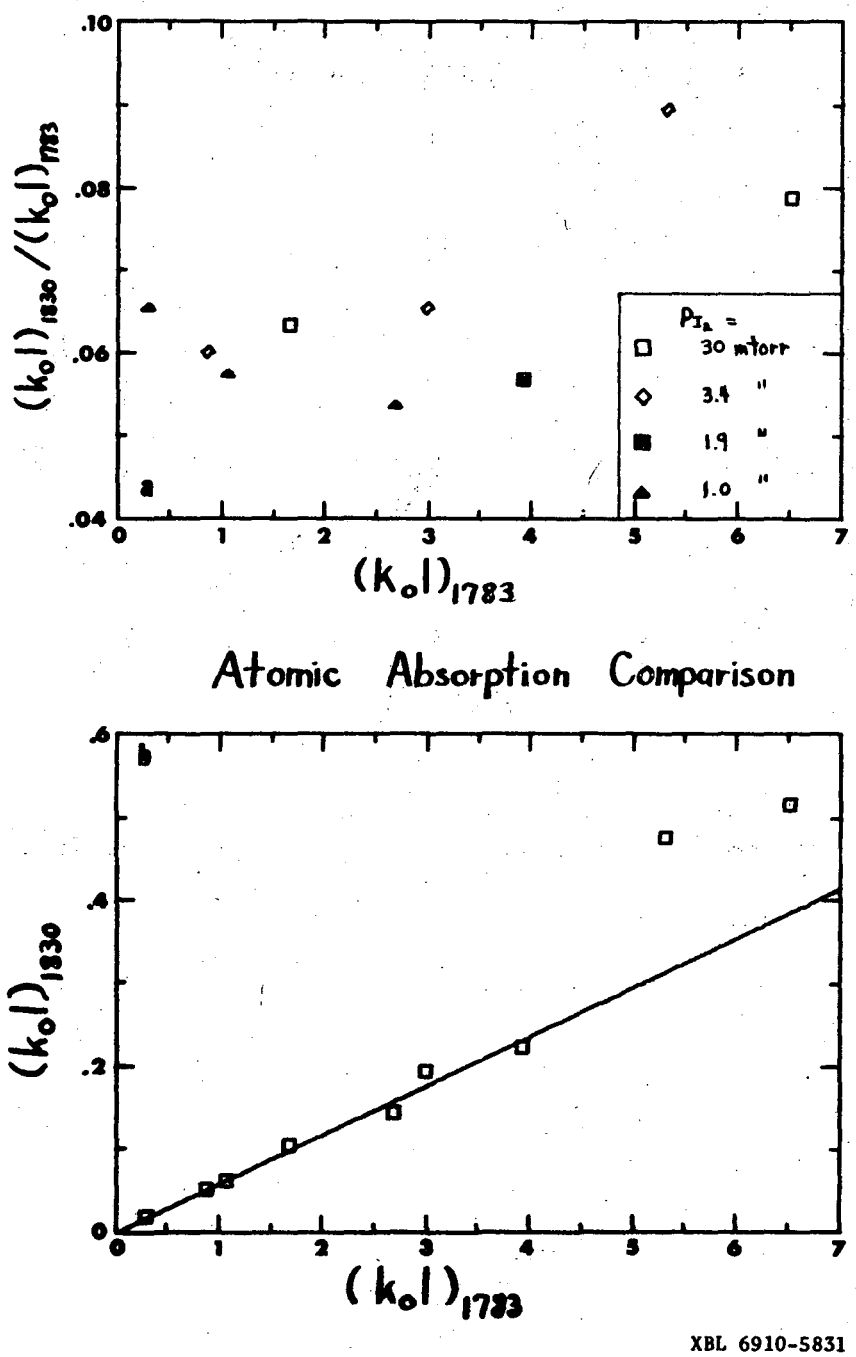

Fig. 13. Results of atomic absorption comparison experiment.

process has already been given:

$$\overline{Ab} = \frac{\Sigma \int E_{\nu i} \left(1 - e^{-k_{\nu i}\ell}\right) d\nu_i}{\Sigma \int E_{\nu i}\, d\nu_i} \qquad \text{(B-14)}$$

The populations of the different hyperfine levels in both upper and lower states should be proportional to their degeneracies, so from (A-11, 12) the intensities of the several components in emission and absorption will be proportional to the line strengths.[1] Therefore, for Doppler source lines

$$E_{\nu i} \propto k_{oi}\, e^{-\alpha'(\nu-\nu_i)^2} \qquad (14)$$

and

$$k_{oi} \propto s_i \qquad (15)$$

If the hyperfine levels are not perturbed severely, the line strengths may be calculated assuming Russell-Saunders type coupling, in which case the s_i values can be taken from the tables given by Condon and Shortley (1951) by making the following identities: $I \leftrightarrow S$, $J \leftrightarrow L$, $F \leftrightarrow J$, where I is the nuclear spin (5/2 for I^{127}) and F is the total angular momentum, $\vec{F} = \vec{J} + \vec{I}$.

Now if we consider the limiting case of very weak Doppler line absorption for all components, we may drop all but the first term (corresponding to linear absorption or a "linear curve-of-growth") in the expression (App. I-5), and we obtain

$$\overline{Ab} = \frac{1}{\sqrt{1+\gamma}} \frac{\Sigma (k_o \ell)_i^2}{\Sigma (k_o \ell)_i} \qquad (16)$$

Evidently we must also modify Eq. (B-11), so that we have

$$\int k_\nu d\nu = \frac{\Delta\nu_D}{2} \sqrt{\frac{\pi}{\ell n 2}}\ \Sigma\ k_{oi} \qquad (17)$$

---

1. We will ignore the possibility of anisotropies introduced by the nature of the discharge, the orientation of the microwave antenna, etc., which could selectively populate some magnetic sublevels and give polarized source radiation.

Then expressing $(k_o \ell)_i$ in terms of the maximum value $(k_o \ell)_m$

$$(k_o \ell)_i = s_i \, (k_o \ell)_m \tag{18}$$

where

$$\begin{aligned} s_i &= 1, \quad i = m \\ &\leq 1, \quad i \neq m \end{aligned} \tag{19}$$

we can see that

$$\overline{Ab} = \frac{(k_o \ell)_m}{\sqrt{1+\gamma}} \; \frac{\Sigma \, s_i^{\,2}}{\Sigma \, s_i} \tag{20}$$

$$\frac{\Delta\nu_D}{2} \sqrt{\frac{\pi}{\ell n 2}} \; (k_o \ell)_m \; \Sigma \, s_i = \frac{1}{8\pi c \nu^2} \; \frac{g_A}{g_B} \; A\ell \tag{21}$$

Recognizing that $\overline{Ab} \sqrt{1+\gamma}$ is the <u>apparent</u> optical depth, calculated assuming a single Doppler line, we see that the hyperfine correction factor is

$$C_{Hf} = \frac{(\Sigma \, s_i)^2}{\Sigma \, s_i^{\,2}} \tag{22}$$

Strictly speaking, this correction factor is valid only in the limit of low absorption and "separate" components. However, C_{Hf} does not change as rapidly as the deviation from the linear growth curve; so as long as we used the full expression (App. I-7) instead of the linear approximation $Ab \sqrt{1+\gamma}$ in calculating the apparent optical depths from our measurements, the results should be usable, even though Ab may be as high as .6 or .7. Partially overlapping components present a problem which can only be solved properly by integrating E_ν and $E_\nu(1 - e^{-k_\nu \ell})$ numerically over all components. However we can establish bounds on the effect of partially overlapping lines by considering the two cases, total separation and total convergence of the components involved.

Clearly Eq. (22) gives the expected results in the simple limiting cases. If there is only one line, $C_{Hf} = 1$. Similarly if there are n

components all at the same frequency, $C_{Hf} = 1$.[1] And for n fully separated, equal components $C_{Hf} = n$. Any overlap or variation in relative strengths must yield a value for C_{Hf} between 1 and n.

From the line-strength tables the maximum possible C_{Hf} value for the 1783 line with ten separate components is 6.75. If some of these coincide, C_{Hf} will be smaller, but since we don't know the hyperfine structure of this line we cannot evaluate this contingency. For $C_{Hf,1830}$ we calculate a maximum value 6.10 for separate components. The Doppler half-width was given earlier as .070 cm^{-1}. From Fig. 9 we can see that two strong components -- (4,4) and (3,2) -- and three or four weak ones -- (1,2), (1,1), (2,3), and (3,4) -- will grossly overlap their neighbors. If we recalculate $C_{Hf,1830}$ on the assumption of coincidence of the (4,4) and (3,2) components we get 5.68. Allowing in addition the (1,1) (2,3) and (3,4) components to converge reduces $C_{Hf,1830}$ to 5.58. Since all the other components (including the strong (5,4) and (4,3) members) display some overlap, the value

$$C_{Hf,1830} = 5.0 \tag{23}$$

should be within 10% of the true value descriptive of the absorption measurements carried out here.

d. Results

From (12b) and (23) we obtain $A_{1830} = 8.7 \times 10^6$/sec, $\tau(^4P_{5/2}) = 115$ nsec. Using a value $C_{Hf,1783} = 6.75$ with (12a) gives $A_{1783} = 2.71 \times 10^8$/sec, in uncanny agreement with Lawrence's result, considering the lack of refinement in the present study. In pure LS coupling the relative strength of the 1783 and 2062 lines has been given earlier as 7.7:1 (including ν^3

1. The sum in the denominator must be taken over all separate components. Therefore if two components k and l coincide, the appropriate term in the sum is

$$s_i^2 = (s_k + s_l)^2.$$

dependence). In that case we would have

$$A_{1783} = .886/(3.6 \text{ nsec}) = 2.46 \times 10^8/\text{sec} \quad (24)$$

if we accept Lawrence's value for the $^2P_{3/2}$ lifetime. Then a comparison with (12a) yields

$$C_{Hf,1783} = 6.1 \quad (25)$$

This value seems more realistic than 6.75, in view of the likelihood of having several of the ten components partially coincide. In addition (24) is consistent with the relative intensities noted in subsection C. In either case, the comparison experiment yields, from (13), $A_{1830} = 7.4 \times 10^6/\text{sec}$. The two determinations are essentially independent, and it is felt that the values

$$\tau(^4P_{5/2}) = 125 \text{ nsec} \quad (\pm 20\%) \quad (26a)$$

$$A_{1830} = 8.0 \times 10^6/\text{sec} \quad (\pm 20\%) \quad (26b)$$

are representative of the precision of this study.

The value for the lifetime of the $^4P_{5/2}$ state is in fair agreement with Lawrence's measured result (90 ± 30 nsec), but differs markedly from his calculated value (63 nsec). From the 125-nsec lifetime and the ~10:1 emission-intensity ratio observed for the 1783 and 2062 lines it appears that the coupling in the $5s^2 5p^4 6s$ configuration of the iodine atom is much closer to the Russell-Saunders case than Lawrence concluded.[1]

By redesigning the absorption cell to include an evacuated "dead" space between the source and absorption chambers it should be possible to effectively isolate the source from the heated cell and avoid the complica-

---

1. Donovan and Husain and coworkers (1965-1968) have carried out an extensive series of experiments on reactions of $^2P_{1/2}$ I atoms produce by flash-photolyzing CF_3I. They have observed all 6 atomic lines 1783 - 2062 in absorption. They give no values for the relative strengths of the lines, but the concentrations of CF_3I they used when detecting 2062 absorption were ~10 times those used when observing 1783 and 1799 absorption, which is in qualitative agreement with the present findings.

tions encountered in the thermal dissociation experiments. Then good data for a wide range of Ab values could enable one to calculate A_{1830} using numerical integration over the entire line shape. The results might provide detailed information about E_ν that could be used to judge the validity of the approximations made here. Such knowledge is of interest to analytical chemists, who increasingly are employing electrodeless discharge lamps to determine atom concentrations by atomic absorption and fluorescence techniques.

IV. SPONTANEOUS PREDISSOCIATION IN I_2 ($B^3\Pi_{0^+_u}$)

A. Detection of Resonance Fluorescence

The methods and results of Section III may be employed to determine iodine atom concentrations in photolysis reactions, using either absorption or fluorescence techniques. Absorption methods involve a straightforward application of the relationships developed previously. However, because of improved signal-to-noise ratios, we prefer a fluorescence method. In that case we must derive additional expressions that relate the observed signals to atomic concentrations.

Winefordner and Vickers (1964) have given equations for the dependence of fluorescent intensity on concentration in a flame. Their efforts were directed toward producing calibration curves in analytical work. It seems worthwhile to derive similar expressions for the situation commonly encountered in photochemical studies, where a cell (often cylindrical) is irradiated at one end and fluorescence is observed at right angles some distance away from the entering light. These equations will of course apply to the detection of I-atom fluorescence in the predissociation cell of Fig. 2.

Consider the arrangement depicted in Fig. 14. The detector sees light emitted from the shaded region. The frequency distribution of the emitted radiation is given by (III-B-8). If the detector is incapable of resolving the line or lines (as is the case for a photomultiplier), it will respond to the total flux of emitted photons, which will in turn be simply proportional to the absorption in the shaded area. The proportionality factor will be a function of the geometry, which we have fixed, the efficiency of the detector, and other variables such as quenching probabilities. For simplicity we will assume the latter are independent

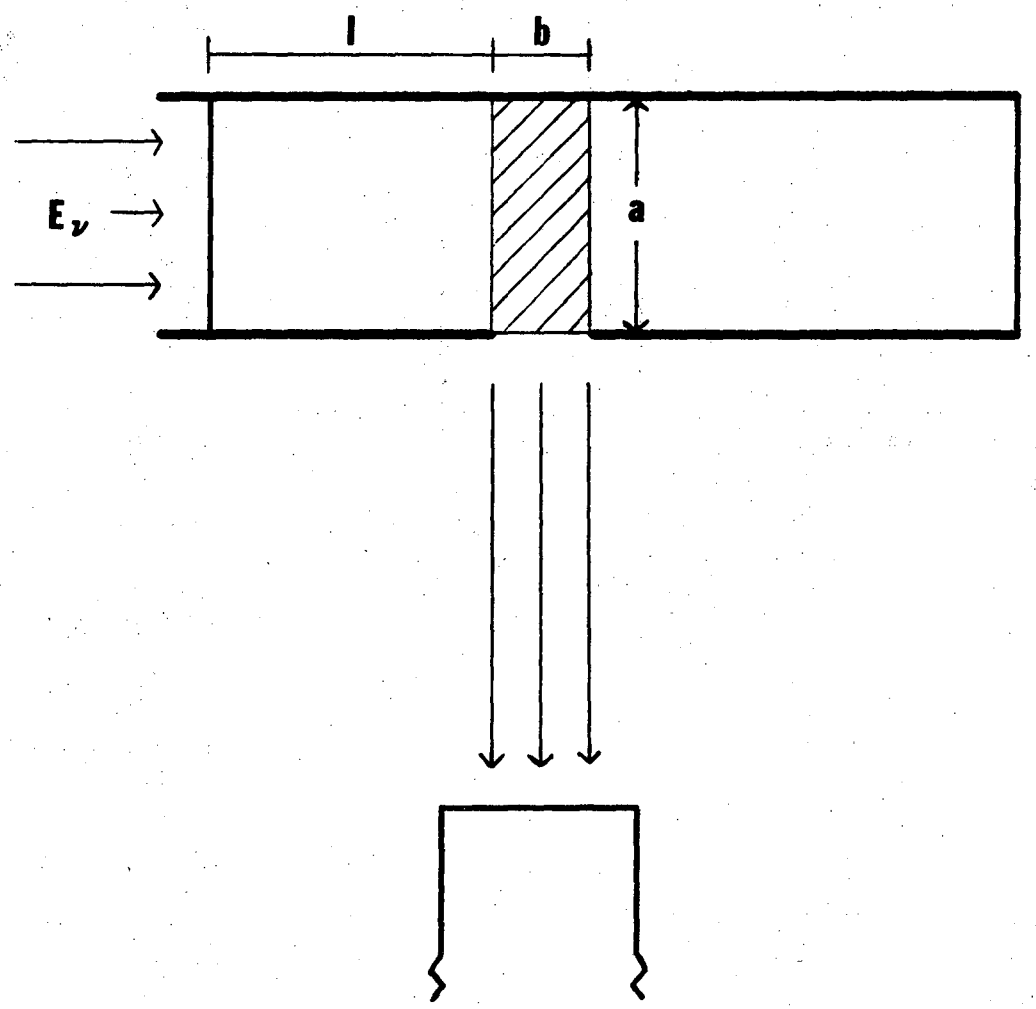

XBL 6910-5809

Fig. 14. Schematic of a fluorescence cell.

of the concentration of emitting particles.[1] The appropriate modification, when required, is obvious. Then

$$\mathrm{Sig}(N) = \mathrm{const} \times (\text{absorption in shaded region}) \quad (1)$$

When $(k_\nu b)$ is small, Eq. (III-B-1) says that the absorption will be proportional to $(k_\nu b)$, which is in turn proportional to the concentration. Recognizing that the incident radiation E_ν must traverse a distance $\sim(\ell + b/2)$ of the cell before it is absorbed, we have

$$\mathrm{Sig}(N) = \mathrm{const} \times \int E_\nu \; e^{-k_\nu(\ell + b/2)}(k_\nu b)\, d\nu \quad (2)$$

Or, considering the effect of the finite depth b, we obtain the more accurate representation

$$\mathrm{Sig}(N) = \mathrm{const} \times \int E_\nu \; e^{-k_\nu \ell}\,(1 - e^{-k_\nu b})\, d\nu \quad (3)$$

Expressions for (2) and (3) are given in Appendix I for a Gaussian E_ν and for an E_ν of the form (III-B-8).

From these equations we see that the signal will depend linearly on the particle density at low concentrations. As N increases, the exciting light reaching the shaded region is progressively attenuated; the signal attains a maximum value and decreases with any further increase in N. Obviously, the linear region is most desirable for quantitative photochemical work, so it is important to utilize concentrations low enough to require only small corrections for non-linearity but high enough to obtain good signal/noise ratios.

---

1. At high concentrations the radiation may "diffuse" out of the cell. If the upper level can decay to the ground state via only one path (I 1830 line, for example), the proportionality constant will remain independent of concentration. If other paths are available, the absorbed energy may exit in some manner not observable by the detector. Thus diffusion of 1783-A radiation through atomic iodine will result in an increased yield of 2062-A radiation at the detector.

A further complication results when a cell of the type shown in Fig. 14 is used: There will be a scattered-light contribution to the total signal. The scattered-light signal will have some constant value at N = 0 and will decrease (neglecting gas-phase molecular scattering) as N is increased, so that the total signal reaching the detector is roughly

$$\mathrm{Sig}(N) = \mathrm{const}_1 \int E_\nu \; e^{-k_\nu \ell} \left(1 - e^{-k_\nu b}\right) d\nu \; . \qquad (4)$$
$$+ \mathrm{const}_2 \int E_\nu \; e^{-k_\nu(\ell + a)} \, d\nu$$

In the second term it is assumed that all the scattered light absorbed is lost to the detector. The ratio $\mathrm{const}_1/\mathrm{const}_2$ will depend on the particular experimental setup. The scattered light can, with proper cell design, be largely eliminated. In some cases, on the other hand, it is desirable to have a scattered-light background. The present work falls in the latter category.

The behavior of Eq. (4) is displayed in Fig. 15. These curves were calculated from the expressions in Appendix I for a Doppler source line and Doppler absorption coefficient. s is the relative line strength, so that k_o is proportional to $s \times N$; γ is the relative line-width parameter introduced in Section III-B. The values of the scaling constants in (4) were chosen to correspond roughly to experimental observations when the predissociation cell was irradiated by visible light at I_2 pressures below 10 mtorr. Concentrations are in arbitrary units, but it is useful to know that the maximum signal falls at $(k_o \ell) = 1.12$ when $\gamma = 1$, $b/\ell = .2$. (Without the scattered-light term the maximum shifts to $(k_o \ell) = 1.22$.) For the range covered by these plots, the approximation (2) gave curves almost imperceptibly different from those calculated with the more complete expression (3).

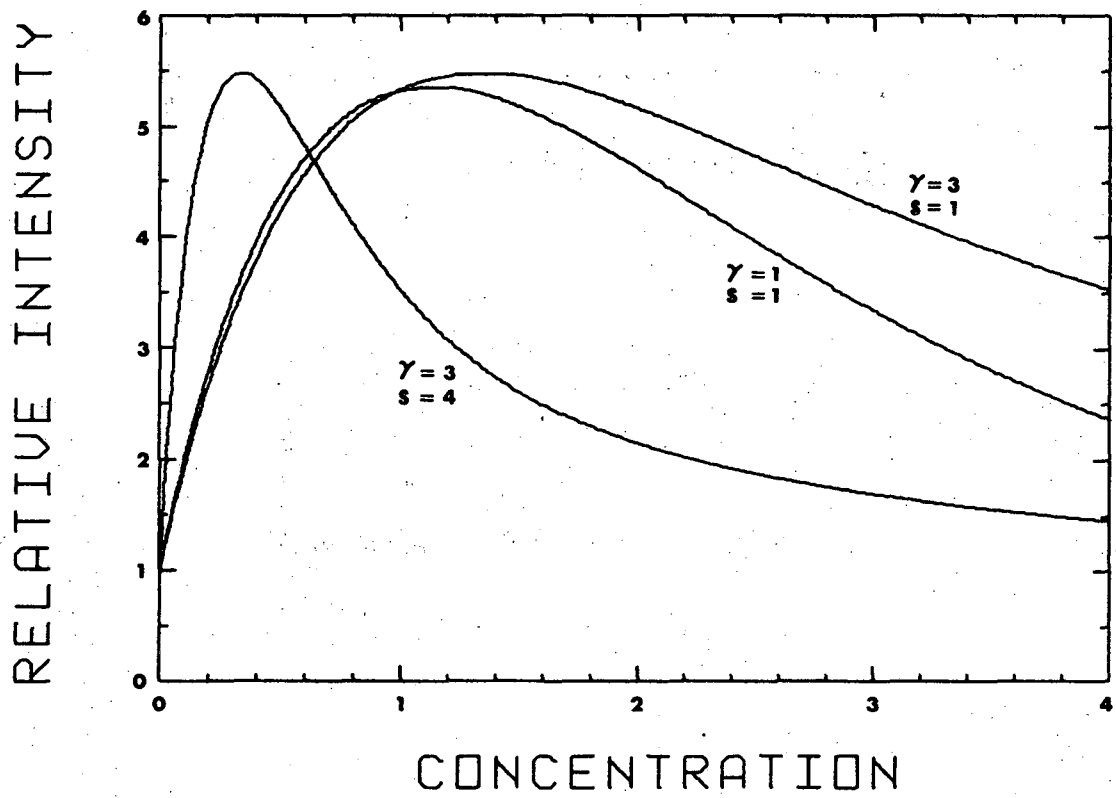

XBL 6910-5810

Fig. 15. Fluorescence function plots. γ is the relative line-width parameter for the Doppler-broadened emission and absorption lines. s is the relative absorption strength, i.e. $k_o = s\ N$. Concentrations are in arbitrary units, such that $N = k_o \ell$ when $s = 1$. Intensities are scaled to a relative 5/1 fluorescence-to-background ratio.

Figure 15 illustrates the importance of having a thorough understanding of the nature of the source and absorption lines in quantitative molecular fluorescence investigations. For example, in a heavy molecule like I_2 a broad source line may excite several partially overlapping rotational lines with different absorption strengths. At high pressures the strong lines will be totally absorbed and the experimental observations will be descriptive of the weaker lines, which may give different and erroneous results, particularly if the property being measured is a function of the rotational quantum number. At the very least, a correction for non-linearity should generally be applied in such studies; preferably the data should be taken at several different ℓ values and extrapolated to $\ell = 0$.[1]

Curves of the type shown in Fig. 15 could be observed for I_2 as well as for I-atoms. The maximum signal occurred at P ~ 55 mtorr. For $\gamma = 3$, $(k_o \ell)$ at the maximum is approximately 1.4. This gives $k_o = 6.4$ cm^{-1} torr^{-1}, in good agreement with the value ~7.5 from the absorption measurements. The relative I_2 fluorescence signal at the maximum was only ~2.6, since a large fraction of the molecular fluorescence falls in a region where the photomultiplier is insensitive.

The absorption by I_2 complicates any quantitative application of the characteristic fluorescence function (4) in calculation I-atom concentrations.[2] At low I_2 pressures the problem should not be severe, and we can calculate from the absorption results, $k_{0,1783}(\text{cm}^{-1}) = 2.7 \times 10^{-13}$ N for T = 300 K, so that the maximum fluorescence signal corresponds to an atomic concentration of 1.0×10^{12} per cm^3. All

---

1. These points have been emphasized repeatedly by Prof. Leo Brewer in private and public communications.

2. At any rate the simple expression (4) will not properly account for the multi-component nature of the I atomic resonance lines.

the measurements were carried out with signals less than 20% of the maximum where $N_I < 1.0 \times 10^{11}/cm^3$.[1] If we compare this to the lowest I_2 concentrations encountered in the experiments ($\sim 5 \times 10^{13}/cm^3$), we see that this photolysis process is indeed a small perturbation on the system.

B. Kinetics of I-Atom Production

1. Proposed Mechanisms

There is on record ample evidence in support of the existence of a spontaneous predissociation decay mode for the B ($^3\Pi_{0^+_u}$) state of I_2 (Chutjian, et al., 1967; Wassermann, et al., 1968; Chutjian and James, 1969). What is still lacking is a quantitative evaluation of this process throughout the region of visible absorption, 5000-6000 A. We shall proceed to derive some expressions for such a quantitative study, which will utilize a comparison technique similar in principle to that employed by Rabinowitch and Wood (1963b) in their definitive work on the quantum yield of quenching in foreign gases.

For excitation in the banded region ($\lambda > 4995$ A) of the B $\leftrightarrow$ X system we must consider the following processes:

$$I_2 + h\nu \xrightarrow{\alpha_\nu \Phi_q(\nu)} I_2^* \qquad (1a)$$

$$I_2^* \xrightarrow{A_T} I_2^\dagger + \text{etc.} \qquad (1b)$$

$$I_2^* \xrightarrow{k_p} 2\,I \qquad (1c)$$

$$I_2^* + I_2 \xrightarrow{k_q} 2\,I + I_2^\dagger \qquad (1d)$$

$$I_2^* + M \xrightarrow{k_M} 2\,I + M^\dagger \qquad (1e)$$

$$I \xrightarrow{k_w} I_{wall} \qquad (1f)$$

---

1. The 1830 and 1783 lines are so different in effective absorption strengths (.059) that one should see two maxima in the fluorescence function. Only one was observed, so it may be assumed that virtually all the photomultiplier signal is from 1783-A fluorescence.

In (1a) $\Phi_q(\nu)$ is the photon flux at frequency ν and α_ν is the absorption coefficient in appropriate units.[1] A_T in (1b) represents the total radiative decay rate to all lower levels. In (1c) k_p is the rate for spontaneous predissociation. k_q and k_M are the constants for quenching by I_2 and by foreign gases, respectively. "Daggers" are included at several points to indicate the possibility of energy transfer in the relevant processes. k_w is a rate constant for wall recombination, the specific mechanism for which will be mentioned below and dealt with in detail in Section V. The rates for the other processes can be represented in the conventional manner, i.e. (1d) implies

$$-\frac{d[I_2^*]}{dt} = k_q\,[I_2]\;[I_2^*]$$

where the brackets indicate concentrations.

Equation (1a) contains an implicit assumption which is unfortunately often incorrect in photochemical studies: namely, that the absorption is small enough so that only the first term in the expansion of $(1-e^{-\alpha_\nu[I_2]})$ need be considered. The observation of less than 10% total absorption is often taken as the criterion for safely applying the linear absorption assumption. This criterion can be disastrously in error for low-pressure gas-phase work, where the absorption occurs in a number of sharp lines. In that case even 1% total absorption of continuous source radiation may imply optical depths of unity or more at the centers of the strong absorption lines, and the assumption of linearity becomes an outright blunder. Later, in the discussion of results, it will be shown that assumption of (1a) introduces an error of several per cent in the predissociation work, even at pressures as low as 10 mtorr. For the present we will accept (1a)

---

1. This α_ν is related to the k_ν used previously by $k_\nu = \alpha_\nu N$; here α_ν is treated as a broad-band parameter, so it is directly related to the measured decadic molar extinction coefficient ϵ_ν. (See Eq. (III-D-9b).)

as valid.

Equations (1b-1e) predict an exponential decay of the I_2^* population. However, as it will turn out in these experiments, the symbol I_2^* will have to represent a total B-state population which is distributed over several v' levels and all thermally accessible rotational levels. If the decay rates vary with v' and J, the observed decay will no longer be exponential, but rather some sort of weighted average of the individual decay curves. In that case the value measured may be explicitly dependent on the method of measurement. For example Cunningham (1968) obtained different lifetimes for the decay of I_2^* in the vicinity of v' = 25 when he used different modulation frequencies in a phase-shift determination. Radiation entrapment can also give deviations from the exponential decay, but such problems are inconsequential in the present situation.[1] Brown, Steinfeld and Klemperer (1964, 1965, 1966) have shown that collisional energy transfer in I_2^* is of a magnitude comparable to the quenching for most collision partners. (I_2^* - I_2 collisions are the noted exception.) Such processes need not be considered in our mechanism; because in the low-pressure limit they do not occur, and in the high-pressure limit 100% quenching is effected, regardless of how much energy transfer precedes it.[2]

Equations (1d) and (1e) correctly represent the quenching of I_2^*, but the indicated products of the quenching are somewhat speculative. Although atoms are known to be produced in the quenching process, the yield of atoms may be something less than two per quenched I_2^* if long-lived intermediates

---

1. An estimate of the effect of entrapment is given by Chutjian, et al. (1967).

2. The foreign-gas quenching results may be affected if transfer occurs to v' levels having noticeably different quenching susceptibility.

such as I_3 and MI_2 can exist.[1]

For the sake of thoroughness we should include mechanisms for vibrational and rotational relaxation and perhaps ortho-para conversion for the ground-state molecules. In the steady-state situation there must be a vibrational cascading occurring for recombining atoms and for the I_2 produced in (1b) and (1d). In view of the very small steady-state concentrations of I_2^* and I, it is unlikely that the ground-state population can be perturbed by more than 1-2%, if we adopt nominal rates for the relaxation processes. Furthermore the experiment offers a qualitative handle on such effects. The I_2 ultraviolet absorption and fluorescence might be expected to decrease or increase if an appreciable fraction of the iodine molecules are in high v" levels, where the Franck-Condon factors could change the absorption. At no time in the course of these predissociation experiments was such an effect observed. Anyway as shown below the comparison nature of the experiment will partially cancel out complications of this type. Therefore the above mentioned processes will be ignored, and $[I_2]$ will be assumed constant with respect to the visible irradiance.

Now we come to the all-important Eq. (1f), the only process given to account for the removal of I-atoms. At the low pressures employed in these studies we expect heterogeneous recombination to predominate over homogeneous (Rabinowitch and Wood, 1936c). The nature of the wall recombination may be complicated; it will be investigated in more detail in Section V. Briefly, a very low (~.001) "sticking" probability will lead to a second-

---

1. The experiment of Rabinowitch and Wood (1936b) indicated that the quenching of I_2^* was accounted for by (1e) and not by the radiationless process $I_2^* + M \rightarrow I_2 + M$. However, the yield of atoms was determined indirectly, from the decrease in $[I_2]$. This unfortunately says nothing about what happens to the I atoms. The same problem arises in all the classic I-atom recombination studies. This deficiency will be overcome in the present work and that discussed in Section V.

order removal, and a moderate (~.1) sticking efficiency will give a first-order disappearance. The former prevailed in the experiments of Wassermann and co-workers (1968); the latter appears to obtain in the present study. In either case the recombination rate may be expressed

$$-\frac{d[I]}{dt} = \frac{k_w [I]^x}{1 + aM + a' [I_2]} \tag{2a}$$

The terms in the denominator are included to account for the diffusion of I-atoms to the walls of the cell. (The form $(1 + a \cdot M)$ will be verified in Section V. Here it is unimportant, because it will be eliminated in the expressions derived below.) When both 1st- and 2nd-order recombination occur to an appreciable degree, (2a) will still represent approximately the overall rate, with $1 < x < 2$. However, it is more correct to express the combined rate as

$$-\frac{d[I]}{dt} = \frac{k_w [I] (1 + b [I])}{1 + aM + a' [I_2]} \tag{2b}$$

In these experiments the deviation from 1st order was small enough that (2a) and (2b) gave essentially the same results.

In the stationary state we have

$$\frac{d [I_2^*]}{dt} = 0 \tag{3a}$$

$$\frac{d [I]}{dt} = 0 \tag{3b}$$

Equations (1) and (3) give, with (2a)

$$[I]^* = \frac{2\alpha_\nu}{k_w} \Phi_q (\nu) \frac{k_p + k_q [I_2] + k_M M}{A_T + k_p + k_q [I_2] + k_m M} [I_2] F([I_2],M) \tag{4}$$

where M represents the concentration of foreign gas and $F([I_2],M)$ is the denominator in (2). The expression

$$R = \frac{k_p + k_q [I_2] + k_M M}{A_T + k_p + k_q [I_2] + k_M M} \qquad (5)$$

contains the information we desire. It is simply the fraction of excited molecules that predissociate. In the limit of high pressure R is unity; the low-pressure limit is $k_p/(A_T + k_p)$ or $k_p\tau$, where τ is the unimolecular lifetime. When x = 1, and $k_q[I_2] \ll k_p$, (4) predicts that [I] will be proportional to $\Phi_q(\nu) \cdot [I_2]$. Such a dependence has been noted by Mayo (1964), and was observed early in this investigation.

Equation (4) does not lend itself to easy evaluation of the quantum yield for predissociation $k_p\tau$. Its use requires accurate knowledge of $F([I_2],M)$ and the characteristic fluorescence function. We can eliminate this problem by comparing $[I]^x$ from (4) with the I-atom concentration produced by excitation above the dissociation limit of the B state. In this case we have, for wavelengths shorter than 4990 A[1]

$$I_2 + h\nu \xrightarrow{\alpha_\nu \Phi_q(\nu)} I(^2P_{1/2}) + I(^2P_{3/2}) \qquad (6a)$$

$$I(^2P_{1/2}) \xrightarrow{k_Q} I(^2P_{3/2}) \qquad (6b)$$

and the same removal mechanism (1f). k_Q in (6b) represents all quenching processes for relaxation of the metastable I-atoms, plus radiative decay, and we assume there are no reactions specific to $I(^2P_{1/2})$ atoms of the form

$$I(^2P_{1/2}) + M \longrightarrow MI \qquad (7a)$$

$$I(^2P_{1/2}) + AM \longrightarrow MI + A \qquad (7b)$$

which can tie up the metastable atoms. This assumption will be supported below, where it will also be shown that the relaxation reactions (6b) are very rapid with respect to the overall atomic removal process (1f).

---

1. The $B \leftarrow X$ continuum actually extends some distance into the "banded" region. This point will be discussed more fully below.

Then

$$[I]^x = \frac{2\alpha_{\nu'}}{k_w} \Phi_q(\nu') \cdot [I_2] \cdot F([I_2], M) \tag{8}$$

Dividing (4) by (8) gives

$$\left(\frac{[I]_\nu}{[I]_{\nu'}}\right)^x = \frac{\alpha_\nu \Phi_q(\nu)}{\alpha_{\nu'} \Phi_q(\nu')} \cdot \frac{k_p + k_q [I_2] + k_M M}{A_T + k_p + k_q [I_2] + k_M M} \tag{9}$$

The application of (9) is obvious. Here we will use the narrow-band interference filters and tungsten lamp described earlier to achieve the excitation. Then we have

$$\left(\frac{[I]_{bi}}{[I]_c}\right)^x = \frac{a_{bi}}{a_c} \cdot R_i([I_2], M) \tag{10}$$

where (a_{bi}/a_c) is the ratio of quanta absorbed by I_2 with "banded" filter i to quanta absorbed using a standard "continuum" filter c. (For a given filter $\Phi_q(\nu)$ is to be the same in all experiments, so that (a_{bi}/a_c) is indeed a constant for banded-region filter i.) Values for (a_{bi}/a_c) may be calculated, or they may be determined experimentally when R = 1.0.

To more properly describe the excitation into the banded region of the I_2 visible absorption, we should include a term to cover the possibility of direct dissociation via an underlying continuum. The $^1\Pi_{1u}$ repulsive state, which is presumably responsible for the spontaneous predissociation, has been predicted (Mulliken, 1940) to contribute about 10% of the overall absorption. In addition the continuum of the $A(^3\Pi_{1u}) \leftarrow X$ transition seems to overlap the $B \leftarrow X$ system at the red end of the latter (Ham, 1954; Mathieson and Rees, 1956).[1] The necessary modification of (10) is simple

---

1. On the basis of the work by Ham (1954), Mulliken has upped his 1940 estimate of the $^1\Pi_{1u} \leftarrow X$ strength to the value given here.

The present treatment implies that the absorptions, $^1\Pi_{1u} \leftarrow X$ and $B \leftarrow X$, and the spontaneous predissociation $B \rightarrow {}^1\Pi_{1u}$ are essentially independent processes. This picture is valid for cases where the coupling between the upper states is relatively weak, but it may be questionable when the mixing becomes strong.

and direct:

$$\left(\frac{[I]_{bi}}{[I]_c}\right)^x = \frac{a'_{bi}}{a_c} R_i([I_2],M) + \frac{a_{ci}}{a_c} \tag{11}$$

where $(a'_{bi} + a_{ci})$ replaces a_{bi} in the discussion of the previous paragraph. The expression on the right will be referred to in future discussions as the experimental yield function, or simply the yield function and will be represented

$$Y([I_2], M) = Y_1 R([I_2], M) + Y_2 \tag{12}$$

Then the quantum yield for unimolecular production of atoms is

$$QY = \frac{Y(0,0)}{Y_1 + Y_2} = \frac{Y_1 R(0,0) + Y_2}{Y_1 + Y_2} \tag{13}$$

$$= \frac{Y_1 k_p T + Y_2}{Y_1 + Y_2} = \frac{Y_{min}}{Y_{max}}$$

Clearly the fractional absorption by the underlying continuum is

$$fr_c = \frac{Y_2}{Y_1 + Y_2} \tag{14a}$$

and that by the "discrete" state is

$$fr_b = \frac{Y_1}{Y_1 + Y_2} \tag{14b}$$

(We must remember that Y, Y_1, Y_2 and R are all functions of the particular filter used for banded-region absorption. The subscript i has been dropped to simplify the notation.)

If we consider the behavior of Y at low $[I_2]$ with no foreign gas M present, we can show that

$$Y \rightarrow Y_1 (k_p\tau + k_q \tau^2 A_T \cdot [I_2]) + Y_2 \tag{15}$$

which is a line with intercept Y_{min} and slope $(Y_1 k_q \tau^2 A_T)$. We can express this slope differently,

$$Y_1 k_q \tau^2 A_T = \Delta \cdot k_q \tau \tag{16}$$

where

$$\Delta = Y_1 A_T \tau \tag{17}$$

Δ is simply the difference $Y_{max} - Y_{min}$. Similarly at high pressures of foreign gas, the following relationship will be useful:

$$Y = Y_1 \left(\frac{1 + c_1/M}{1 + c_2/M} \right) + Y_2 \tag{18}$$

where

$$c_1 = \frac{k_p + k_q [I_2]}{k_M} \tag{19a}$$

$$c_2 = \frac{A_T + k_p + k_q [I_2]}{k_M} \tag{19b}$$

Having derived the relationships we will need, we now return to the problems involving $I(^2P_{1/2})$ atoms.

2. Relaxation of Metastable Iodine Atoms

The above derivation required the supposition that processes (6b) are rapid and that reactions (7) do not occur. If either of these assumptions fails to hold, the comparison procedure will give erroneous results, because the detection method "sees" only ground-state I-atoms.

Donovan, Husain, and co-workers (1965-1968) have published a series of papers on $I(5^2P_{1/2})$ reactions with various gases. They used a method of time-resolved kinetic spectroscopy which allowed them to detect the presence of both ground-state ($^2P_{3/2}$) and metastable ($^2P_{1/2}$) I-atoms through their absorption lines at 1783, 1799, and 2062 A. By flash-photolyzing CH_3I and CF_3I, they were able to produce exclusively $^2P_{1/2}$ atoms.

Abstraction reactions of the type (7b) were found to occur in the cases, M = Cl_2, Br_2, ICI, and IBr. In all other cases collision-induced spin-orbit relaxation dominated the removal of $^2P_{1/2}$ atoms, as demonstrated by the simultaneous increase in $I(^2P_{3/2})$. (At long time delay, the latter

disappeared and the ultraviolet absorption of I_2 was observed.) In the noble gases, decay was limited by diffusion to the walls; in molecular gases it occurred in homogeneous collision processes. Deactivation probabilities on collision were quoted for more than a dozen quenching gases. For N_2, O_2, and I_2, values of 3.0×10^{-6}, 5.6×10^{-2}, and 7.1×10^{-2} were given. (I_2 was the most efficient quencher found.)

Although the evidence against reactions of the type (7) is strong (except for the four cases mentioned earlier), it is difficult to exclude the possibility entirely, as concentrations of $I(^2P_{1/2})$ and $I(^2P_{3/2})$ were not determined absolutely by the above authors. On the other hand the constancy in relative concentrations with different quenchers makes it seem likely that any effects of the type (7) were unmeasureable in their experiments. This would place an upper limit of ~5% on the fraction of $I(^2P_{1/2})$ atoms removed by attachment or abstraction reactions in, for example, N_2, O_2, and I_2. Meyer (1968) found that $^2P_{1/2}$ I-atoms abstract I from CH_3I and noted that other workers had produced IO and IO_2 in processes of the type (7). In addition there were some indications of the occurrence of (7) in this lab when M was O_2.[1] However, the data of Donovan and Husain are the best quantitative measure of this problem, and we will accept their results as justification for the exclusion of (7) from the mechanism.

There remains the question of the relative magnitudes of the rates for $I(^2P_{1/2})$ relaxation and for overall recombination of I-atoms. The results to be discussed in Section V give a lowest mean recombination

---

1. Use of air as a quencher in the predissociation cell led to permanent changes in the "poisoned" surfaces, including fogging by a white deposit. These changes could have involved $I(^2P_{1/2})$, O_3 or a number of other possible species.

lifetime $\tau_r(=1/k_w)$ of ~3 msec for an untreated cell. The rate has not yet been measured in a "poisoned" cell, but qualitatively τ_r seemed to be an order of magnitude greater. With $\tau_r \doteq 30$ msec, at $P(I_2) = 1$ mtorr (lower than any pressure actually used), the I-atoms undergo ~150 collisions before recombining; the concentration of $I(^2P_{1/2})$ would be practically negligible after ~50 collisions with I_2. This calculation may be entirely academic though, as we note that the mean free path is ~50 mm at $P(I_2) =$ 1 mtorr, so that the average iodine atom collides with the cell walls about as often as with I_2 molecules. Donovan and Husain (1966) point out that the efficiency for relaxation of $I(^2P_{1/2})$ in wall collisions is fairly high. In that case we should reopen the question of reactions (7) occurring on the acid-treated surfaces of the cell. The author was unable to locate any studies of such processes, but fortunately the experimental data give some estimate of this possibility. The results indicate it can affect the accuracy of the measured quantum yields by at most 10%, probably much less.

It was possible to check for absorption by $I(^2P_{1/2})$ experimentally using the procedures outlined in (III-D). The 1799, 1844, and 2062 lines all gave detactable absorption in both treated and untreated cells. Although the resonance-line absorption increased ten-fold in the treated cell, the $^2P_{1/2}$ absorption remained constant within the precision of the measurements, indicating the acid poisoner had no effect on the decay of the $^2P_{1/2}$ atoms. However, this comparison was made at a pressure of ~30 mtorr, where homogeneous quenching might have obscured any changes in the wall relaxation processes. The lowest I_2 pressure for which both 1783 and 1799 absorption were measured in a treated cell was 9 mtorr, where the absorptions were 85% and < 5%. (The measurement at 1799 A appeared to be even lower than 5%, but the uncertainty was high because of low signal/noise ratio.)

According to Lawrence (1967) and Donovan and Husain (1968), the absorption strengths of the 1799 and 1783 lines are approximately equal.[1] In that case the above measurements indicate the $I(^2P_{3/2})$ concentration is about 80 times that of $I(^2P_{1/2})$. If we assume the broad continuum source produces atoms in the ratio $N_I(^2P_{3/2})$: $N_I(^2P_{1/2}) = 5:1$, all but 7% of the metastable atoms have relaxed to the ground state in the steady-state situation.

From this discussion the complications involved in comparing the concentrations of I-atoms produced in banded-region excitation with the concentrations of initially non-identical atoms from continuum excitation are minor, and we may proceed to measure the low-pressure quantum yield of iodine atoms using our comparison technique.

C. Collection and Treatment of Data

1. Procedures

The experimental approach to the problem is already obvious from the relationships derived in Subsection B. Equation (B-15) predicts a linear dependence of the yield function on $[I_2]$ in the limit of low iodine pressures. From the quenching data of Chutjian, et al. (1967), we can estimate that the deviation from (B-15) at $P(I_2) = 20$ mtorr is about 15%, so a plot of Y vs. $P(I_2)$ should be reasonably linear for pressures lower than this. In the high-pressure limit Y goes to Y_{max}, but there are complications inherent in reaching this limit using I_2 alone to produce the quenching. The ultraviolet absorption by I_2 is so strong that at pressures greater than ~75 mtorr the fluorescence signal actually decreases when the visible source is turned on; and visible light from the iodine lamp can develop high residual concentrations of atoms. On the other hand we can use a foreign

1. This is in good agreement with the theoretical line strengths for Russel-Saunders coupling. Unfortunately the absorption at 2062 A was too weak for a quantitative determination of the relative 1799 and 2062 absorption strengths. Qualitatively the results supported the findings of Section III.

gas such as Ar or N_2 to predissociate $I_2^*(B)$ and thereby obtain values for the foreign-gas quenching constant k_M as well as the desired Y_{max} at each wavelength. (B-18) is the appropriate relationship.

The experiments were carried out over a period of two months, using the arrangement of Fig. 6. In a given run, one or two points were recorded for each of the twelve interference filters at constant foreign-gas and I_2 pressures. Before each low-pressure (no foreign gas) run, the cell was freshly evacuated in the manner described in Section II; afterwards (~4 hours) the cell was checked for possible leakage. In the foreign-gas runs cylinder-grade N_2 was used as the quencher.[1] With the I_2 frozen out, the vacuum line and cell were flushed several times before the cell was filled with the desired amount of N_2; the pressure was determined to ±.03 torr with the aid of an oil manometer.

In the low-pressure work, the I_2 pressure ranged from 1.5 to 16.5 mtorr, corresponding to cold-finger temperatures between -27 and -6 C. The iodine vapor pressures were taken from the tables mentioned in Section III-D. In the foreign-gas runs, N_2 pressures of .75-11 torr proved suitable, and the I_2 pressure was held at 1.6 mtorr by cooling the cold finger to -26 C in a slush of o-xylene. At the higher N_2 pressures it was necessary to wait as much as 1/2 to 1 hour to establish a constant iodine concentration. With no foreign gas present the I_2 vapor appeared to equilibrate with the cold finger as fast as the latter could be cooled.

The iodine lamp cold finger was cooled in a bath of ethanol and dry ice at ~-80 C. Under these conditions the UV output was quite sufficient and the visible output was tolerable. At the start of a run it was necessary to wait 15-20 minutes for the lamp's ultraviolet output to stabilize, as indicated by the attainment of a fairly level

1. $I_2^*(B)$ is so efficiently quenched by most molecules that any possible impurities should give a negligible error in the results for k_{N_2}.

background signal of scattered light and I_2 fluorescence. During the run the lamp generally weakened with time, but it displayed no problematic instability as long as the bath temperature was kept constant.

Each recorded data point was an average of 3-5 measurements for the 4919-A continuum filter and 3-10 measurements for the particular banded-region filter. For each measurement the tungsten strip lamp was turned on for 10-12 seconds, long enough to establish the steady state. (With N_2 present the points required slightly longer, ~15 seconds.) The signals were recorded in a "sandwiching" fashion, illustrated in Fig. 16, in order to compensate for possible drifts in I-lamp power and I_2 pressure. They were subsequently normalized to a constant background before being converted to an experimental signal ratio (Sig_b/Sig_c). A correction for non-linearity, discussed below, was applied to produce each value of Y. For every banded-region filter a total of 9-12 points were obtained for the determination of each of the desired limits.

2. Non-linearity Correction

Earlier we assumed for simplicity that the recombination of the I-atoms proceeded according to (B-2a), and we used that equation to subsequently derive the expression for the yield function. It was pointed out that (B-2b) is a theoretically more plausible expression for the combined 1st- and 2nd-order wall recombination. We can determine the unknown constant x in (B-2a) from the slope of a plot of $\ln \Phi_q$ vs. $\ln [I]$, as is clear from (B-4). Alternatively we can determine a value for b in (B-2b) from a plot of Φ_q vs $[I]$.

$$[I]\,(1 + b\,[I]) = \Phi_q \times F'\,([I_2], M) \qquad (1)$$

In order to obtain even relative values for [I] we must correct the observed signals for non-linearities of detection as dictated by the

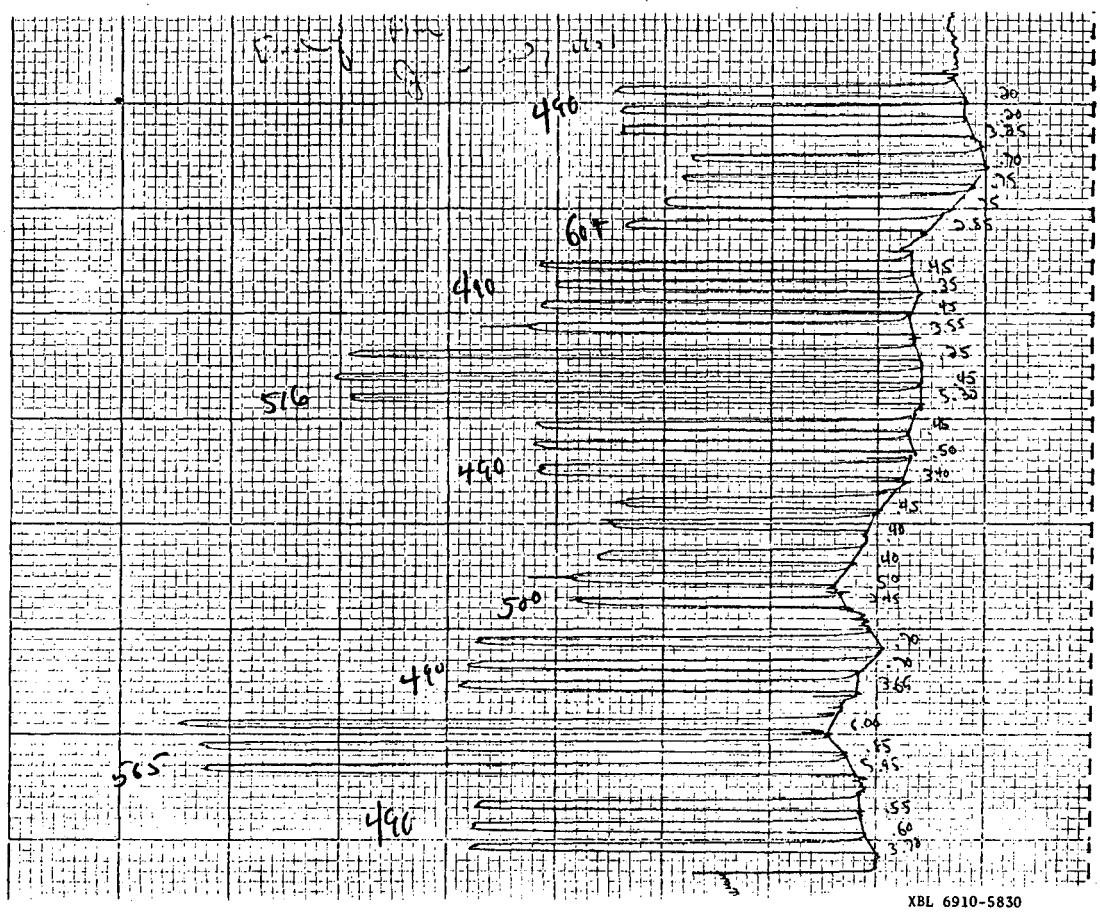

Fig. 16. Sample data from predissociation experiment. Here $P(N_2) = 0.96$ torr, $P(I_2) = 1.6$ mtorr. Wavelengths for the filters were recorded in nanometers. An average baseline was filled in, and the measured signals were recorded in millivolts.

characteristic fluorescence function derived in Part A. Rather than do this we can simply lump the non-linearities of recombination and signal detection together and obtain

$$\left(\frac{Sig_b}{Sig_c}\right)^{x'} = Y \tag{2a}$$

or

$$\frac{Sig_b\ (1 + b'\ Sig_b)}{Sig_c\ (1 + b'\ Sig_c)} = Y \tag{2b}$$

Then we obtain the value of x' or b' as above, from the appropriate relationship between the signal (Sig) and the relative intensity of exciting light.

Preliminary work indicated the values of x' and b' in (2) were functions of the I_2 pressure and the total magnitude of the signals involved. The logarithmic plots gave, under various conditions, values of x' from 1.04 to 1.14, a range ten times the individual standard deviations. The foreign-gas data generally gave values around 1.06; the low-pressure data averaged ~1.10. Furthermore the logarithmic plots generally exhibited slight positive curvature. The curvature would be expected for a mixed order of recombination, and the variation of the slope may be interpreted as a result of being in different regions on the fluorescence-function curve. Eventually the form (2b) was adopted for the correction. Although b' behaved in a similarly dissatisfying manner, fitting the data to (2b) gave statistically slightly better results than for (2a). Figures 17 and 18 illustrate the typical behavior.

Since values for b' seemed to vary with experimental conditions, it was felt desirable to determine the correction independently for each data run. To minimize dependence on the magnitude of the fluorescence

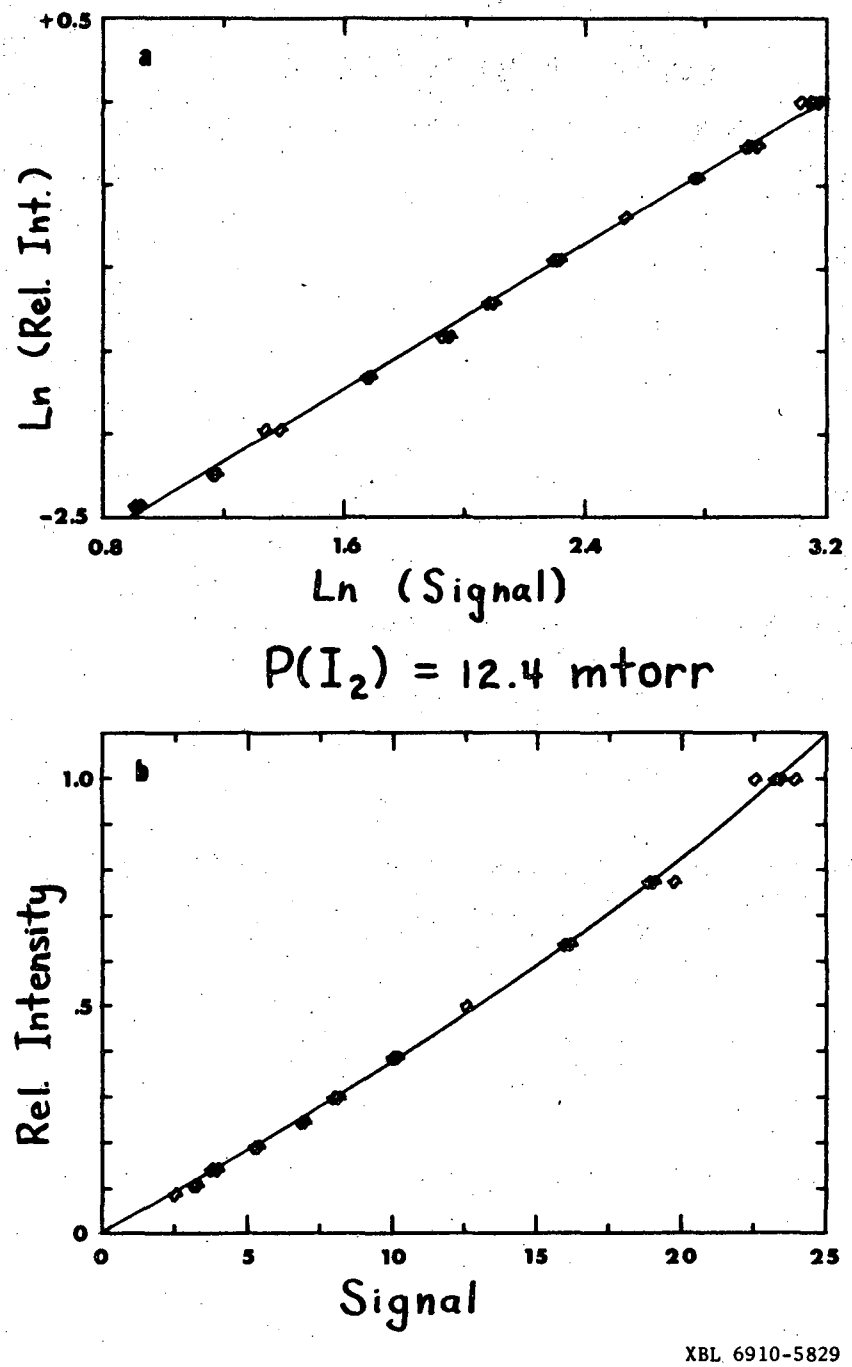

Fig. 17. Relationship between relative intensity and signal for excitation at 5462 A. $P(N_2) = 0$; $P(I_2) = 12.4$ mtorr.

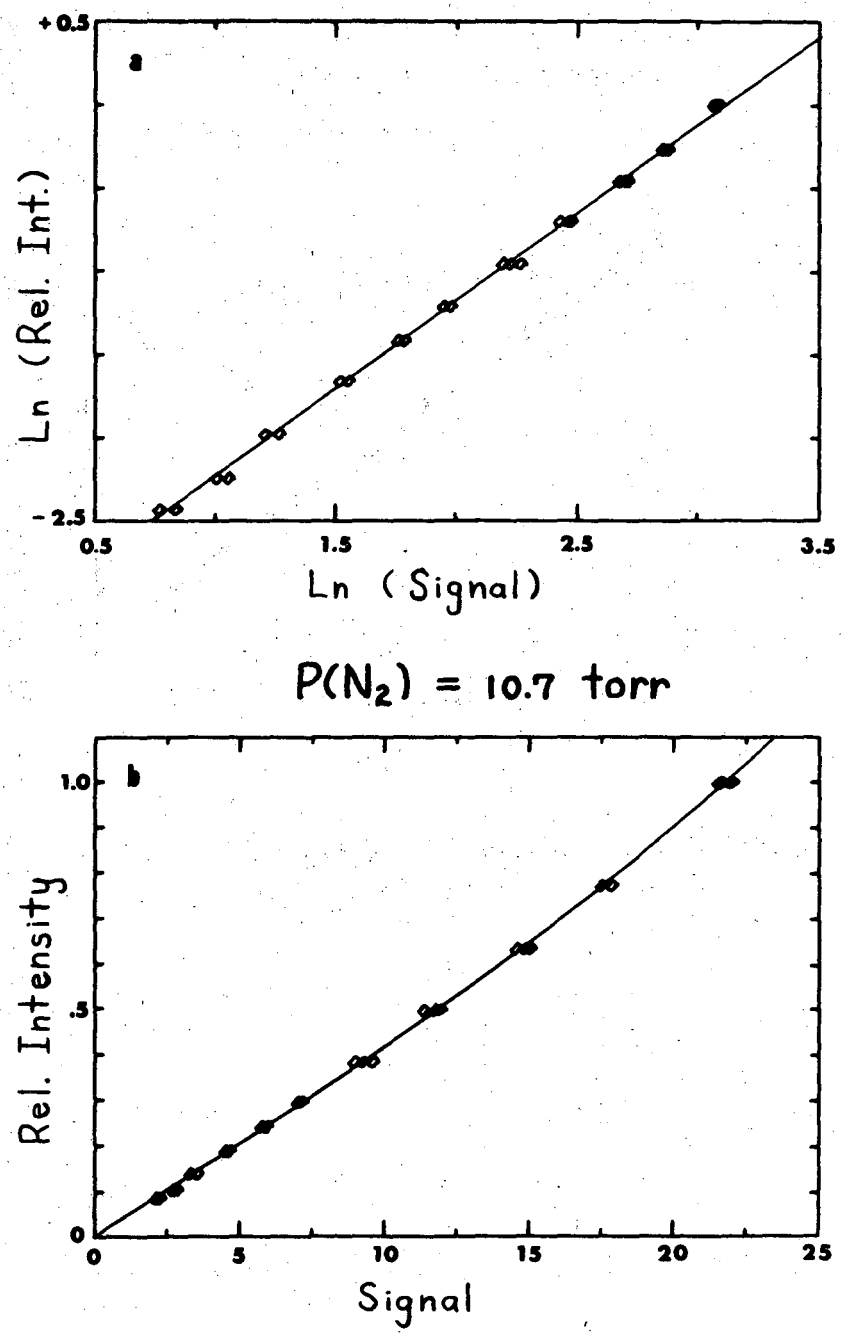

XBL 6910-5826

Fig. 18. Relationship between relative intensity and signal for excitation at 5462 A. $P(N_2)$ = 10.7 torr; $P(I_2)$ = 1.6 mtorr.

signal, cardboard diaphragms were used to mask down the condensing lenses. In this way the maximum working fluorescence signal was always adjusted to 10-15% of the maximum in the characteristic fluorescence function. Data of the type shown in Figs. 17 and 18 were recorded using the calibrated neutral density filters in combination with the interference filter having peak transmission at 5462 A.[1] Points were acquired going from low to high density and back again, to compensate for possible temporal changes (assumed to be "linear") in the lamp output and iodine concentration; each point here represented a single on-off operation of the tungsten lamp.

Despite the esthetically unpleasing aspects of this non-linearity treatment, the net effect on the measured quantum yields was small. It was greatest when the high- and low-pressure limits of Y were farthest apart, where it amounted to ~4%.

D. Results and Discussions

1. Unimolecular Quantum Yield of Iodine Atoms

a. Yield function plots

Results for the twelve banded-region interference filters are displayed in Figs. 19-30. The upper plots show the performance of Y in the high-pressure limit. The solid curves are the least-squares best fits of the points to a modified form of (B-18),

$$Y = Y_{max}\left(\frac{1 + c_1/P_{N_2}}{1 + c_2/P_{N_2}}\right) \qquad (1)$$

which amounts to ignoring the continuum contribution to the total atomic yield. For most of the filters this will turn out to be a good assumption, as will be evident later. For the cases where the continuum contri-

1. The 5462-A filter was chosen because it gave the largest signals. For comparison several runs were made with the continuum filter peaked at 4919 A; no significant difference was observed. Unfortunately this result does not prove the recombination is equivalent in the two regions. For example, $^2P_{1/2}$ atoms could have a much higher sticking probability and never be seen by the detector.

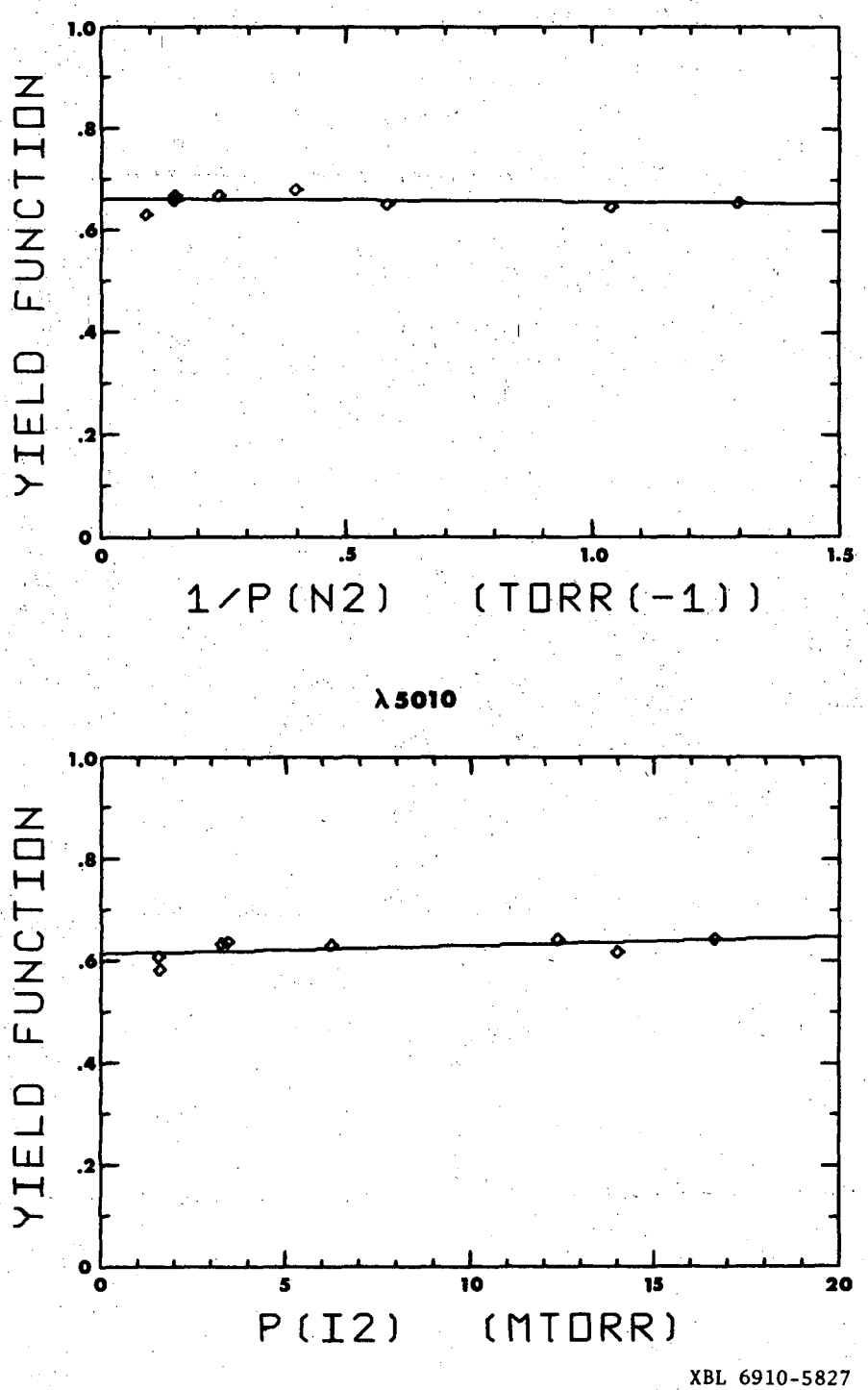

Fig. 19. Experimental yield function plot for 5010 A.

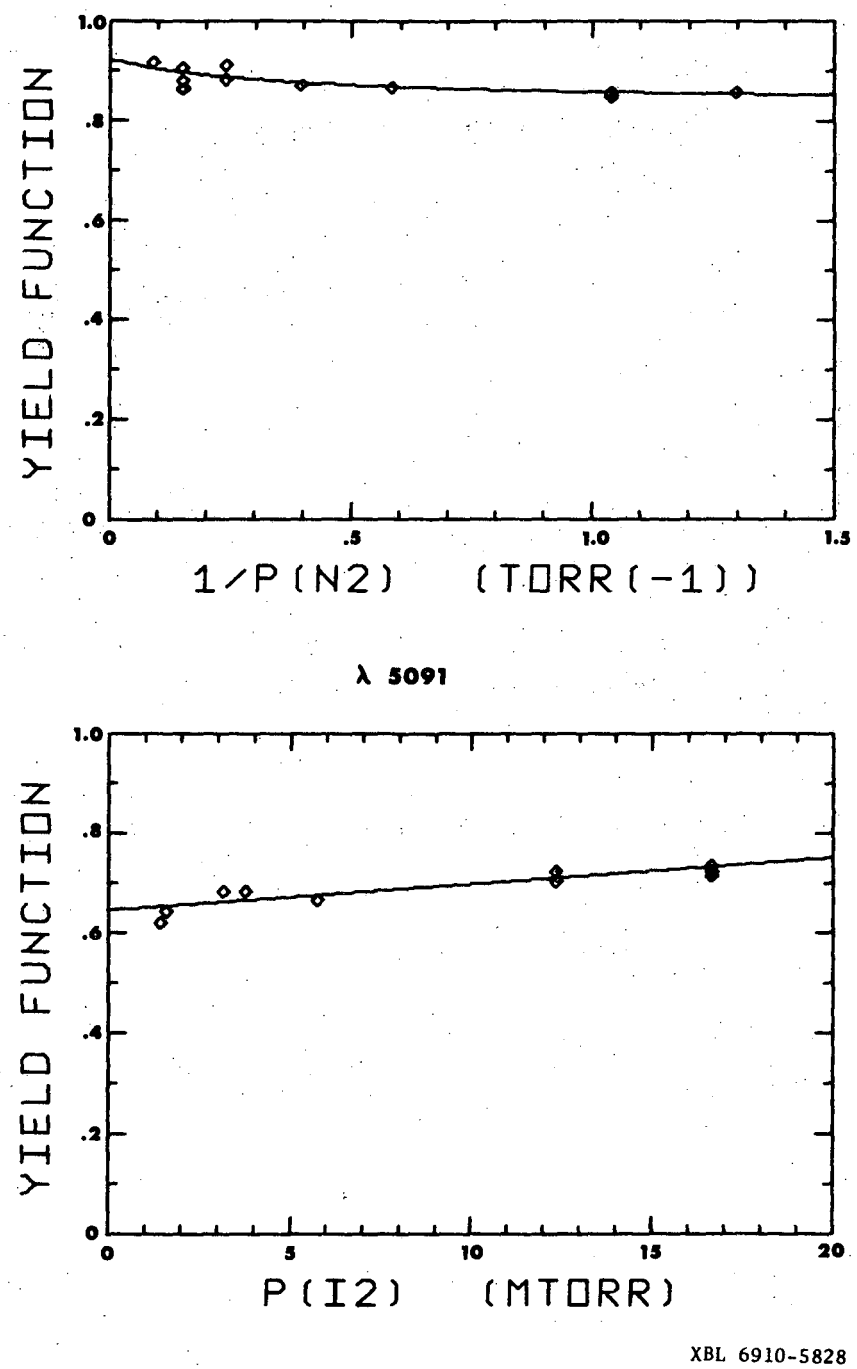

XBL 6910-5828

Fig. 20. Experimental yield function plot for 5091 A.

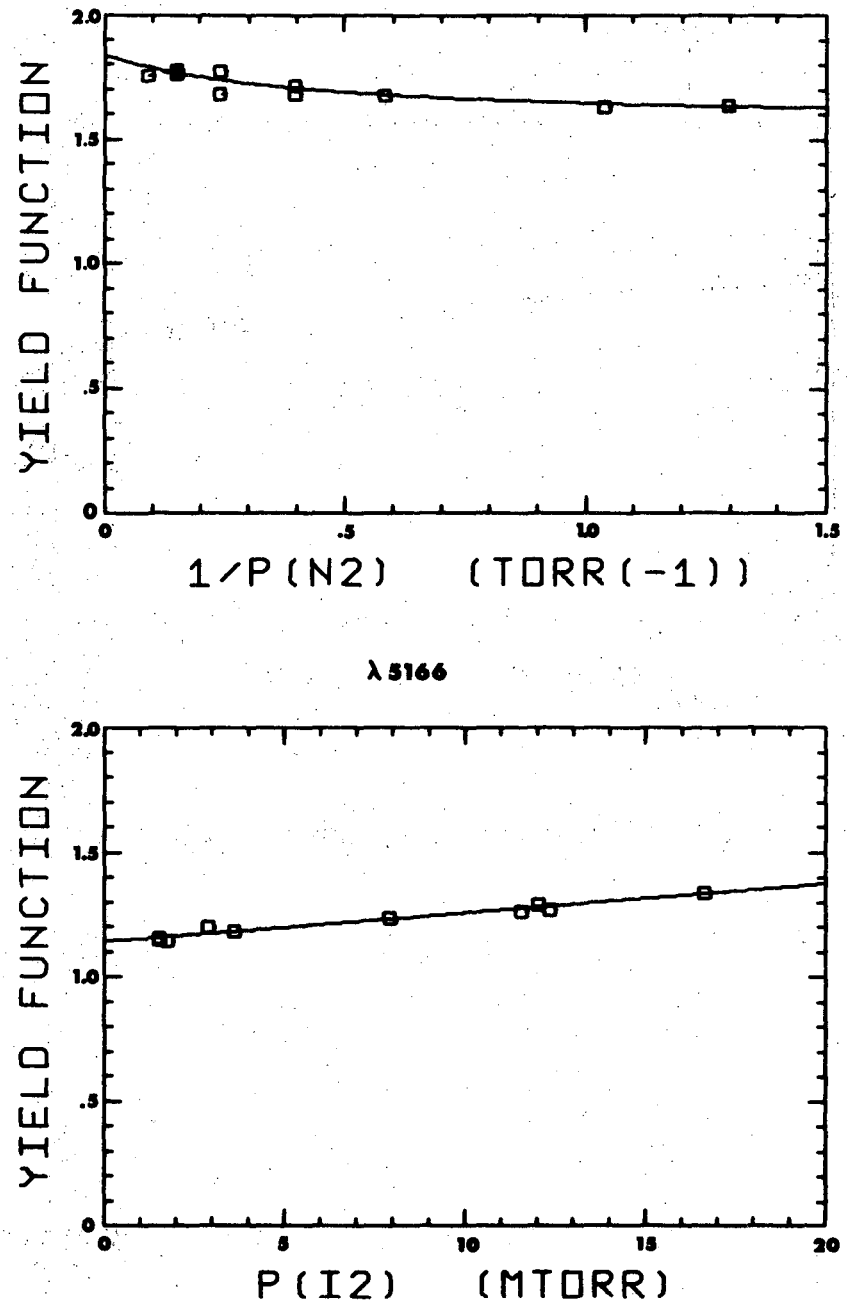

XBL 6910-5821

Fig. 21. Experimental yield function plot for 5166 A.

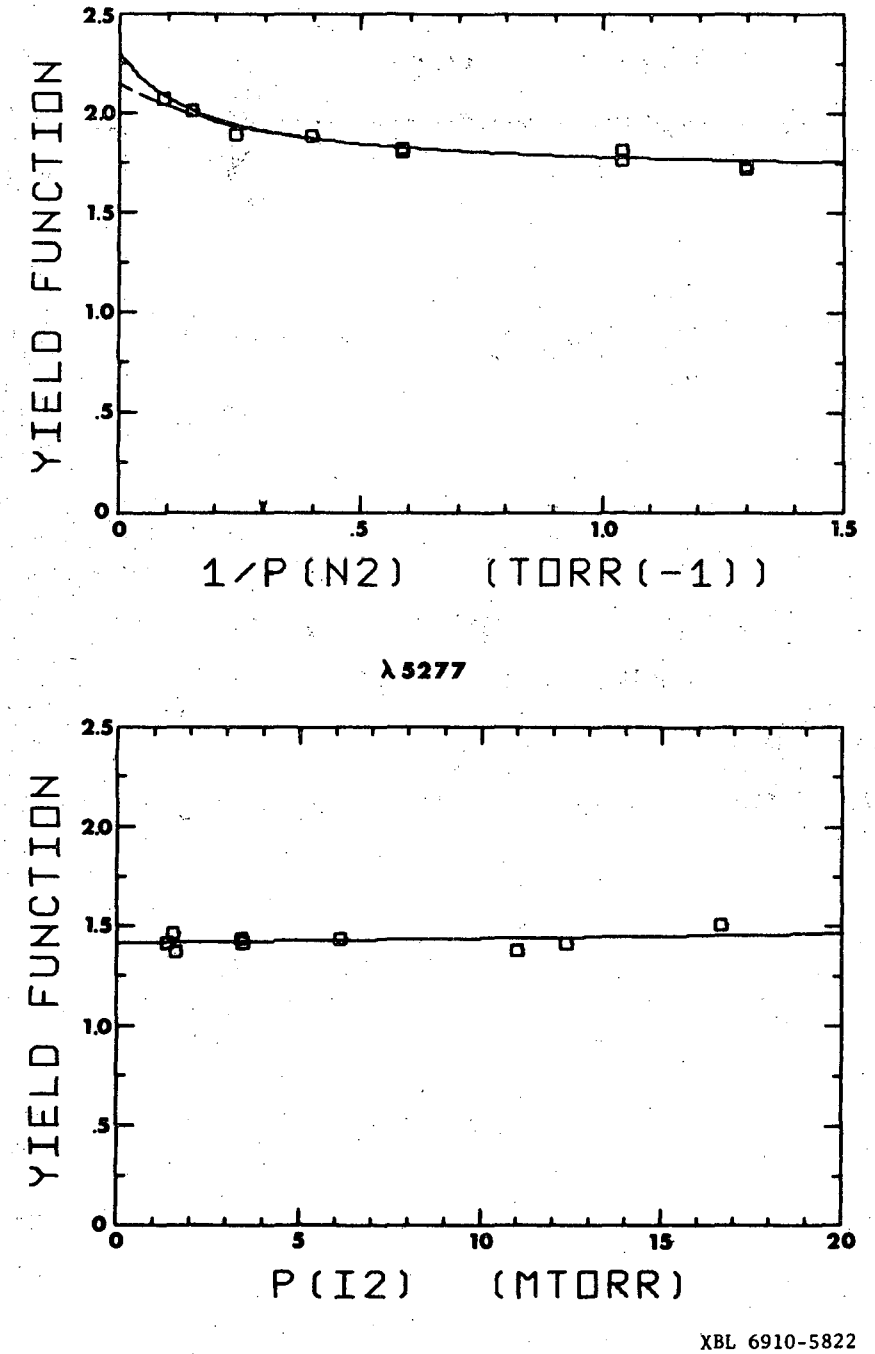

XBL 6910-5822

Fig. 22. Experimental yield function plot for 5277 A.

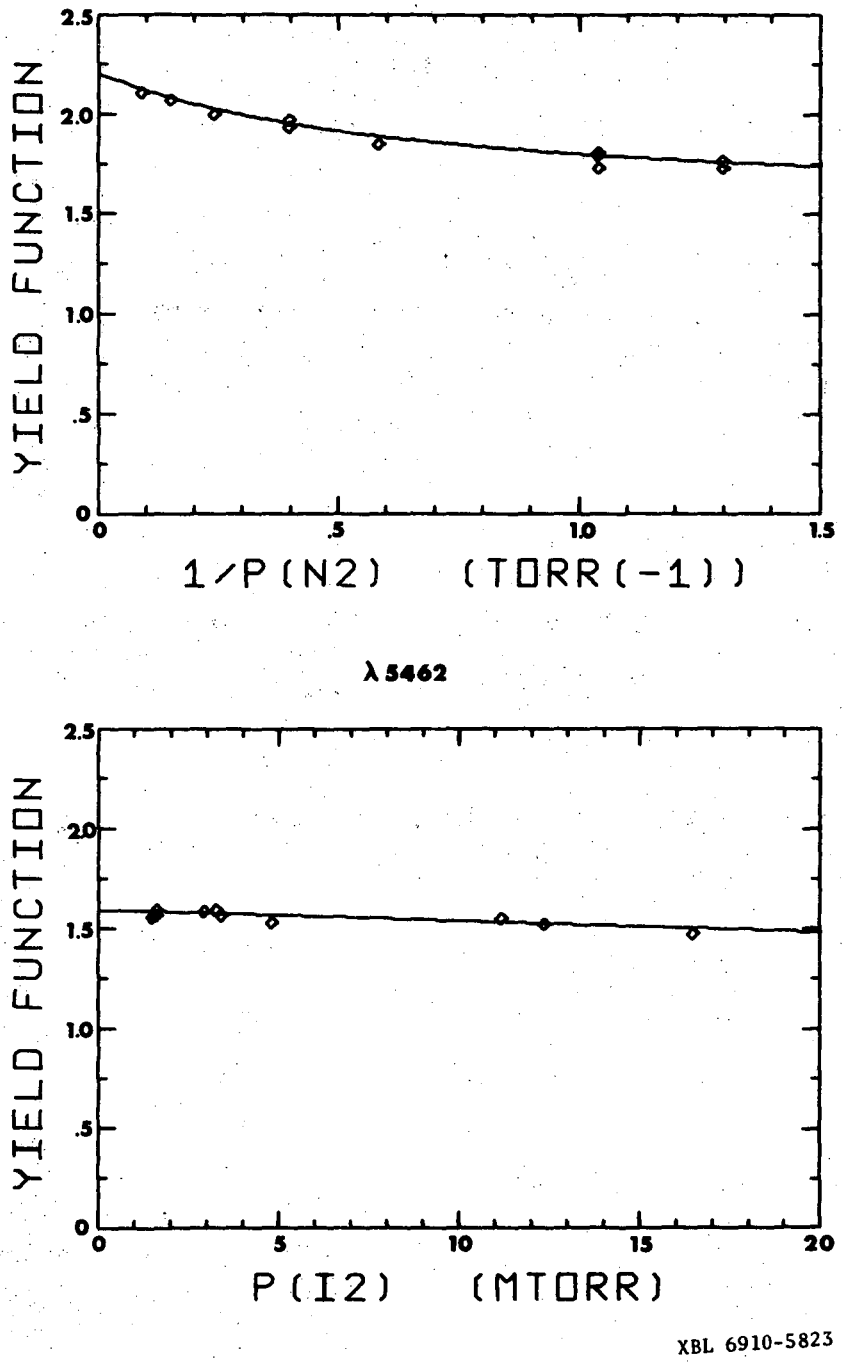

Fig. 23. Experimental yield function plot for 5462 A.

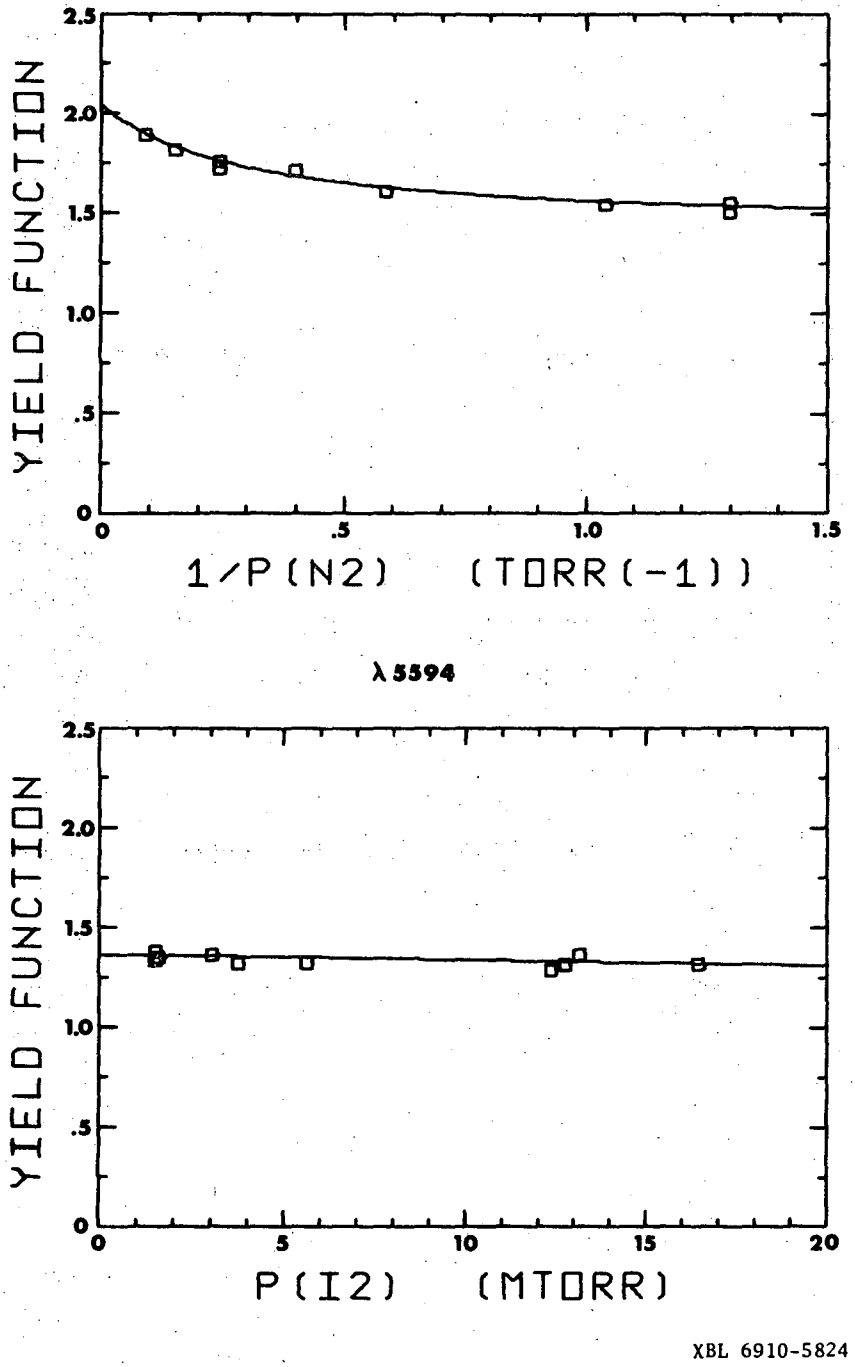

Fig. 24. Experimental yield function plot for 5594 A.

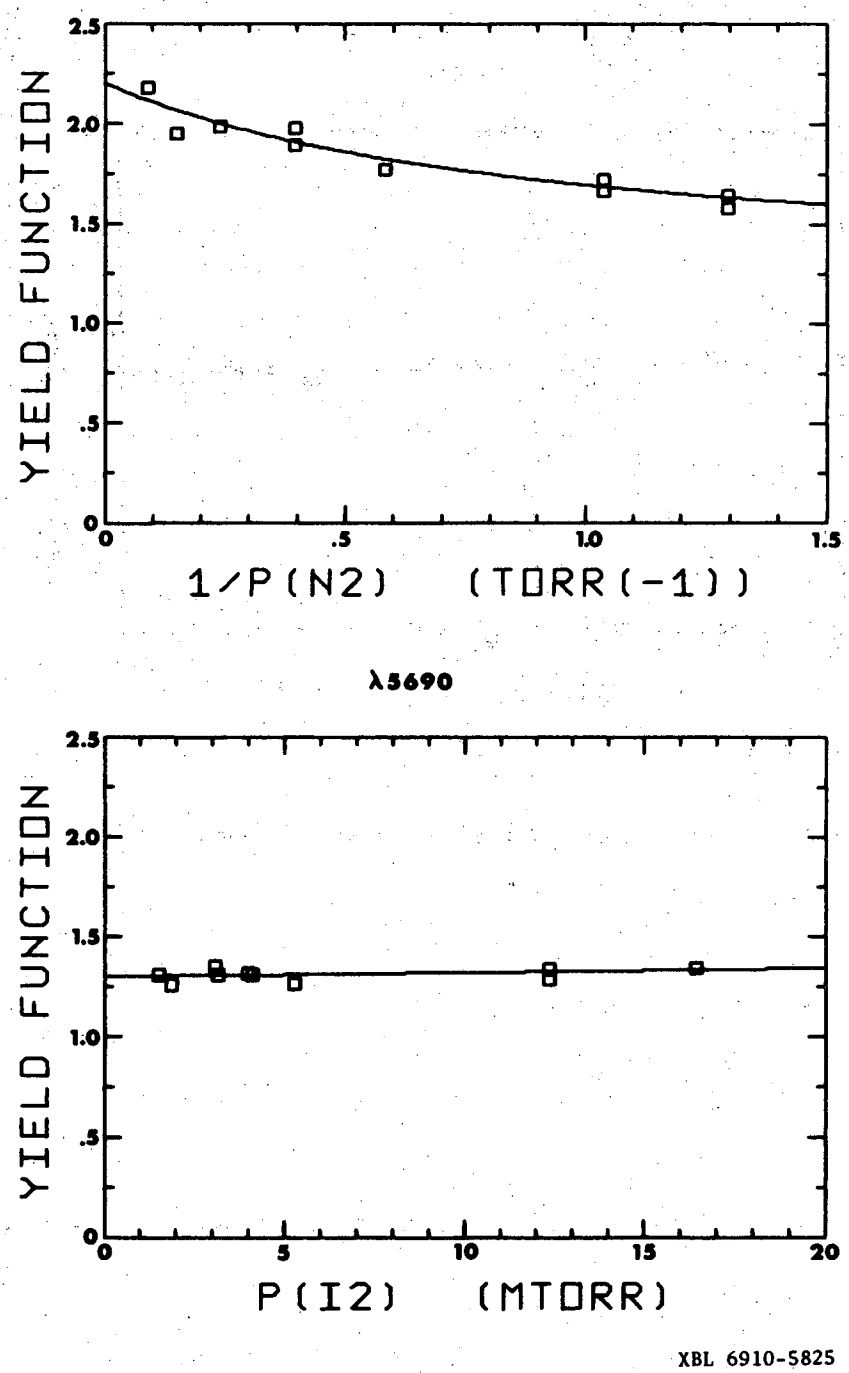

Fig. 25. Experimental yield function plot for 5690 A.

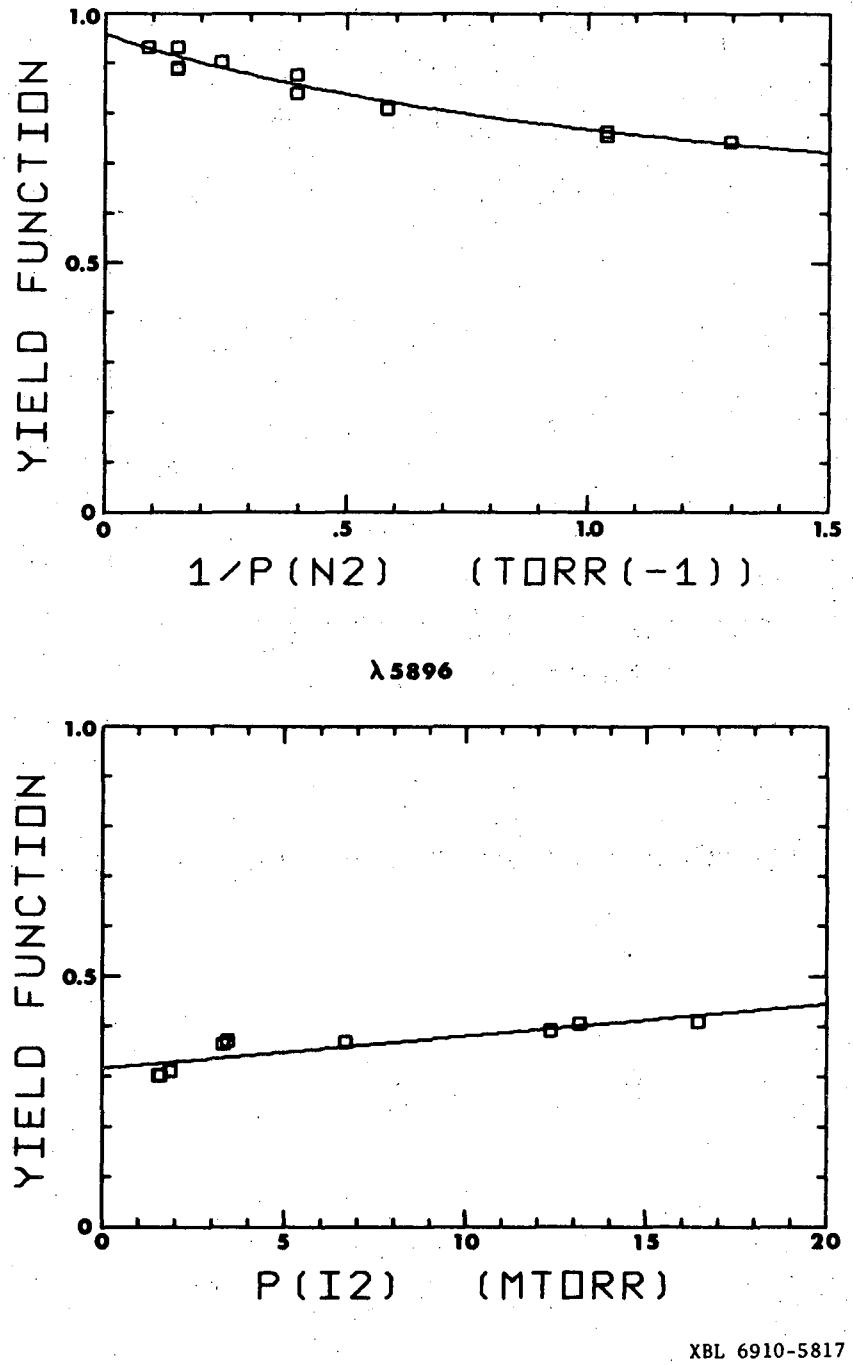

XBL 6910-5817

Fig. 26. Experimental yield function plot for 5896 A.

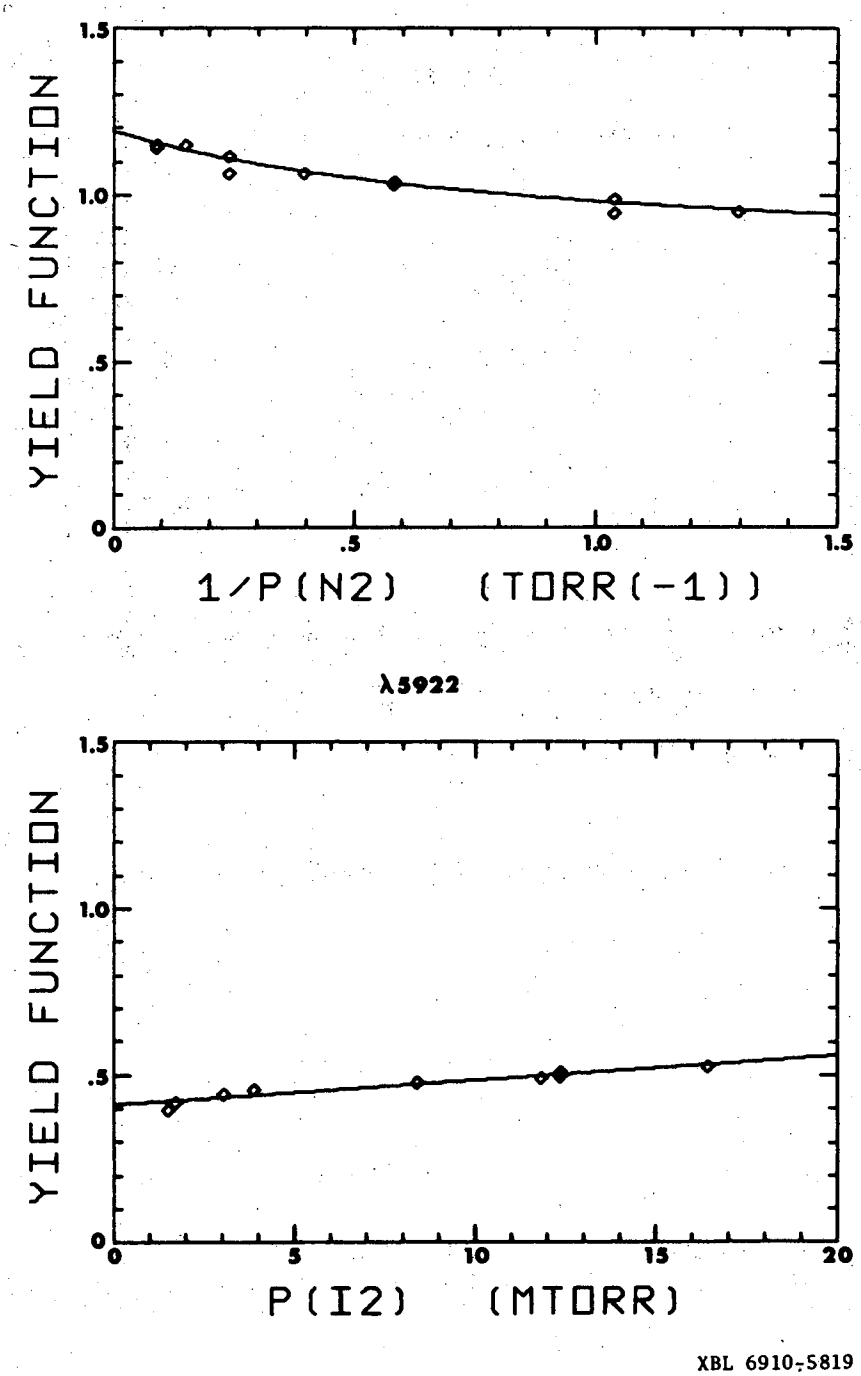

Fig. 27. Experimental yield function plot for 5922 A.

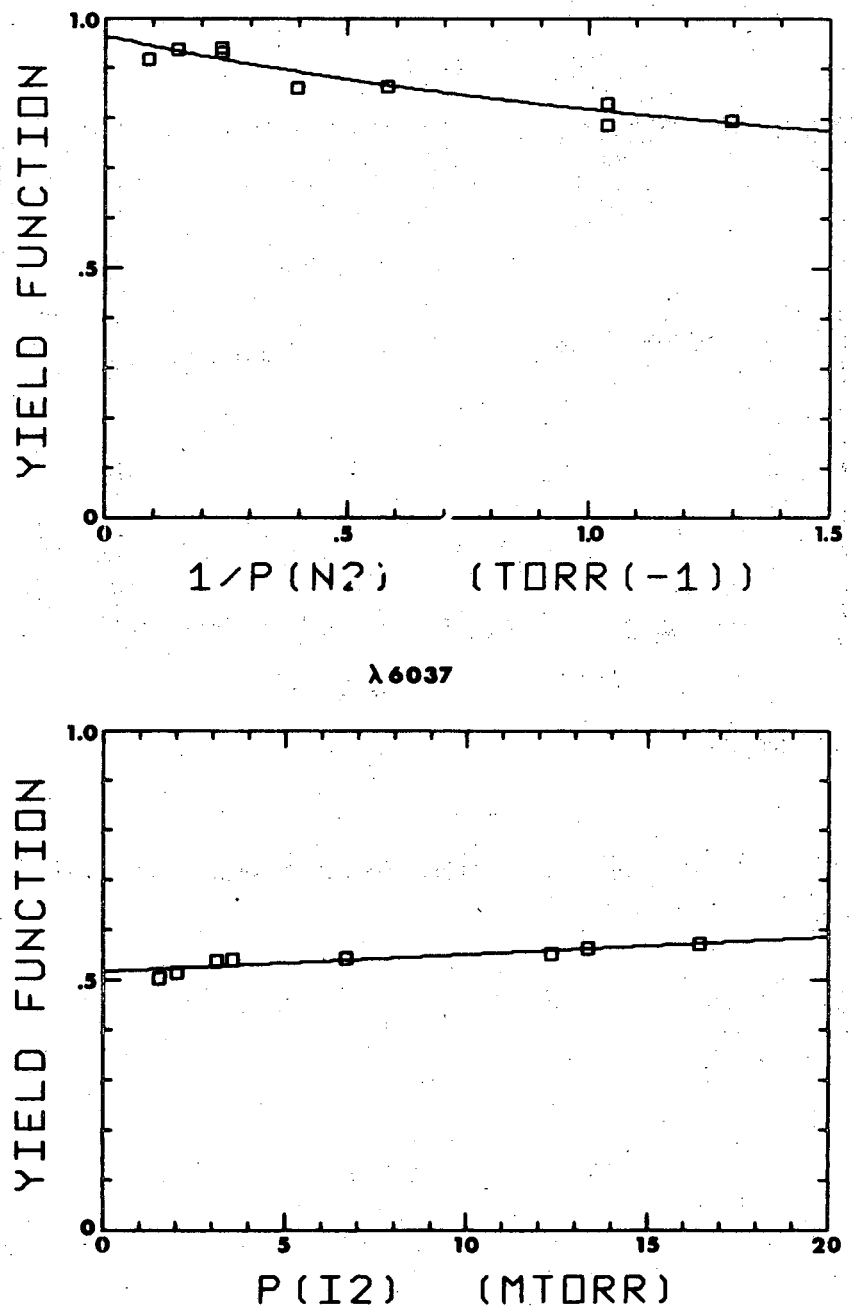

XBL 6910-5820

Fig. 28. Experimental yield function plot for 6037 A.

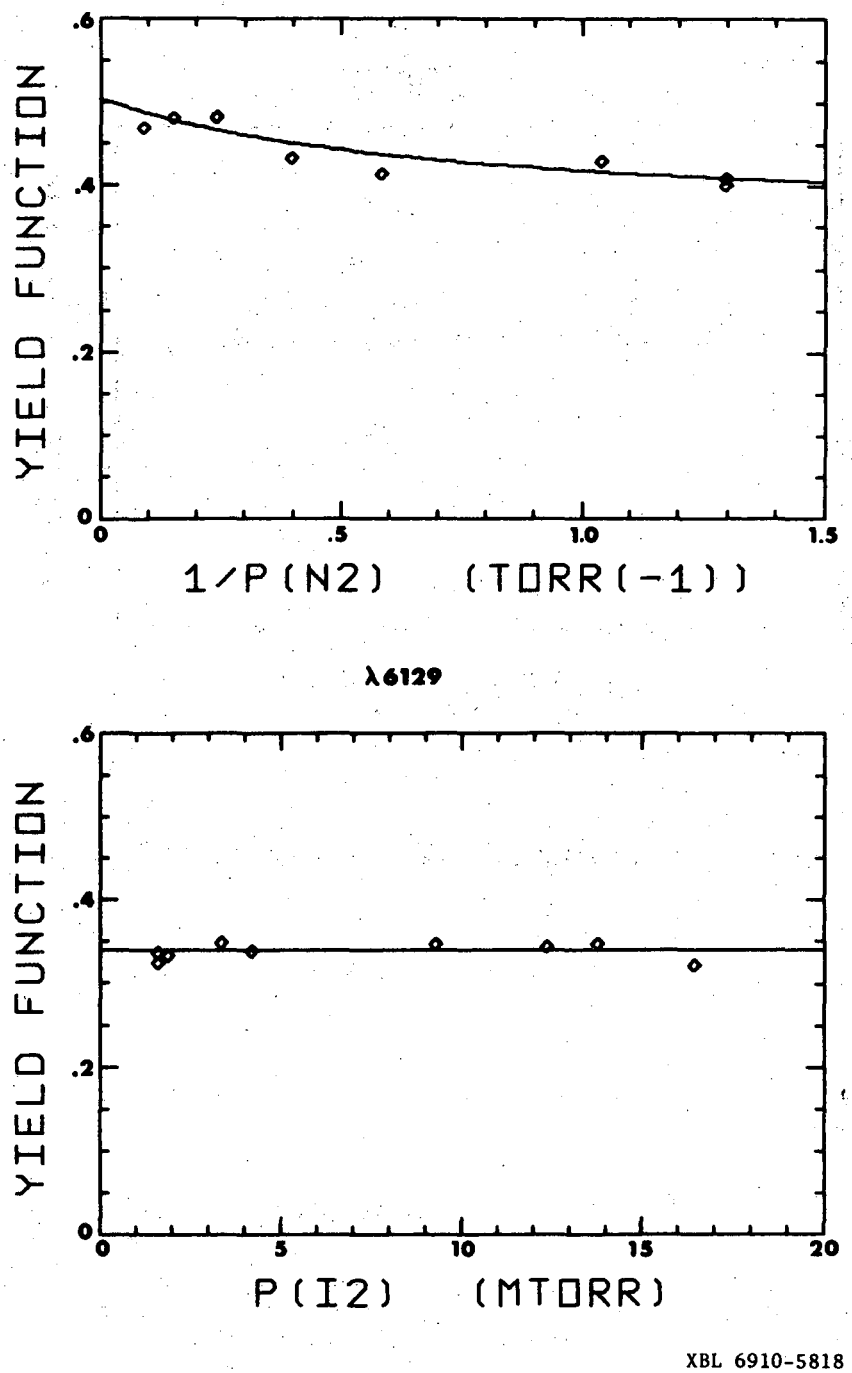

Fig. 29. Experimental yield function plot for 6129 A.

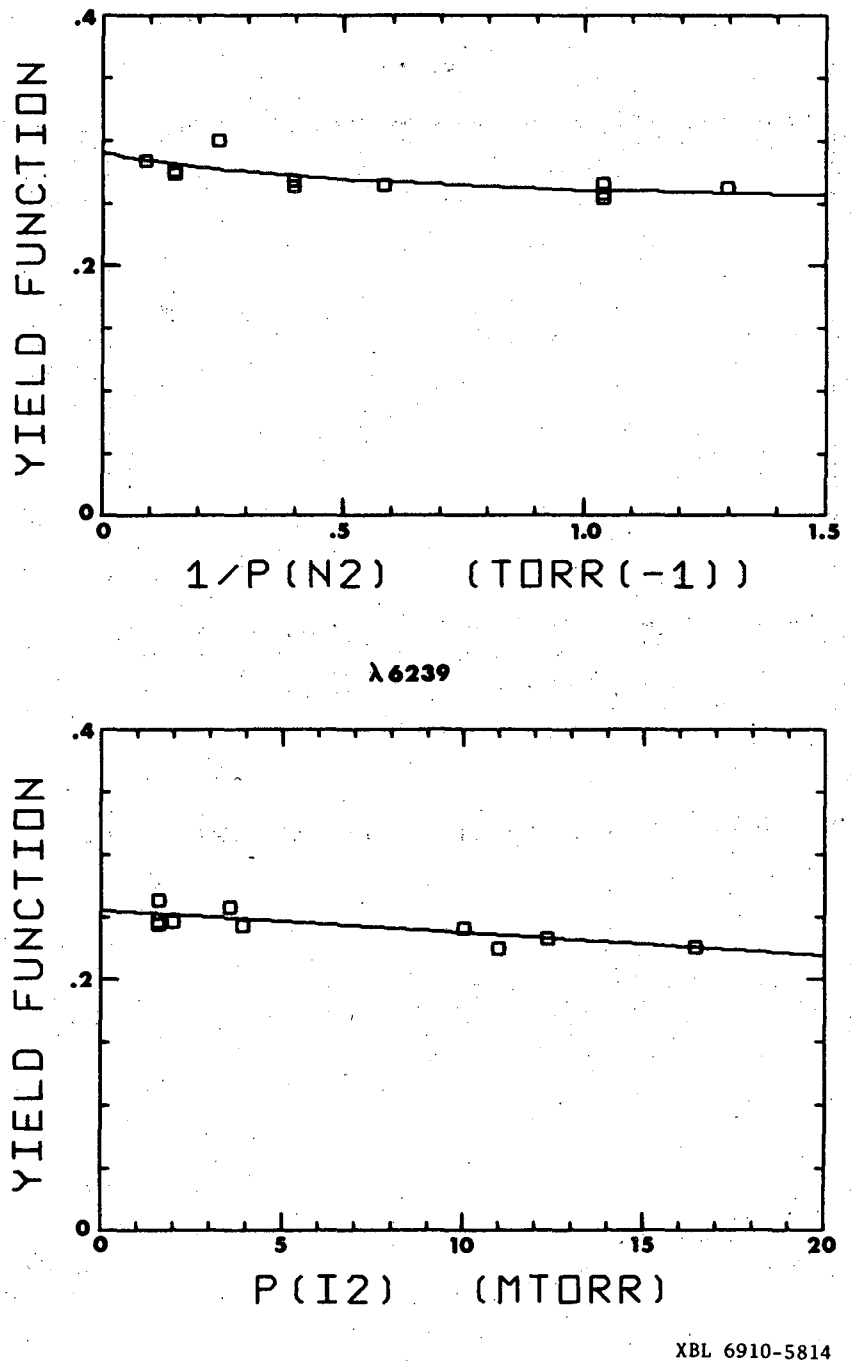

Fig. 30. Experimental yield function plot for 6239 A.

bution is not small, (1) remains a useful form for obtaining the intercept $Y_{max} = Y_1 + Y_2$; but c_1 and c_2 no longer have the significance indicated in Eqs. (B-19).[1] The calculated curves have the expected form, except for the results at 5277 A (and possibly at 5594 A), where the abrupt upswing near $1/P(N_2) = 0$ appears to be a mathematical artifact rather than a physical reality. Hence, the intercept in the 5277 plot was adjusted downward from 2.30 to 2.15, still within the standard deviation (which was unusually high for this particular set of points). The fit routine understandably failed to converge for the data at 5010 A, so the intercept was taken from a linear fit in this case.

The low-pressure results are illustrated in the lower plots. A good linear dependence is found for each filter. However, some of the slopes are anomalously low, with negative values occurring at λλ5462, 5594, and 6239. It is clear from (B-15) that negative slopes cannot arise from our proposed mechanism, so some unforeseen process or complication must be occurring. Several possibilities are discussed in Part 2 of this subsection. The quenching results will be dealt with in Part 4. However, we note for the sake of comparison that the greatest values for the self-quenching cross section are found at 5091 and 6037 A, where $d^2 \simeq 50\ A^2$, substantially lower than Chutjian's values, 66 and 74 A^2, respectively.

The results of the least-squares fits are summarized in Table 2.[2] Table 3 gives the quantum yields for unimolecular dissociative processes, obtained from the ratio Y_{min}/Y_{max}. (The values in parenthese for 5277 A

---

1. The least-squares fit of the high-pressure data to the form (1) followed the general methods outlined in the book by Deming (1964). The three quantities Y_{max}, c_1, and c_2 were treated as independent variables and determined by an iterative procedure from initial guesses. The results were used only to obtain the Y_{max} values; quenching constants for N_2 were obtained in a separate computation, detailed below.

2. As an indication of the reliability of these measurements, only eight or ten points of the total ~250 obtained were discarded before producing these results. The rejections were based on statistical and experimental grounds.

Table 2

PREDISSOCIATION EXPERIMENT

LOW PRESSURE RESULTS

WAVELENGTH (A)	NO. POINTS	INTERCEPT	ST. DEV.	SLOPE	ST. DEV.
5010	8	.615	.011	.00167	.00121
5091	10	.645	.010	.00524	.00090
5166	10	1.144	.008	.01160	.00088
5277	9	1.417	.022	.00251	.00262
5462	11	1.593	.009	-.00569	.00124
5594	10	1.361	.014	-.00264	.00149
5690	10	1.301	.016	.00220	.00198
5896	9	.318	.012	.00634	.00136
5922	9	.412	.009	.00729	.00094
6037	8	.517	.007	.00343	.00072
6129	9	.339	.006	.00006	.00063
6239	10	.255	.004	-.00183	.00048

FOREIGN GAS (N2) RESULTS

(DATA FIT TO FUNCTION Y = C(1+A/P)/(1+B/P))

WAVELENGTH (A)	NO. POINTS	INTERCEPT(C)	ST. DEV.	A	SDA	B	SDB
5010	9	.664	.008	0.	0.	0.	0.
5091	11	.924	.043	2.59	5.32	2.87	5.90
5166	13	1.837	.052	2.11	1.89	2.48	2.20
5277	10	2.302(2.15)	.143	4.48	2.47	6.11	3.62
5462	11	2.202	.048	1.04	.54	1.50	.71
5594	9	2.040	.075	2.36	.99	3.40	1.44
5690	10	2.201	.100	.60	.72	1.08	1.02
5896	11	.957	.021	.37	.43	.71	.57
5922	11	1.190	.023	.72	.52	1.09	.67
6037	9	.963	.029	.23	.69	.45	.86
6129	9	.503	.031	1.02	1.67	1.44	2.16
6239	11	.290	.017	1.27	3.34	1.53	3.84

Table 3

PREDISSOCIATION STUDY

QUANTUM YIELD RESULTS

WAVELENGTH (A)	ATOMIC QUANTUM YIELD	ST. DEV.
5010	.926	.020
5091	.698	.034
5166	.623	.018
5277	.616 (.66)	.039
5462	.723	.016
5594	.667	.025
5692	.591	.028
5896	.332	.014
5922	.346	.010
6037	.537	.018
6129	.673	.043
6239	.878	.053

are the adjusted results, mentioned above.) We can see from Table 3 and Fig. 31 that the yield increases at both ends of the banded spectrum of I_2, with possibly an additional maximum at ~5450 A and a minimum at ~5900 A. The total quantum yield will be further analyzed in terms of contributions from direct dissociation and spontaneous predissociation in Part 3.

The quantum yield results in Table 3 are in excellent agreement with the findings of Chutjian and James (1969), whose work indicated 67% spontaneous predissociation at 5450 A and 33% at 5900 A. When the effects of underlying continuum absorption are considered below, the agreement will diminish only slightly. Wassermann and co-workers (1968a,b) observed "parallel" production of atoms in continuum and banded-region excitation down to pressures even lower than those employed in this study. Their results were presented in a log-log display, which obscures the detailed pressure dependence; however, interpreted in terms of the mechanism given in this work, their parallel behavior indicates 100% predissociation and 0% fluorescence. As was noted in Section II, acid-treated quartz continues to degas slowly for weeks or months; if the cells used by Wassermann, et al. were not freshly evacuated before their experiments, quenching by impurities could have produced their high yields. Interestingly enough, their earlier results (Falconer and Wassermann, 1966) from a study of the photosensitized isomerization of cis-butene-2 indicated a low-pressure atomic yield of 77% for 5460 A excitation, in good agreement with the present findings.

b. <u>(v'v") Distributions</u>

Knowing the Franck-Condon factors for the B-X system enables us to calculate the distributions of v' and v" levels involved in the absorption process for the various filters. Chutjian and co-workers (1967) have given approximate v' regions excited for most of the filters used in this

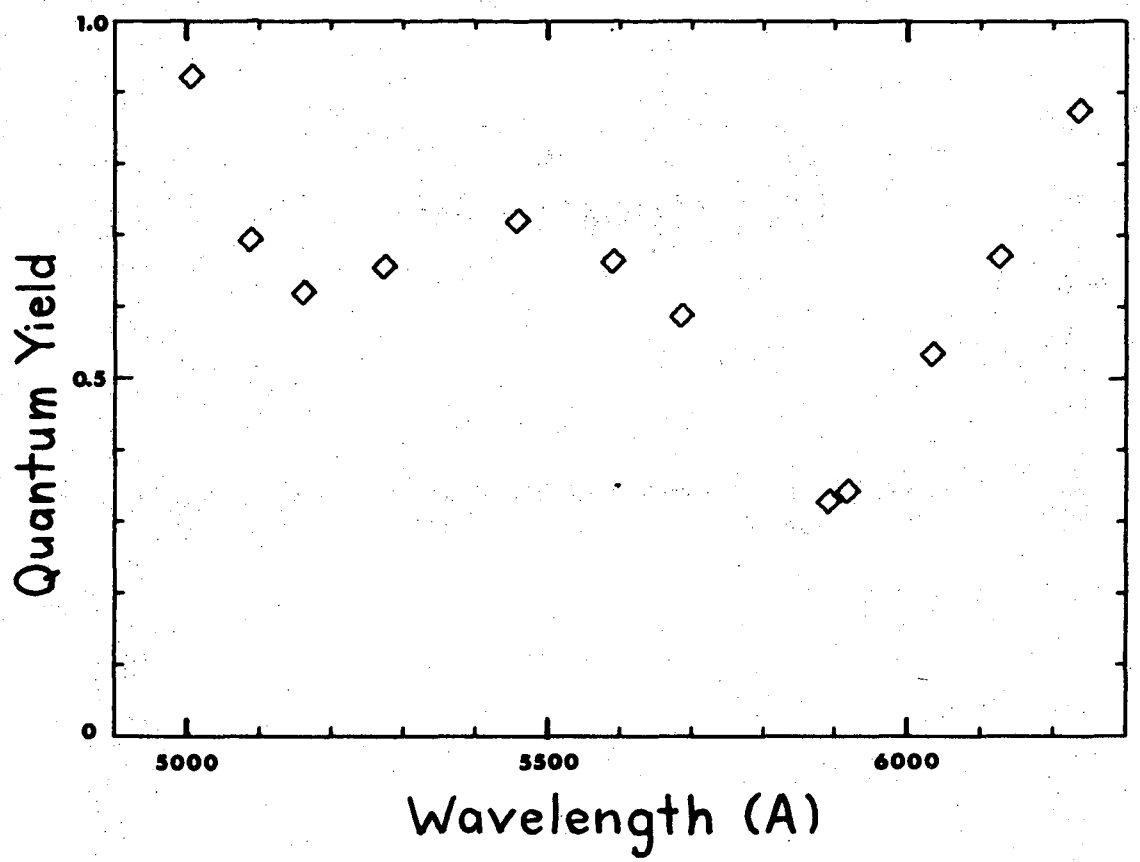

XBL 6910-5815

Fig. 31. Quantum yield for unimolecular dissociation of $I_2^*(B)$ as a function of excitation wavelength.

work, but r-centroids and v" distributions are lacking. In addition, several of the filters used here were not used in their work. Therefore a computer routine was written to calculate the desired information for the new filters and was used to recalculate the distributions for the old.

From formulas given in Section III we know that the absorption by a given rotational line will be proportional to the rotational line strength (divided by the degeneracy $(2J''+1)$), the Franck-Condon factor, the frequency of the transition, and the population of the absorbing state. The last of these is governed by the rotational degeneracy and Boltzmann factor. To calculate the total absorption for a given filter, we must sum all the contributing lines.

$$\text{Absorption} \quad \propto \bar{\nu} \ \Sigma \ F_\lambda \ s_{J,i} \ e^{-\epsilon_i/kT} \ |\langle v''|v'\rangle|^2 \qquad (2)$$

where F_λ is the wavelength distribution of quanta for source and filter, and the sum is carried out over all rotational lines in the region of transmission for the particular filter. Here the wave number $\bar{\nu}$ for the transitions is treated as a constant for a given filter, in which case it will have no effect on the (v',v") distributions. Later, in comparing the total excitation for different filters, $\bar{\nu}$ will be included.

The calucations were carried out assuming the source quantal distribution was constant over the transmission band of the filter and taking F_λ to be a Gaussian function of λ.[1] For this case s_J was $(J+1)$ for the R branch and J for the P branch, and the 5:7 intensity alternation due to nuclear spin degeneracy was ignored.[2] The Franck-Condon factors used were those calculated by Cunningham to v' = 47,[2] all for rotationless RKR

1. The Gaussian form seemed to represent the transmission of the filters fairly well over the region $F_\lambda > 10\% \ F_{\lambda,max}$.

2. See footnotes, Section III-D.

potential curves. The frequencies of the lines were calculated from the constants of Steinfeld, et al. (1969) for the B state and Verma's results for the X state,[1] and were converted to standard-air wavelengths with the help of Edlen's (1953) formula. The computation included lines of both R and P branches up to J = 300 (well over 99% of the total rotational population), for all bands with v" = 0-5 having origins within 2-3 filter half-widths on the red side and 3-4 half-widths on the blue side of the filter transmission maximum.

The results are summarized in Table 4. The distributions for the 5010 and 5091 filters are guesses based on the conclusions of Steinfeld and co-workers (1969).[2] All other tabulated values resulted from the computation procedure outlined above, except that some "guessed" F-C factors were used in the calculation for the 5166-A filter. It is interesting to note how difficult it is to absorb into low v' levels at the red end of the spectrum. For the 6037, 6129, and 6239 filters the v' population distribution changes only slightly, while the v" distribution shifts to higher levels, as the absorption "climbs" up the right-hand wall of the X-state potential curve. The average r-centroids descriptive of the absorption process change only slightly -- from 2.701 A at λ5462 to 2.806 A at λ6239.

---

1. The value of Steinfeld, et al. for $\omega_e y_e'$ appears to be missing a minus sign. With this change, the calculated energies are in agreement with earlier results of Steinfeld, Zare, Jones, Lesk, and Klemperer (1965). Verma's ΔG values were used to produce the constants ω_e = 214.577, $\omega_e x_e$ = .6524, $\omega_e y_e$ = .005974, for the first six vibrational levels of the ground state.

2. These authors point out that their constants are good only to v' ~ 52. Even with poor constants the F-C factors up to v' ~ 60 should be suitable in this type of calculation involving low v" levels. However, the version of Zare's program on hand was not capable of performing the numerical integrations for the vibrational functions when the integration intervals were too large, a situation which arises when trying to compute functions for high v' levels and low v" levels for states with greatly differing r_e values. Therefore only levels to v' = 47 were obtained.

Table 4. Filter characteristics and I_2 $B \leftarrow X$ excitation distributions

Wavelength (A)	Maximum Transmittance	Half-width (A)	v' levels	v" levels
4919	.60	66	(continuum)	0 (5%),1 (40%),2 (45%)
5010	.59	30	75-95	0 (20%),1 (40%),2 (35%)
5091	.73	28	55-75	0 (45%),1 (30%),2 (20%)
5166	.78	47	40 (5%),41 (9%),42 (11%) 43 (11%),44 (9%),45 (7%) 46 (5%)	0 (67%),1 (25%),2 (8%)
5277	.77	50	33 (12%),34 (20%),35 (21%) 36 (15%),37 (9%), 38 (5%)	0 (93%),1 (2%),2 (4%)
5462	.77	51	24 (9%),25 (24%),26 (25%) 27 (16%),28 (10%),29 (5%)	0 (81%),1 (13%),2 (5%)
5594	.73	56	19 (6%),20 (19%),21 (21%) 22 (20%),23 (17%),24 (8%)	0 (56%),1 (40%),2 (1%) 3 (3%)
5690	.45	138	16 (6%),17 (11%),18 (16%) 19 (18%),20 (17%),21 (12%) 22 (8%)	0 (39%),1 (53%),2 (5%) 3 (3%)
5896	.78	58	12 (9%),13 (21%),14 (20%) 15 (24%),16 (14%)	0 (8%),1 (44%),2 (42%) 3 (2%),4 (3%)
5922	.72	85	11 (6%),12 (14%),13 (21%) 14 (21%),15 (19%),16 (10%)	0 (6%),1 (41%),2 (45%) 3 (5%),4 (3%)
6037	.81	86	9 (6%),10 (13%),11 (22%) 12 (24%),13 (18%),14 (9%)	0 (2%),1 (20%),2 (51%) 3 (25%),4 (1%),5 (2%)

Table 4 (continued)

Wavelength (A)	Maximum Transmittance	Half-width (A)	v' levels	v" levels
6129	.54	84	8 (9%),9 (18%),10 (24%) 11 (24%),12 (14%),13 (5%)	0 (0%),1 (8%),2 (39%) 3 (45%),4 (6%),5 (2%)
6239	.37	96	6 (5%),7 (13%),8 (22%) 9 (26%),10 (20%),11 (10%)	0 (0%),1 (2%),2 (19%) 3 (50%),4 (28%),5 (1%)

According to Kronig's (1928) results the predissociation rate for the transition $0_u^+ \rightarrow 1_u$ should be proportional to $J(J+1)$. In that case the "effective" v' distributions might more properly be calculated by including this J dependence in the sum (2). The effect would be to shift the distributions to slightly lower v' levels, with perhaps $\Delta v' = -1$. In the present study spectral resolution was too low to allow for a meaningful analysis of k_p in terms of individual rates $k_p(v')$, so this modification was not felt to be worthwhile. A method for observing the predicted $\sim J^2$ dependence will be described below.

2. Possible Systematic Errors

a. Geometrical, Thermal, and Associated Complications

Previously we noted the anomalous behavior of the yield function at low $P(I_2)$. There are a number of possible complications which could account for the small slopes in the low-pressure data plots. Fortunately we can dismiss most of them forthwith.

It is doubtful that "geometrical" errors could have been introduced into the procedures in other than random ways, in which case they would detract from the precision of the results but would not affect the accuracy. The focusing of the tungsten lamp, the masking of the condensing lenses, and the positioning of the cell at the outset of each run were all operations which could conceivably introduce wavelength-dependent differences. A more serious problem was the positioning of the filters for each set of readings. In this case a slight tilt off the normal to the incident light beam would cause a shift to the blue in the transmission peak, so care was taken to employ constant orientation at all times.

Although the subsidiary transmission peaks in the visible were "blocked" for all the filters used, substantial transmission in the IR

was observed for several. One of these (5462 A) was checked for the possibility of atom production outside the visible region. Absolutely no signal was observed for excitation in the UV and IR spectral regions.

In the arrangement used in these experiments (Fig. 6) the image of the tungsten filament was focused roughly in front of the fluorescence window in the predissociation cell, diverging only slightly at both ends of the cell. This arrangement insured that virtually all atoms were produced in a region removed from the cell walls, since the $I_2^*(B)$ molecule can travel less than 1 mm during its lifetime. On exiting, the light beam was directed through the iodine atomic source. This had no apparent effect on the lamp as indicated by the constancy of the scattered-light background signal on irradiation by the unfiltered tungsten lamp with the I_2 frozen out of the cell.

The presence of residual concentrations of atoms, produced by visible absorption from the iodine lamp, could lead to concentration-dependent errors. If the recombination of the I-atoms is not strictly linear, the relation between the yield function and the incremental atomic concentrations will be different at high and low $P(I_2)$ values, because the background atomic concentration increases with $P(I_2)$. Of course the signal vs. [I] dependence changes even more radically, as the background included fluorescence from I_2 and the residual I-atoms. However, the non-linearity correction method is essentially a calibration procedure, and as such should account for all these effects within the flexibility of the quadratic form used for the correction. (To check on this, a few points were measured at $P(I_2) = 30.5$ mtorr and found to agree with the data at lower pressures.) In no way can such effects account for the spread of slopes from negative values to

values near the anticipated results in the low-pressure yield function plots.

All thermal complications in the experiments were negligible. Heating by microwaves and by the discharge lamp increased the temperature locally at one end of the cell by 10-20 degrees, or as much as 60-80 degrees at the lamp window, a very small area. Homogeneous thermal pyrolysis is impossible for the low exciting-light levels used. A rough calculation shows that at most one in 200 I_2 molecules absorbs a photon (energy ~75-100 kT) in each second. At the low pressures of these experiments, each I_2 molecules collides with the walls 10^2 to 10^4 times per second. Furthermore most (~60-80%) of the absorbed energy is dissipated in recombination at the walls, so the temperature gradient in the cell must be exceedingly small. As with the other problems, thermal effects can not possibly explain the variety of slopes observed in the low-pressure data plots.

Dissociation of I_2 by microwaves was considered by Wassermann, et al. (1968b) and found not to occur. A quantitative estimate of this possibility could not be obtained from the present work, but no changes were observed when the cell was shielded with metal foil.

b. Non-linear Absorption

Non-linear absorption is a likely cause of the variation in slope for the low-pressure data. The second term in the expansion of $(1 - e^{-\alpha_\nu [I_2]})$ has a negative sign, which would tend to decrease the slopes. The effect would be more pronounced in regions where the absorption comes from a few very strong lines and would be nominal in regions where many weak lines overlap to give a semi-continuous absorption. The continuum absorption at 4919 A can be assumed linear for all iodine concentrations used here.

We can estimate the magnitude of the effect using the line absorption results of Chutjian and James (1969). From the relationships in (III-A), we calculate an A value of 2.1×10^4/sec for an individual rotational line in the (25,0) band at ~5460 A. The corresponding k_o value for a Doppler absorption coefficient is $k_o(cm^{-1}) = 5.6 \times 10^{-15}$ N. At room temperature the fraction of I_2 molecules in, for example, the J" = 30 level of v" = 0 is .0050; and $k_o \ell$ = .20 for the predissociation cell at $P(I_2)$ = 20 mtorr. From Eq. (III-B-16) we see that the deviation from linear absorption is 6-7% for this particular line (R or P) under these conditions.

We may broaden this approach to include all the rotational lines in the band. Then the total band absorption, assuming no overlapped rotational lines, is proportional to

$$\text{Band Absorption} \propto \sum_{J=0} \left[(k_o\ell)_J - \frac{(k_o\ell)_J^2}{2\sqrt{2}} + \ldots\right] \qquad (3)$$

and

$$(k_o\ell)_J = 6.5 \times 10^{-14}\, N_{J,v''=0} \qquad (4)$$

so that

$$\text{B.A.} \propto 6.5 \times 10^{-14} \sum_{J=0} \left[N_{J,v''=0} - \frac{6.5 \times 10^{-14}}{2\sqrt{2}} N^2_{J,v''=0} + \ldots\right] \qquad (5)$$

The deviation from linearity is simply the absolute value of the ratio of the second term to the first term in the summation. We have

$$\sum N_{J,v''=0} = \frac{N_T}{1.55} \qquad (6a)$$

$$\sum N^2_{J,v''=0} = \left(\frac{N_T}{1.55}\right)^2 \frac{1}{q_r^2} \sum (2J+1)^2 e^{-2(\theta r/T)J(J+1)} \qquad (6b)$$

With a little effort it can be shown that the sum in (6b) is for this case approximately

$$\Sigma \ (2J+1)^2 \ e^{-2\left(\theta_r/T\right)J(J+1)} = \frac{q_r}{2} \left(1 + \sqrt{\frac{\pi \ q_r}{2}}\right) \qquad (7)$$

so that

$$\Sigma \ N_J^2 = \left(\frac{N_T}{1.55}\right)^2 \frac{1}{2 \ q_r} \left(1 + \sqrt{\frac{\pi \ q_r}{2}}\right) \qquad (8)$$

Therefore the desired ratio is

$$\left| \frac{\text{2nd term}}{\text{1st term}} \right| = 1.26 \times 10^{-16} \ N_T \qquad (9)$$

With an iodine pressure of 20 mtorr, the deviation from linear absorption is accordingly 8% for the (25,0) band.[1] This value was calculated assuming $|Re|^2 = .837$ debye^2. Mulliken[2] has estimated a value of 1.34 for $|Re|^2$, which would increase the non-linearity to ~12%. Allowance for overlapping lines could raise the deviation considerably. For example, when the rotational constants fulfill the relationship $(B_{v'}/B_{v''}) = \frac{n}{2+n}$ for integer values of n, the lines R(J) and P(J-n) will coincide exactly when the terms in $J^2(J+1)^2$ are negligible; and the deviation from linearity will be twice as great. For the (23,0) band the above ratio is .6655, so that R(J) and P(J-4) will overlap for much of this band. In general, though, the probabilities for coincidences of strong lines will be small, so that overlapping lines should raise the deviation only 2-3% (absolute).

From Fig. 23 the yield function for 5462-A excitation is 7% lower at 20 mtorr than at $P(I_2) = 0$. The calculated increase from quenching, taking $\tau = 6.7 \times 10^{-7}$ sec and $k_q = 1.53 \times 10^4$/(sec mtorr), is 7.5%. The

1. The inclusion of additional terms in the equivalent width relationship will decrease this value a bit. For instance when $(k_o \ell)$ is .30, the 2nd term is 10.6% of the 1st in absolute value, and the 3rd is .87%.

2. See the discussion below on continuum contributions to the total absorption. The value 1.34 is calculated from Mulliken's revised dipole strength of 582×10^{-20} cm^2. The latter is obtained from the extinction curve, but it is not clear which curve was used.

non-linearity in the absorption would give a net change of ~ -4% in Y at 20 mtorr, in fair agreement with the observations. The behavior of Y at 5091 and 5166 A, and in the 5900 A region is in near agreement with predictions from Chutjian's (1966) results; and we note that in these regions the absorption is spread out among a larger number of weaker lines, so the total absorption is expected to be more linear. The results at 6129 and 6239 A should likewise display little deviation from linear absorption; unfortunately they do differ markedly from expected behavior. Consequently the non-linear absorption effect must be accepted as only partial explanation for the anomalies.

The values for the zero-pressure intercepts cannot possibly suffer from non-inear absorption complications, because points were measured at pressures down to 1.5 mtorr, where deviations are entirely negligible for all wavelengths. Similarly the high-pressure intercepts should be free of such effects, though such phenomena as collision-sensitized absorption could lead to errors. Such a possibility seems remote, particularly for the low N_2 pressures employed here.

Several authors have discussed the phenomenon of pressure-narrowing of rotational lines in electronic spectra of some diatomic molecules (Breene, 1957; Bird, 1963). If this phenomenon occurs in I_2, it must of course increase the deviation from linear absorption and lead to more negative slopes in the low-pressure data plots. No estimate of the magnitude for such an effect can be given by this writer at present.

c. Metastable Iodine Atoms and I_3

Earlier we discussed the relaxation of $I(^2P_{1/2})$ atoms in a semi-quantitative way and argued that any errors from these complications should be small, though possibly not negligible. Quantitatively we

can show that the ratio of $^2P_{1/2}$ atoms to $^2P_{3/2}$ atoms produced in steady-state excitation into the continuum is

$$\frac{[I(^2P_{1/2})]}{[I\ (^2P_{3/2})]} = \frac{k_w'}{k_w' + 2k_Q} \qquad (10)$$

where k_Q represents the total rate for relaxation to the ground state by all processes. k_w' is the wall-recombination rate, assumed to be the same for both types of atoms; it is a function of $P(I_2)$ and $P(N_2)$. From the results of Donovan and Husain, we calculate the constant k_Q to be $(8 + 67 + 260)/\text{sec} = 335/\text{sec}$ when $P(N_2) = 10$ torr and $P(I_2) = 1.6$ mtorr. The three terms in the sum represent radiative decay, quenching by N_2, and quenching by I_2, respectively. From the earlier discussion k_w' is guessed to be less than 30/sec, giving a ratio of ~.045 in (10), for an error of less than 3% in Y_{max}.

A comparison of the observed values for Y_{max} with those calculated from the extinction coefficient of Rabinowitch and Wood reveals a discrepancy of ~25% as indicated in Table 5. The calculated Y_{max} values were taken from the product of extinction coefficient, filter area, and the black-body quantum flux (including emissivity correction) at each peak transmission wavelength, all relative to the excitation at 4919 A. The 25% disparity may be indicative of an incorrect value for the extinction coefficient ϵ_ν at ~4900 A. In this regard, it may be noted that Rabinowitch and Wood (1936b) obtained yields of 1.14 and 1.10 for collisional quenching by foreign gases at high pressures. They assumed a yield of 1.00 above the dissociation limit and calculated the relative absorption, in the three regions they investigated, from their own extinction coefficient measurements. On the other hand extinction coefficients are generally easy to measure for continuous absorption, but the banded region values could be too low if the lines were not adequately broadened by the foreign

Table 5. Comparison of observed Y_{max} values with those calculated from extinction curve of Rabinowitch and Wood

Wavelength (A)	Y_{max} (obs)	Y_{max} (calc)	$\frac{Y_{max}(obs)}{Y_{max}(calc)}$
4919	1.00	1.00	1.00
5010	.66	.59	1.13
5091	.92	.76	1.21
5166	1.84	1.50	1.23
5277	2.15	1.69	1.27
5462	2.20	1.64	1.34
5594	2.04	1.52	1.34
5690	2.20	1.91	1.15
5896	.96	.76	1.26
5922	1.19	.95	1.25
6037	.96	.74	1.30
6129	.50	-	-
6239	.29	-	-

gases they used. In that case one would still expect the values to be good in regions of weak absorption by many lines, and the observed/calculated ratio in Table 5 should decrease to ~1.0 for these regions.

By allowing for the possibility of a very high sticking probability for $^2P_{1/2}$ atoms in wall collisions, we might increase the explainable disparity between observed and calculated Y_{max} values to 10-15%, certainly no more. Thus it seems likely that reactions of the type (B-7) may be non-ignorable.

$$I\ (^2P_{1/2}) + M \rightarrow IM \qquad \text{(B-7a)}$$

$$I\ (^2P_{1/2}) + AM \rightarrow IM + A \qquad \text{(B-7b)}$$

When spectroscopic-grade argon was used as a quencher, the results were in good agreement with those measured using N_2, so the latter seems a poor candidate for M in (B-7).[1] I_3 is thought to be a fairly stable complex by some kineticists, but its existence has never been proven by direct methods. If I_2 can react preferentially with $^2P_{1/2}$ I atoms and tie up an appreciable fraction of the latter in the I_3 complex, experimental values of Y_{max} will be too large. This hypothesis would predict yields <u>lower</u> than unity in the work of Rabinowitch and Wood (unless I_3 absorbs strongly in the region of the I_2 B-X system), because their I-atom concentrations were determined from the decrease in the I_2 visible absorption. The results of both studies are consistent with the following mechanism:

$$I\ (^2P_{3/2}) + I_2 \xrightarrow{k_1} I_3 \qquad \text{(11a)}$$

$$I\ (^2P_{1/2}) + I_2 \xrightarrow{k_2} I_3 \qquad \text{(11b)}$$

---

1. Results at six wavelengths using P(Ar) = 10 torr were all lower than the fitted curves for N_2 in Figs. 19-30. The average discrepancy was -3.1%, in keeping with the lower efficiency of Ar as a quencher of I_2*(B) (Berg, 1933).

$$I_3 + I \xrightarrow{k_3} 2\ I_2 \qquad (11c)$$

$$I_3 + M \xrightarrow{k_4} I_2 + M + I\ (^2P_{3/2}) \qquad (11d)$$

k_2 must be much greater than k_1, because the overall recombination is predominantly heterogeneous; and k_3 must be large enough to keep the stationary-state I_3 concentration low. Furthermore (11c) must be significant relative to (11d), or the net reaction is simply the quenching of $I(^2P_{1/2})$.

At low pressures we should consider, in addition to (11), the reactions of $^2P_{1/2}$ atoms with the walls. If $^2P_{1/2}$ atoms are removed from the reaction vessel with probability unity per wall collision, the values of Y_{min} would be too large by nearly a factor of 2. The error would decrease with $P(I_2)$, as an increasing fraction of the (1/2) atoms relax to (3/2) before reaching the cell walls. The "well-behaved" data at 5091, 5166, and 5900 A show that such effects must be small. Furthermore if such an error were large, we might expect to find some Y values measured at low $P(N_2)$ lower than the measured Y_{min}: None of the data plots exhibits such a behavior. We conclude that the results for Y_{min} are at most 10% too high.

One additional process involving I_3 should be mentioned:

$$I_2^*(B) + I_2 \longrightarrow I_3 + I \qquad (12)$$

If the quenching proceeds in this manner, with (11c) accounting for the removal of I_3, the net slope in the low-pressure yield function would be halved. Also, the efficiency of (12) could vary with v'. There is no reliable way of evaluating this possibility in these experiments, though the results for k_q at 5091 and 5900 A indicate that the quenching

in those regions follows the conventional mechanism, (B-1d).

In conclusion it is felt that most the deviations from the predicted behavior for Y in the low-pressure plots can be attributed to effects of non-linear absorption, with a possible error of + 10% in Y_{min} because of wall reactions involving $^2P_{1/2}$ atoms.[1] If the error in the relative extinction coefficients is 15%,[2] the measured values of Y_{max} may be in error by + 10%, due to small steady-state concentrations of $^2P_{1/2}$ atoms and reactions of the type (11). The possible systematic errors in Y_{min} and Y_{max} are both in the same direction, so that the error in the quantum yield is felt to be less than 10% from all processes considered here.

3. Continuum Absorption in the Banded Region

a. Calculations and Comparisons

The results in Table 3 say nothing about the relative contributions of direct dissociation and spontaneous predissociation to the total first-order dissociative yield. Mulliken has predicted that the $^1\Pi_{1u}$ state should contribute 10% of the total absorption strength in the visible bands of I_2.[3] The present total yields compare favorably with the results of Chutjian and James (C and J, 1969) for spontaneous predissociation alone,

1. The abnormally low slopes for wavelengths 6129 and 6239 remain somewhat puzzling. None of the hypotheses is completely satisfying, though the anomalies are probably due to wall reactions of $^2P_{1/2}$ atoms and slight errors in the non-linearity calibration procedure, which are magnified at these low Y values.

2. Some experimental support for this contention is presented in the next section.

3. Mulliken's revised dipole strengths are 8.8, 33.6, and 582×10^{-4} A^2 for the $A \leftarrow X$, $^1\Pi_{1u} \leftarrow X$, and $B \leftarrow X$ systems, respectively. The relative absorption strengths must include a factor of 2 for the doubly-degenerate $^1\Pi_{1u}$ state.

which tends to support Mulliken's assessment. On the other hand C and J's results for absorption between rotational lines indicate the $^1\Pi_{1u} \leftarrow X$ contribution may be as much as 25%. In that case the apparent agreement between total yield and predissociative yield may be fortuitous.

We may approach the question of the underlying continuum in a different way. C and J give values for $|Re|^2$ for the discrete transitions $B \leftarrow X$. We can calculate from these a low-resolution extinction coefficient and compare it with the measured ϵ_ν. Any disparity might be attributable to additional transitions falling in the same spectral region.

Most of the work for such a computation has already been done in assigning the (v',v") distributions for the absorption process. If we consider the absorption coefficient k_ν to be a low-resolution parameter for the band absorption, we can write

$$\int k_\nu \; F_\nu \; d\nu \;=\; \frac{1}{8\pi c} \; \Sigma \; \nu_i^{-2} \; A_i \; F_{\nu i} \; N_i \qquad (13)$$

based on the expressions in Section III. F_ν is a sort of resolution parameter, in this case the interference filter transmission profile. The calculation could equally well be done for a rectangular "slit" of arbitrary breadth. However if the breadth is made too narrow, the result for k_ν may show vibrational structure. The sum is carried out over all rotational lines of significance for the "filter" F_ν. If k_ν varies slowly with respect to F_ν, we have

$$\int k_\nu \; F_\nu \; d\nu \;=\; k_\nu \int F_\nu d\nu$$

$$= \frac{8\pi^3}{3hc} \; \frac{N}{q_r \; q_v} \; |Re|^2 \; \Sigma \; F_{\nu i} \; \nu_i \; s_{Ji} \; e^{-\epsilon_i/kT} \; |\langle v'|v''\rangle|_i^2 \qquad (14)$$

When ν_i is averaged and removed from under the summation sign, the remaining sum is precisely the result from the earlier calculations, Eq. (D-2). For $\int F_\nu d\nu$ we take the area under the filter in Angstroms and convert it to cm^{-1}; for this calculation the error introduced by this rough conversion in negligible. The partition functions q_r and q_v have been given earlier as 5.55×10^3 and 1.55, respectively. (ϵ_i is again the energy above the lowest level.) The value found for $|Re|^2$ by C and J for the (25,0) band was .837 debye^2. For the 5462-A filter. $\int F_\nu d\nu$ = 41.8 A or 140 cm^{-1}. The value for the sum (with $\bar{\nu}$ removed) in (14) was found to be 353, and $\bar{\nu}$ is taken to be 18,300 cm^{-1}. The resulting value for $k_\nu(cm^{-1})$ is 1.87×10^{-18} N. Using (III-D-9b) we obtain a value of 490 liter mole^{-1} cm^{-1} for the decadic molar extinction coefficient.[1]

The number 490 compares rather poorly with the value ~675 taken from the curve of Rabinowitch and Wood. Similarly the calculated (using $|Re|^2 = 1.14$) extinction coefficient at 5896 A is 167, or 15% lower than R and W's value of 200. However, from C and J's data for absorption between the lines in the banded region, we calculate continuum contributions of 170 and 35 to the total extinction coefficient at 5460 A and 6020 A, respectively, which brings their results into excellent agreement with R and W's extinction curves. These values represent 25% of the total I_2 extinction at their respective wavelengths; this indicates that the $^1\Pi_{1u} \leftarrow X$ absorption parallels that by $B \leftarrow X$ and is considerably stronger than all previous estimates.

---

1. Another way to approach this problem is to sum all the equivalent widths in a fixed interval and then divide by the width of the interval. The resulting expression for ϵ_ν is exactly the same as that given by Eq. (14).

The matter of the effect of pressure and path length on the absorption spectrum of I_2 has an interesting history, having gone through two complete cycles in the literature already. The first apparent measurement of the gas-phase extinction coefficient was reported by Vogt and Koenigsberger (1923). They used saturated I_2 vapor at several temperatures from 48 to 400 C; their results varied radically with both temperature and pressure. Loomis and Fuller (1932) noted the appearance of increased absorption for $v' > 12$ when oxygen was added to their absorption cell; they ascribed the effect to an increased transition probability due to a collision-induced predissociation. Kondratjew and Polak (1933) carried this line further. They located three apparent maxima (at $v' = 22, 29, 39$) in the absorption of I_2 in the presence of N_2, O_2 and HCl, which they attributed to increased absorption strengths due to crossings of the B-state potential curve by one (0^+g) and two (1_u) states.[1] Unfortunately they failed to consider the dependence of the effect on path length and I_2 concentration, which would have been crucially important in their 3-meter cell at their I_2 pressure of .188 torr. In 1936 Rabinowitch and Wood remeasured the extinction coefficient, using various pressures of air, He, and Ar to broaden the absorption lines. At low foreign-gas pressures they observed "humps" in the absorption similar to those noted in earlier works. As the foreign-gas pressure was increased, the apparent absorption coefficient in the 5000-5600 A region increased gradually, leveling off at a pressure of ~500 torr for all three gases. Since further increases in foreign-gas concentration failed to change ϵ_ν, they attributed the apparent irregularities in the low-pressure spectrum to effects of absorption path length and dismissed the notion of strengthened absorption from induced predissociation.

---

1. Their reasoning seems to be in error here, as the (1_u) states are the states allowed in <u>spontaneous</u> predissociation.

The "limiting" curve of R and W has been the accepted extinction curve for I_2 up to the present decade. In 1964 Goy and Pritchard re-opened the investigation, rejecting R and W's conclusions to propose the existence of weak foreign gas-I_2 complexes. Ogryzlo and Thomas (1965) then demonstrated conclusively that R and W's interpretation was in fact correct. They varied independently the path length and concentrations and even studied the line-broadening directly; their results leave no doubt that the irregularities in the absorption spectrum of I_2 are a function of the detailed nature of the discrete line absorption.

Although the apparent anomalies in the spectrum have been attributed to path-length problems, there may still be a weak, "smooth" contribution to the overall absorption strength from foreign gas-I_2 interactions. For example the several reported extinction coefficients differ even in the region of continuous absorption, where path length problems disappear (for moderate instrumental resolution). Furthermore, the pressure-broadened extinction curve of R and W is still 15-20% below the absorption in inert solvent. Mulliken feels the limiting curve of R and W is not sufficiently pressurized and that it should agree more nearly with the extinction in inert solvent.[1] Evidently the obvious experiment -- a measurement of ϵ_ν at very low total absorption, for pure I_2 and various admixtures of foreign gas -- has not been carried out. Sulzer and Wieland (1952) did measure the extinction coefficient of pure I_2 vapor at temperatures 600 to 1050 C, using three different concentrations and three separate path lengths. Although these authors indicate that some sort of check on the validity

---

1. Mulliken has so indicated in a letter to H. O. Pritchard.

of Beer's Law was made, they fail to note whether an extrapolation was necessary. In any case their I_2 concentrations were high enough that extrapolations might not have accurately eliminated the possible pressure effects, even if they did demonstrate adherance to Beer's Law. Their integrated extinction coefficient $\int \epsilon_\nu \, d\nu/\nu$ was 15% lower than that calculated from R and W's curve (Brewer, et al., 1963).

From the earlier evaluation of the absorption non-linearity, the measured value for ϵ_ν should be within 5% of the true value when the total absorption is less than 1%. Such small differences can be measured accurately with the proper equipment, and an extrapolation to zero absorption should give ϵ_ν values free of path length complications. Although the author was not prepared to carry out such an experiment with any degree of thoroughness, a cursory check on the extinction yielded values of $\epsilon_{\lambda 5277} = 680$ liter mole^{-1} cm^{-1} and $\epsilon_{\lambda 4919} = 410$, both lower than R and W's limiting curve.[1,2] The ratio $\epsilon_{\lambda 5277}/\epsilon_{\lambda 4919} = 1.67$ is in fair agreement with the experimental results in Table 5, supporting the suggestion made earlier that the limiting extinction curve of R and W may be in error, particularly in the region of continuous absorption. More precise measurements are needed to provide a definite answer to this question.

---

1. In a 13.7-cm absorption cell a pressure of 30.5 mtorr I_2 gave an average of 2.9% absorption with 12% standard deviation at 5277 A. This gives an apparent absorption coefficient $\epsilon_\nu = 574$, but the non-linearity at 3% absorption should be about 20%, giving a corrected value of 680 liter mole^{-1}cm^{-1}.

At 4919 A, .161 torr I_2 gave 10.5% (±.6%) absorption for an extinction coefficient of 408. No correction is warranted here, because the absorption is supposed to be continuous. The value 408 represents an average value over the bandwidth of the filter and does not necessarily apply for absorption at the specific wavelength of the peak transmittance.

2. R and W's curve gives 825 and 650, respectively for these two wavelengths.

b. Experimental Observations

It was difficult to assess by experimental methods the contribution of direct dissociation to the total atomic yield in these experiments. Inserting an I_2 "filter" into the path of the exciting light demonstrated that a sizeable fraction of the atoms were coming from discrete line absorption, as expected. A 5-cm cell containing I_2 at room temperature decreased the signal by 25% at 4919 A, 46% at 5462 A, and 31% at 5900 A; the measured low-resolution attenuation by the I_2 filter at these wavelengths was 25%, 25% and 21%, and a blank gave a 13% decrease. From previous calculations we would expect the useful narrow-line exciting radiation to be even more completely eliminated by the filter than indicated by the 46% decrease at 5462 A. Therefore the continuum contribution appears to be appreciable.

In the calculation of the (v',v") distributions we obtained values for the summed excitation given in Eq. (D-2). If we divide the observed Y_{max} values (corrected for the relative black-body distribution of the tungsten lamp) by the summed excitation (including ν dependence), and plot these values versus v', the resulting curve should be nearly linear, with deviations from the horizontal indicative of the variation in $|Re|^2$ for the absorption. If continuous absorption contributes to Y_{max}, the curve may be less well-behaved.

The results of such a comparison are illustrated in Fig. 32. Clearly something intersting is happening at v' = 12 and below. It is unlikely that $|Re|^2$ is changing so suddenly over this narrow range of v', so the sharp upswing undoubtedly represents the onset of another transition, probably involving the continuum of the $A(^3\Pi_{1u})$ state. This interpretation is in general agreement with the sketchy results of Mathieson and Rees

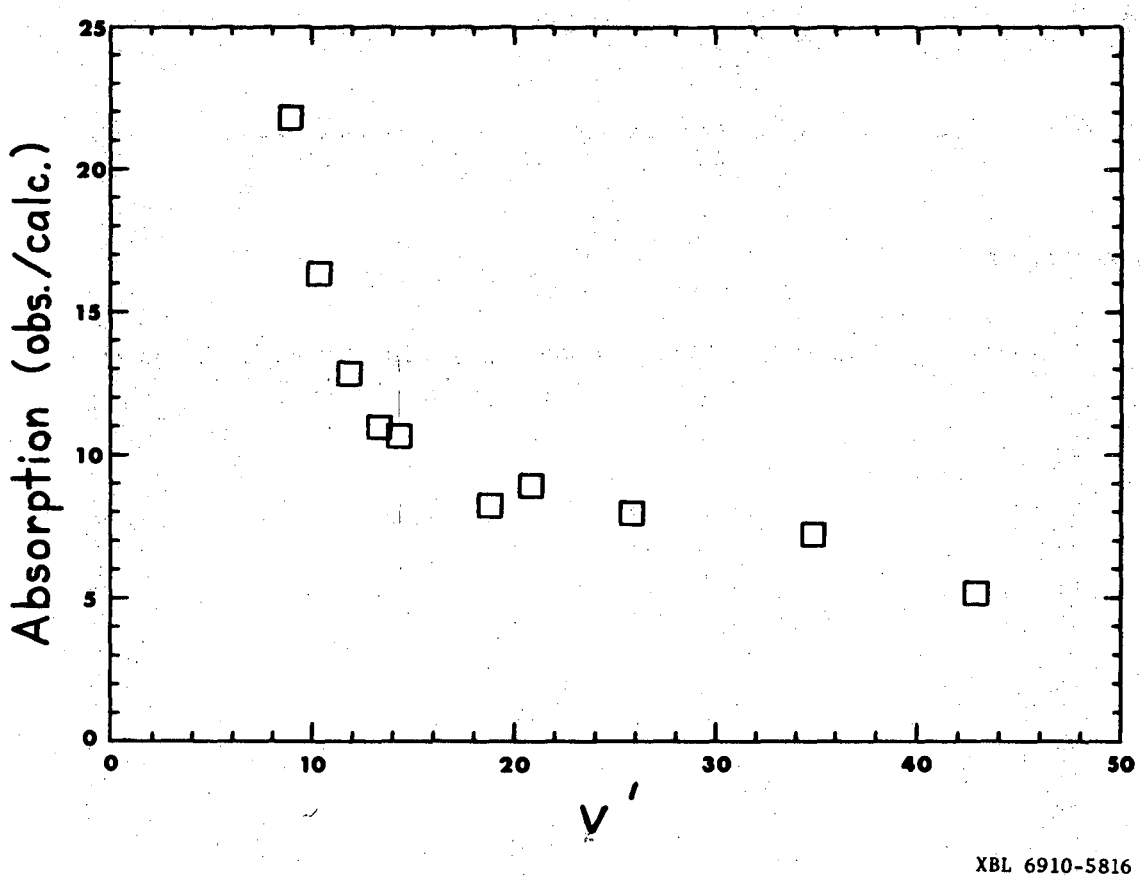

Fig. 32. Plot of relative observed/calculated absorption as a function of v'.

(1956, p. 761) and the findings of Ham (1954), except that Fig. 32 shows the A ← X continuum extending further toward shorter wavelengths than has generally been supposed.[1] At 6240 A, the A ← X continuum amounts to at least 45% of the total absorption. Unfortunately data were not recorded at longer wavelengths.

The apparent extension of the A ← X absorption to shorter wavelengths is consistent with the possible 25% contribution of the $^1\Pi_{1u} \leftarrow X$ absorption to the total visible band strength. Mulliken's calculations (1934, 1940) relate absorption strength for the $^1\Pi_{1u} \leftarrow X$ transition to the positions and relative strengths of the A ← X and B ← X systems. A shift to shorter wavelengths for the maximum of the A ← X absorption corresponds to increased strength for the $^1\Pi_{1u} \leftarrow X$ absorption. The latter is not manifested in any obvious way in Fig. 32, but that is as expected from C and J's results, where a parallel absorption is indicated. This behavior is also consistant with the presumed location of the $^1\Pi_{1u}$ state (shown in Fig. 34).

The trend in the points for v' > 12 in Fig. 32 demonstrates that the transition moment is <u>decreasing</u> at smaller r-centroid values.[2] The relative change in $|Re|^2$ with v' is in close agreement with the findings of C and J. In the limit of large internuclear distances the value of $|Re|^2$ must decrease and approach the value for the weak $^2P_{1/2}$ - $^2P_{3/2}$ atomic

---

1. Locating the maximum and assessing the relative strength of the A ← X absorption requires resolving the visible and infrared spectrum into two peaks. The outcome of such a resolution, carried out in an "eyeball" manner, may reflect the designs of the investigator. When the Franck-Condon factors can be calculated accurately (as is the case for I_2 B-X), the resolution can be carried out unambiguously, as was done here.

2. Recall that, for absorption from low v" levels, the r-centroids decrease with increasing λ and v'. Values given earlier were 2.806 A and 2.701 A for 6239 and 5462 A excitation, respectively.

transition. Therefore $|Re|^2$ must possess a maximum value which falls in the neighborhood or r = 3.0-3.4 A. The decrease for r < 3.0 A is an unexpected result; it may, however, indicate the approach to case (a) coupling, where the $^3\Pi_u$ - $^1\Sigma_g^+$ transition becomes spin-prohibited.

In assessing the relative contributions of continuum absorption and spontaneous predissociation to the total dissociative quantum yield, we must arbitrarily assign the contribution from the parallel $^1\Pi_{1u} \leftarrow X$ absorption. The value 20% is reasonably consistent with both Mulliken's predictions and C and J's results. Equations (B-14, 17) can be used to achieve the desired resolution.

The resulting analysis is given in Table 6. The tabulated lifetime values represent rough averages of the results of Chutjian (1966), Wolff (1967), Cunningham (1968), and Grimes,[1] summarized in Table 7. All values in parentheses are based on A_T values obtained from a smooth interpolation of the points in Fig. 33, where the resolved total radiative decay rates are plotted versus v'. Four points calculated by C and J from absorption measurements are included for comparison.

The results are very encouraging. We see that the radiative decay rate varies smoothly with v', as would be expected from the behavior of the average ν^3 and r-centroid values; and the irregularities in the total decay rates reported by Chutjian and co-workers (1967) are in general accounted for in terms of the competing spontaneous predissociation, which fluctuates in magnitude with v'. Chutjian (1969) has demonstrated that such fluctuations are expected for predissociation to a repulsive state lying just to the left of the B-state potential curve, because the bound-state and continuum wave functions alternately fall "in step"

1. Unpublished direct-decay results. Chutjian's value for τ at 5087 A appears now to be in error.

Table 6. Analysis of I_2 visible absorption and B-state decay processes

Wavelength (A)	Absorption: Fraction Continuum	Absorption: Fraction Banded	$I_2^*(B)$ Decay: Fraction Fluorescence	$I_2^*(B)$ Decay: Fraction Predissociation	$1/\tau$ (10^5/sec)	A_T (10^5/sec)	k_p (10^5/sec)
5010	.80	.20	.37	.63	6.7	2.5	4.2
5091	.40	.60	.50	.50	6.2	3.1	3.1
5166	.25	.75	.50	.50	4.7	2.4	2.3
5277	.20	.80	.42	.58	9.7	4.1	5.6
5462	.20	.80	.34	.66	14.9	5.1	9.8
5594	.20	.80	.42	.58	15.8	6.6	9.2
5690	.20	.80	.51	.49	(13.7)	(7.0)	(6.7)
5896	.20	.80	.83	.17	9.4	7.8	1.6
5922	.20	.80	.82	.18	(10.1)	(8.3)	(1.8)
6037	.30	.70	.66	.34	13.7	9.0	4.7
6129	.45	.55	.59	.41	(15.3)	(9.0)	(6.3)
6239	.55	.45	.27	.73	(35)	(9.4)	(25)

( ) - based on "smooth" interpolation of A_T values from experimentally measured τ values.

Table 7. Summary of measured lifetime values
(10^{-7} sec)

Wavelength (A)	Chutjian (Phase-Shift)	Wolff (Direct Decay)	Grimes (Direct Decay)	Cunningham (Phase-Shift)
5011	17.5 ± 1.5	(9.99)	9.8 ± 4	
5087	42.2 ± 6	11.3 ± .8	16.8 ± 1	19.7 ± 2.0* 20.6 ± 3.0†
5168	24.1 ± 3	(10.8)	18.9 ± 4	
5277	9.66± .5	(8.40)	10.9 ± 1	
5461	7.69± .3	6.28 ± .40	6.42± .3	5.66 ± .6* 7.4 ± .4†
5592	6.89± .33	(6.74)	5.78± .3	
5895	11.4 ± .6	8.02± .55	13.1 ± 1.1	9.8 ± .7
6040	6.79± .33	(7.16)	8.3 ± 3.5	

( ) - inexhaustive measurements

* 1 MHz modulation frequency
† 360 kHz modulation frequency

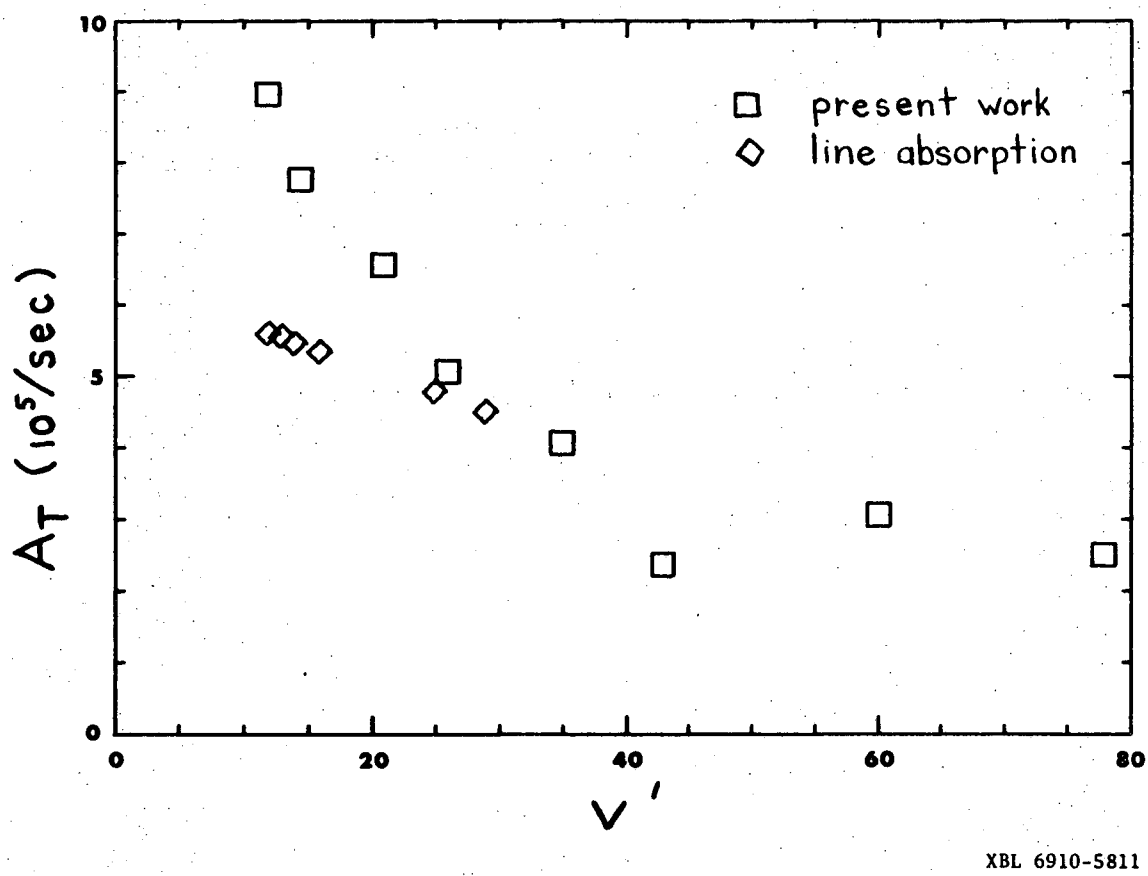

Fig. 33. Resolved total radiative decay rate as a function of v'.

and "out of step" with each other. It is interesting to note that k_p is predicted to be ~25×10^5/sec at 6039 A (based on the smooth extrapolation of the A_T values in Fig. 33). As a result the B-state lifetime for excitation at this wavelength should be ~3×10^{-7} sec, much smaller than any heretofore measured value.

There is one apparent inconsistency in Fig. 33: C and J's calculated radiative decay rates fall noticeably below the experimental points for v' < 20. In view of the uncertainties involved in both works, the discrepancy is not terribly alarming. For example C and J assume a constant $|Re|^2$ value of 1.03 debye^2 in calculating their total transition rates. Since $|Re|^2$ apparently attains a maximum value greater than ~1.15 at some internuclear distance beyond 3.0 A, these calculated rates could easily be too low. An increase to an average value of $|Re|^2$ = 1.30 for emission from v' = 12 would give respectable agreement between the two studies.

From Fig. 33 the lifetime value at 5166 A would appear to be too great. The value used here was an average of the numbers obtained by Grimes and Chutjian; Wolff's sketchy results are in better areement with the measured atomic yields. Ezekiel and Weiss (1968) measured an even longer lifetime of $30 \pm 5 \times 10^{-7}$ sec in this region. They used 5145 A excitation from an argon-ion laser, so they were exciting low J values in the (43,0) band, whose origin falls at 5144.5 A. (Their own analysis indicated J values lower than 10.) In that case their long lifetime may reflect the predicted J(J+1) dependence in k_p.

Table 7 shows the relative continuum absorption increasing at both ends of the visible bands. The continuum absorption at the red end has already been assigned to the A ← X system. The increase at short wavelengths is based on a semi-quantitative resolution of B ← X absorption

into a "continuum" peak and a "banded" peak, recognizing that the maximum in the former may actually lie to the red of the dissociation limit at 4985 A. These appears to be widespread neglect of this point in the literature.[1,2] At room temperature, only 65% of the I_2 molecules are in the lowest vibrational level. For v" = 1,2,3 the dissociation limit falls at 5038, 5093, and 5148 A, respectively.[3] Furthermore the Franck-Condon principle favors absorption by excited v" levels over the ground level for radiation in the 5000 A region.[2] Thus the dissociation continuum of the B ← X system extends a considerable distance into the "discrete" region, in principle all the way to 13,150 A!

4. Collisional Quenching of $I_2^*(B)$

a. Review

The quenching by foreign gases of the visible fluoresence from the B state of I_2 has been the subject of numerous investigations in the last sixty years. Franck and Wood (1911) first reported the phenomenon, noting that the apparent reddening of the fluoresence light indicated the effect

1. A good example is the study by Callear and Wilson (1967) of the reactions of $^2P_{1/2}$ I-atoms with propane. They attributed some of their observations to a translational energy "boost" above the dissociation limit, when actually a large part of their yield can be explained in terms of the discussion here.

2. Steinfeld and co-workers (1969) suggested that, because of the relative paucity of rotational structure near the (v"=0) dissociation limit, more than one continuum may be involved in the absorption. They point out that the Franck-Condon factors for transitions(v',0) are very small for v' levels near the dissociation limit; by the same token the continuum absorption from v" = 0 must be practically negligible. The F-C factors are more favorable for absorption out of excited v" levels, so that most of the absorption in this region is probably still B ← X, though present indications are that $^1\Pi_{1u}$ ← X may contribute ~25%. (The latter transition could contribute more than 25% if the two absorptions are not quite parallel, i.e. if the $^1\Pi_{1u}$ potential curve crosses the B-state curve as shown in Fig. 34.)

3. For J" levels of appreciable population (30-60) these limits lie 10-20 A farther to the red. Thus the often quoted 4995-A convergence limit represents a "practical" limit.

was stronger in the green bands. Berg (1933) obtained a quantitative measure of the quenching by I_2, N_2, O_2 and Ar; his results for Ar in three different spectral regions supported the previous observations. Turner (1928, 1931, 1932), by detecting atomic resonance-line absorption, demonstrated convincingly that ground-state I-atoms were being produced in the quenching process. He further suggested that this collisional predissociation might be due to enhancement of a weak spontaneous predissociation. The work of Rabinowitch and Wood (1936b) further confirmed the predissociative mechanism. The absorption studies of Loomis and Fuller (1932), Kondratjew and Polak (1933), and Goy and Pritchard (1964) were interpreted in terms of collisional predissociation but were later shown to be in error. (See the discussion above.)

Eliashevitch (1932), and Rössler (1935) observed that vibrational energy transfer was about as probable as collisional quenching for a number of foreign gases, and that both mechanisms had rates exceeding the gas-kinetic collision rates. The works of Arnot and McDowell (1958) and Polanyi (1958) supported these findings, but a more realistic estimate of the unimolecular I_2^* (B) lifetime by Polanyi indicated the rates were only one order of magnitude greater than gas-kinetic collision rates, and not two as had been suggested by earlier workers. To account for the great efficiency of I_2 as a quencher, Polanyi suggested that the mechanism in this case might involve a sensitized predissociation, in which I_2^* transfers it energy to its collision partner and the latter dissociates, leaving the originally excited molecule in a vibrationally excited level of the ground electronic state.

Steinfeld, Klemperer, and Brown have reported a series of comprehensive experiments on collisional quenching and energy transfer (1964-1966). Some of their rates may be as much as 30-50% too high from failure

to properly take into consideration the nature of the fluorescence function discussed in (IV-A). However, even with such corrections their results display a v' dependence. On the other hand the definitive work by Chutjian, et al. (1967) showed clearly that the I_2 self-quenching cross sections vary only ~10% with excitation from 5000 to 6000 A. Their results have been supported by other direct lifetime measurements (Wolff, 1967; Cunningham, 1968; Grimes and Davis, 1968), and by an independent fluorescence quenching measurement (Kummler and McCarty, 1967). If the results of Klemperer and co-workers be further corrected in accord with the fluctuating nature of the I_2^* unimolecular lifetime, it is likely that the apparent v' dependence for quenching by molecules other than I_2 will disappear also.[1] It is still possible, however, that I_2 is such an efficient quencher that it "swamps" any detailed v' dependence that might be revealed in the quenching by other gases. No adequate theoretical explanation of the quenching in $I_2^*(B)$ is yet at hand; and the detailed nature of the process, including the states responsible for it, are still matters of speculation.[2]

b. Experimental Results

Some quenching data can be gleaned from the results of the predissociation experiments. These experiments are less than ideal for such purposes, because all the information is contained in the difference $\Delta = Y_{max} - Y_{min}$. If the fluorescence fraction at zero pressure is small, systematic errors in Y_{max} and Y_{min} may negate the results.

---

1. The "unquenchability" for v' < 8, noted by Steinfeld (1966) may be valid. Direct observations of lifetimes in this region would be useful. However, from the (v',v") distributions calculated earlier, these low v' levels can probably only be populated substantially in very hot cells.

2. See, however, the recent work of Degenkolb, et al. (1969), in which some reference is made to unpublished work of Steinfeld and comrades.

The expression for the I_2 self-quenching rate has been given in Eq. (B-16) as

$$k_q = \frac{\text{slope}}{\Delta\tau} \tag{15}$$

For the foreign-gas quenching we have, from (B-18)

$$k_M M = 1/\tau \left[\frac{\Delta}{Y_{max} - Y} - \left(1 + \frac{k_q [I_2]}{1/\tau}\right)\right] \tag{16}$$

Strictly speaking, Y_{max} and k_M are not independent variables in these experiments; but Y_{max} is statistically so precise relative to k_M, that for practical purposes we may treat the two independently. The second term in the brackets in (16) was ~1, as the I_2 pressure was very low.

The constants $k_q\tau$ and $k_M\tau$ were obtained in the units (mtorr^{-1}) and (torr^{-1}), respectively. The corresponding rates (kP) may be converted to concentration rates and thence to reaction cross sections,

$$kP = k'N = \Pi d^2 \left(\frac{8kT}{\pi\mu}\right)^{1/2} N \tag{17}$$

μ is the reduced mass for the collision partners, and d^2 is the customarily reported collision cross section. In our case, for T = 300 K,

$$d^2_{N_2-I_2} (A^2) = 1.97 \times 10^{-6} k_M \tag{18a}$$

$$d^2_{I_2-I_2} (A^2) = 4.42 \times 10^{-3} k_q \tag{18b}$$

The results are given in Table 8. (The necessary lifetime values were taken from Table 6.) The unphysical negative values of d^2 for I_2 self-quenching are omitted, but we can see that they lie in the region of strong absorption from v" = 0, in line with the non-linear absorption explanation. (Slopes at 6129 and 6239 A were anomalously low, but were also highly uncertain.) The values at 5900 A and near 5100 A are roughly 2/3 those measured by Chutjian.

The cross sections for N_2 quenching appear to be smaller than gas-kinetic values, contrary to most previous results. In general the k_M

Table 8. Collisional quenching results

	N_2 quenching			I_2 self-quenching		
λ (A)	$k_M\tau(\text{torr}^{-1})$	$d^2(A^2)$	% St. Dev.	$k_q\tau(\text{mtorr}^{-1}\times10^{-2})$	$d^2(A^2)$	% St. Dev.
5011	-	-	-	3.4	101	73
5091	1.	1.2	80	1.9	51	17
5166	1.4	1.3	55	1.7	35	8
5277	.7	1.4	30	.35	15	100
5462	.5	1.4	25	-	-	-
5594	.35	1.1	20	-	-	-
5690	.65	1.7	35	.25	15	90
5896	2.1	3.8	25	1.0	41	22
5922	2.2	4.3	35	.95	42	13
6037	1.7	4.5	35	.75	47	21
6129	.6	1.7	50	-	-	-
6239	.1	.9	160	-	-	-

values agree with those obtained by Berg (1933) and Brown and Klemperer (1964), except that there appears to be a decrease in the green region, in disagreement with all prior studies. This apparent decrease is felt to be a manifestation of the previously suggested systematic error in Y_{max}. For example, if Y_{max} is 15% high, the apparent quenching rates will be about one third the true values for the green filters, where only 30% of the $I_2^*(B)$ molecules fluoresce at zero pressure. For the yellow filters (5900 A), where the fluorescence fraction is 65%, the error in Y_{max} is less important.

Despite the problems, the results in Table 8 are reasonably consistent with the proposed mechanism (B-1). A method of atom detection cannot be expected to provide accurate collisional predissociation data when the fluorescence fraction is very small. However, for a molecule with 100% fluorescence yield at zero pressure, the method is in principle at least as good as direct observation of fluorescence, perhaps better, in that problems involving the fluorescence function are circumvented. Direct lifetime measurements have, of course, the same advantage.

c. Quenching Mechanism

The absence of pronounced v' dependence in I_2 self-quenching lends support to the suggestions of Turner (1931) and Cunningham (1968), that the collisional predissociation is simply an ehanced spontaneous predissociation. As a third body approaches an I_2 molecule the potential curves in Fig. 34 shift about. It is conceivable that this shifting could "trigger" the spontaneous predissociation by improving the Franck-Condon overlap between the $^1\Pi_{1u}$ and B states. In that case the collisional quenching might be expected to retain some of the J(J+1) dependence predicted for the spontaneous predissociation.

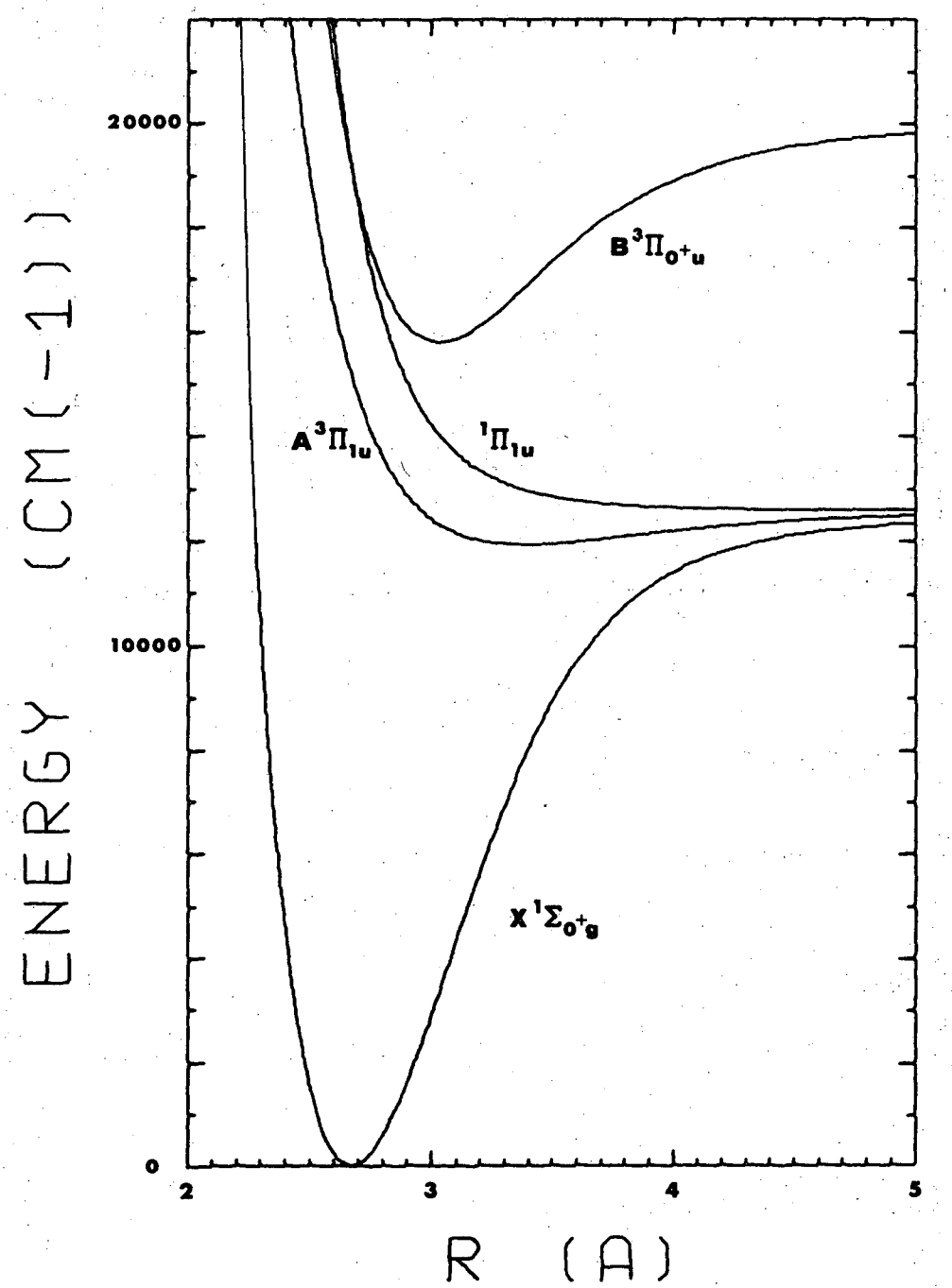

XBL 6910-5812

Fig. 34. Potential diagram for several low-lying states of I_2.

A preliminary investigation of the emission spectrum of I_2 at various concentrations failed to show any J dependence in the quenching (Gee and Tellinghuisen, 1969). Fluorescence and emission bands have a profile which is characteristic of the temperature of the system. If the quenching is strongly J-dependent, the emission bands should progressively "cool off" as the I_2 pressure is increased. Densitometer tracings of weak emission spectra from a Tesla-coil-excited discharge of I_2 at pressures of 20 mtorr and 200 mtorr were qualitatively identical, indicating no pronounced J dependence in the quenching.

Conventional ("no selection rules") collisional predissociation can occur via any one of half a dozen predicted repulsive states, to be mentioned in the next topic. The author is not prepared to predict which of these, if any, should display a strong J dependence. The lack of specific v' dependence may indicate that the repulsive state or states responsible for the quenching cross the B-state curve near the minimum or on the inner branch.

5. I_2 Potential Diagram

The possible electronic states for I_2 have been derived and discussed in detail by Mulliken (1934, 1940) and Mathieson and Rees (1956). A number of recent experimental works have generally proven Mulliken's predictions for the low-lying states to be correct. Therefore the present discussion will be pleasantly brief.

There are ten states arising from $^2P_{3/2} + {}^2P_{3/2}$ atoms, ten from $^2P_{1/2} + {}^2P_{3/2}$, and three from $^2P_{1/2} + {}^2P_{1/2}$. These are conveniently enumerated in a table given by Mathieson and Rees. Of the 23 states only three (X, A, B) have been observed and accepted by general consensus. These three plus the now strongly evident $^1\Pi_{1u}$ state are shown in Fig. 34.

The X and B curves are from RKR calculations; the A curve is a Morse function based on Brown's data (1931); the $^1\Pi_{1u}$ curve is the one used by Chutjian (1969) to calculate sample predissociation rates. The results of this study indicate that the repulsive branch of the A state may lie a bit nearer to the B curve than shown here. Similarly the 1u may be closer to the B state at low v' levels than indicated by Chutjian's adopted r^{-12} form for this repulsive state.

Of the seven remaining states which correlate with ground-state iodine atoms, two are predicted to be stable -- the 0_u^- and 2_u (both $^3\Pi$). Degenkolb and co-workers (1969) have attributed the magnetic quenching of the B state to a 0_u^- state, but they fail to note that there are two 0_u^- states which lie in this region. The magnetic quenching is presumably caused by the 0_u^- ($^3\Sigma^+$) state, which should lie above the 0_u^- ($^3\Pi$); so the latter remains unseen. The 2_u state has been tentatively identified as the lower state involved in the famous emission system at ~3450 A (Wieland and Tellinghuisen, 1969). It appears to have an appreciable dissociation energy of 2000 - 2500 cm^{-1} and a vibration frequency greater than 100 cm^{-1}. The remaining states -- $^3\Pi_g$ (0^+, 1, 2) and $^3\Delta_u(3)$ -- are all predicted to be repulsive by Mulliken. The collisional quenching likely involves some or all of these.

Aside from the B state, none of the states which correlate with ($^2P_{1/2}$ + $^2P_{3/2}$) has been seen. Degenkolb et al. located the 0_u^- state crossing the inner branch of the B curve, in which case the 2700-A continuum absorption may involve a state with these atomic products. Such a picture is compatible with the feelings of Mulliken, but contrary to the interpretation of Mathieson and Rees. This region of the state diagram is in need of additional theoretical and experimental work.

6. Future Work

The results for Y_{max} suggested possible errors in the extinction curve of Rabinowitch and Wood. It was pointed out that accurate measurements of ϵ_ν in the limit of zero absorption should finally settle the question of the effects of foreign gases and solvents on the absorption spectrum of I_2. Such measurements, carried out with the filters used in these experiments, could be used to assess more realistically the magnitude of the errors in Y_{max}. With a measurement of the iodine atom heterogeneous recombination rate in N_2, reactions (11) might be more quantitatively evaluated. An accurate determination of the extinction by pure I_2, extended to the infrared region, could permit a complete resolution of the $A \leftarrow X$, $B \leftarrow X$, and $1_u \leftarrow X$ contributions to the total absorption, using the method present here. In addition the variation of the B-X transition moment could be observed for a greater range of r-centroid values; ϵ_ν values for higher temperatures would be useful here.

The question of v' dependence in the quenching of $I_2^*(B)$ by foreign gases could be answered by direct lifetime methods. The region of low v' values (<10) seems of particular interest. Direct lifetime measurements using line sources might also enable one to verify the predicted $J(J+1)$ dependence of k_p. Alternatively a quantitative comparison of the fluorescence and emission bands with calculated band profiles should reveal this dependence. Since the predissociation rate varies radically with v', one could probably identify bands of widely divergent apparent temperature all in the same spectrum; the "cooler" bands would then correlate with greater $k_p(v')$ values. The failure to observe such phenomena might inspire a re-evaluation of predissociation theory; or it could simply indicate a necessity to include the rotational-vibrational interaction in the calculation of the overlap integrals.

There is one important question not treated in this study: Why is the predissociation in I_2 so weak ($\sim 10^6$/sec) when allowed predissociations generally have rates of 10^{10} - 10^{12}/sec? Chutjian's computations (1969) demonstrate that the overlap integrals between the bound and continuum state change little as the 1_u state is made to cross the inner branch of the B-state curve, so the answer is not simply a matter of crossing or not crossing. According to Chutjian's numbers and certain sum rules, the maximum possible rate would be $\sim 5 \times 10^8$/sec. Two thoughts come to mind:
(a) The "strong" predissociations are not really so strong after all.
(b) The low rate for I_2 may be characteristic of this particular relative orientation of the bound and continuum states, i.e., the former embedded in the latter. In this case is seems plausible that an intersection on the right branch of the bound state could give much better overlap, because the cancellation which occurs across the domain of the bound state for the I_2 case would not be present for a right-branch intersection. Calculations of the type done by Chutjian should be extended to cover a variety of relative positions for the bound and continuum states; they might have something very interesting to say about this matter of weak and strong spontaneous predissociation.

V. HETEROGENEOUS RECOMBINATION OF IODINE ATOMS

A. Introduction

The homogeneous recombination of iodine atoms

$$I + I + M \xrightarrow{k_r} I_2 + M \qquad (1)$$

has served as a topic for numerous experimental and theoretical investigations. Equation (1) is by now perhaps the most thoroughly studied reaction of this type; in many kinetics texts it is presented as the classic example of a termolecular reaction. The book by Johnston (1966, Chpt. 14) includes a fine summary of the work in this area.

The recombination of iodine atoms was first examined experimentally by Rabinowitch and Wood (1936c), who used a photostationary method to produce I atoms in the presence of various foreign gases. After correcting for thermal effects, these authors were able to show that, at pressures greater than ~100 torr, the recombination proceeded according to

$$-\frac{d[I]}{dt} = 2\, k_r\, [I]^2/M \qquad (2)$$

At lower pressures wall reactions played an important role in the net recombination. For the homogeneous process the constant k_r varied by as much as an order of magnitude for the foreign gases used, with recombination occurring in one in 530 I-I collisions in one atmosphere of He and one in 50 in one atmosphere of CO_2. With the development of flash photolysis techniques by Norrish and Porter (1949), it became possible to study process (1) dynamically. In the first few years of work in this field, different labs recorded discordant values for k_r, at which time it was realized that thermal complications associated with the intense flashes were causing large errors. By eliminating or correcting for these effects, the various workers have been able to obtain generally consistent results for most

foreign gases M. The outstanding exception is $M = I_2$, where the estimates still range over a factor of four (Christie, 1962).

Much of the theoretical interest in I-atom recombination is aimed toward evaluating the relative contributions of two proposed mechanisms for the reaction:

$$I + I \underset{k_{-1}}{\overset{k_1}{\rightleftharpoons}} I_2^* \qquad (3a)$$

$$I_2^* + M \xrightarrow{k_2} I_2 + M$$

$$I + M \underset{k_{-1}}{\overset{k_1}{\rightleftharpoons}} IM \qquad (3b)$$

$$IM + I \xrightarrow{k_2} I_2 + M$$

Eq. (3a) is known as the energy-transfer mechanism, and Eq. (3b) is usually called the bound-complex mechanism. Calculations indicate that the latter is the dominant process for all but the simplest 3rd body M (Johnston, 1966). Experimentally the two cases are practically indistinguishable, because both I_2^* and the proposed complexes IM are generally not very stable. However, for the case of a stable complex IM, mechanism (b) predicts that the removal of iodine atoms will be first order in [I], even though the overall recombination (1) remains second order. The case $M = I_2$ is suspected to be of this type, as I_3 has been predicted to be stable by about 5 kcal/mole (Bunker and Davidson, 1958). Unfortunately it has not been possible to detect I_3 either directly or indirectly (from 1st-order removal of I) in any of the existing kinetic studies.

One feature common to all the experimental studies mentioned above was the indirect observation of I atoms via I_2 visible absorption. Because of signal precision problems it has been necessary to use high-

power arcs or violent flashes of 1000 joules or more total energy, which introduced the thermal problems noted above. The latter were found to diminish as the pressure of the diluent gas was increased; but it has remained impossible to observe directly the recombination of I atoms in pure I_2 vapor. The method of atomic fluorescence spectroscopy utilized in Section IV of this work could serve as a powerful new tool in investigating reactions of I atoms; in particular it might provide some answers to the questions about I_3 in mechanism (3b).

B. Kinetics

1. General Considerations

We can predict on intuitive grounds what sort of behavior the I-atom recombination will exhibit in a cell containing low pressures of I_2. From the work of Rabinowitch and Wood (1936c) the rate-determining reaction is diffusion-controlled wall recombination for foreign-gas pressures lower than 50-100 torr. In pure I_2 vapor homogeneous recombination may prevail at pressures much lower than this, because of the great efficiency of the I_2 molecule as a third body. However, we expect wall recombination to predominate at pressures lower than ~ 0.5 torr, though the net recombination may include an appreciable contribution from homogeneous processes.

At very low I_2 concentrations (~ 1 mtorr), where the I-atom mean free path is greater than the dimensions of the cell, the I-atom removal should become independent of the I_2 pressure. In the limit of zero pressure it should approach a constant rate determined solely by the nature of the surfaces and the dimensions of the cell. The mechanism may be summarized as follows:

$$I \underset{k_{-1}}{\overset{k_1}{\rightleftharpoons}} I_{wall} \tag{1a}$$

$$I + I_{wall} \xrightarrow{k_2} I_{2,wall} \tag{1b}$$

$$I_{2,wall} \xrightarrow{k_3} I_2 \tag{1c}$$

If we assume that (1c) is reasonably rapid, so that the presence of I_2 molecules on the surface has no effect on the removal of I atoms, we can apply the steady-state approximation to I_{wall} and get

$$-\frac{d[I]}{dt} = 2\,k_1[I]\left\{\frac{k_2\,[I]}{k_{-1} + k_2\,[I]}\right\} \tag{2}$$

In deriving (2) we assumed the number of available sites on the surface was essentially infinite, which may be a poor approximation. We can use the adsorption-isotherm approach to obtain a more complete expression. If θ is the fraction of available sites that are occupied, the adsorption is proportional to $(1-\theta)$, and desorption and reaction (b) are both proportional to θ. If the surface concentration is in equilibrium with the gas-phase concentrations at all times, analogous to the steady-state approximation made above, we have

$$-\frac{d[I]}{dt} = 2\,k_1\,[I]\left\{\frac{k_2[I]}{k_{-1} + (k_1 + k_2)[I]}\right\} \tag{3}$$

Both (2) and (3) predict that the I-atom removal will be a process of mixed order with respect to [I], as was postulated in Section IV. However, the form of the total removal rate is seen here to differ from the simple expression $C[I]\,(1 + b[I])$ used earlier. When $k_{-1} \ll (k_1 + k_2)[I]$, (3) predicts an exponential decline of [I] from some initial value $[I]_0$.

There is one qualification to this statement: If the "sticking" efficiency is very high (~1), the removal time for a given atom will be a function of its distance from the walls of the cell; in that case the net decline will be non-exponential.

As we increase the I_2 pressure the I-atom removal rate should decrease, as the atoms must diffuse through the I_2 vapor to reach the walls. Until the homogeneous recombination sets in, the rate should go as $[I_2]^{-1}$. In terms of this mechanism the removal of the I atoms can be expressed as

$$-\frac{d[I]}{dt} = \frac{C\,[I]^2}{(1 + C'[I])(1 + a[I_2])} \tag{4}$$

It is interesting to note that (3) and (4) predict that the deviation from 1st-order kinetics in [I] should decrease as [I] increases. The dependence of signal on irradiance in the predissociation work seemed to indicate just the opposite behavior. This suggests that an additional process of the form

$$I + I \xrightarrow{\text{wall}} I_{2,\text{wall}} \rightarrow I_{2,\text{vapor}} \tag{5}$$

may be operative. Of course the homogeneous recombination must occur along with the surface reactions, though we do not expect it to predominate at I_2 pressures below ~ 1 torr. We can write

$$I + I_2 \underset{k_{-1}}{\overset{k_1}{\rightleftharpoons}} I_3 \tag{6a}$$

$$I_3 + I \xrightarrow{k_2} 2\ I_2 \tag{6b}$$

as one of the many possible mechanisms involving the I_3 complex. If I_3 is relatively stable, the bulk removal of iodine atoms under transient conditions will be essentially first-order in both [I] and $[I_2]$, and we might observe a deviation from the $(1 + a[I_2])^{-1}$ dependence in Eq. (4).

2. Diffusion Kinetics

A proper treatment of the diffusion equation indicates that (4) does not give the exact I_2-pressure dependence for the recombination rate. Kovacs and co-workers (1968) have investigated diffusion and wall de-excitation of vibrationally excited CO_2 in cylindrical cells. Their situation was entirely analogous to the present one, and we may use their mathematical relationships to describe the wall reactions of I atoms.[1]

The decay of the atom concentration is determined by the diffusion equation

$$\frac{\partial N}{\partial t} = D \nabla^2 N + \Gamma' N \tag{7}$$

where D is the diffusion constant and Γ' represents the volume removal rate, which will be assumed to follow 1st-order kinetics. The boundary conditions on the solutions are fixed by the continuity equation

$$\int_{\text{surface}} \text{flux} \cdot \vec{dS} = \int_{\text{volume}} \frac{dN}{dt}\, dv \tag{8}$$

If we let β represent the wall reflection probability and $\bar{v}$, the mean speed of the I atoms, the outward flux at the wall is

$$\text{flux} = (1 - \beta) \left[\frac{1}{4} N \bar{v} - \frac{1}{2} D\left(\frac{\partial N}{\partial r}\right)\right]_{\text{wall}} \tag{9}$$

The solution for N is a sum of Bessel functions of various orders; according to Kovacs, et al., the nonzero-order terms decay rapidly, leaving

$$N \propto J_0 \left(\frac{xr}{r_0}\right) e^{-\Gamma t} \tag{10}$$

---

1. Here we assume, in anticipation of the results, that the wall removal of I is strictly first order. Also, for simplicity we will neglect problems concerning the finite length of the cell. The errors introduced by such a move should not be fatal in this particular study.

where

$$\Gamma = \frac{x^2 D}{r_o^2} + \Gamma' \tag{11}$$

J_o is the zero-order Bessel function and r_o is the cell radius; x is the solution to (8), which appears in the form

$$x\, J_1(x) - \frac{\bar{v}\, r_o}{2D}\left(\frac{1-\beta}{1+\beta}\right) J_o(x) \tag{12}$$

At low pressures Γ approaches a constant value

$$\Gamma_o = \frac{\bar{v}}{r_o}\left(\frac{1-\beta}{1+\beta}\right) \tag{13}$$

For intermediate I_2 concentrations the pressure dependence of Γ is complex, but at high pressures x approaches a constant, so that $\Gamma - \Gamma'$ displays an $[I_2]^{-1}$ behavior. Thus the overall pressure dependence is approximately that given in the earlier discussion, Eq. (B-4) when the homogeneous removal rate Γ' is negligible.

C. Results and Discussion

The data were obtained using the flash photolysis arrangement described in Section II. The cell used here was the same one used in the predissociation work. Prior to these experiments it had been flamed out under vacuum, charged with distilled, resublimed I_2, and sealed off. Oscilloscope tracings were recorded for [I] decay curves at total I_2 pressures ranging from 4 to 160 mtorr.

Typical tracings are illustrated in Plate 2. Photo (d) exhibits effects of non-linearity in the fluorescence function, discussed in Section IV-A. To avoid complications of this sort, the flash was attenuated with neutral density filters, so that the maximum observed signal was less than ~ 25% of the maximum in the characteristic fluorescence function.[1]

1. From the discussion in Sec. IV-A we see that the flash is dissociating less than .1% of the I_2 in the cell, so the perturbation on the system is negligible.

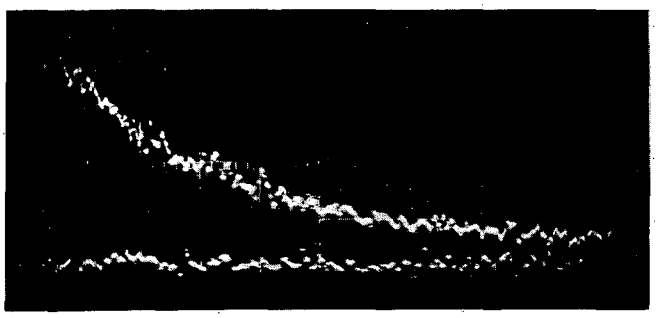

(a) $P(I_2)$ = 8.5 mtorr
1 msec/div.

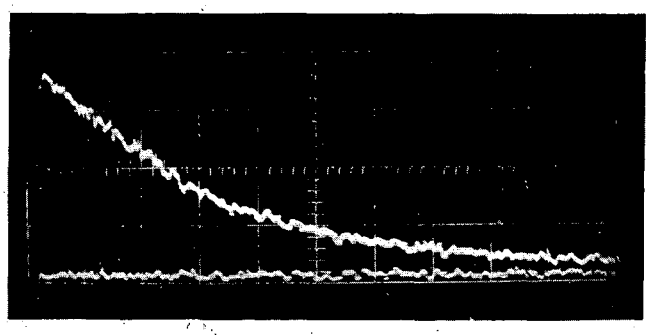

(b) $P(I_2)$ = 56 mtorr
2 msec/div.

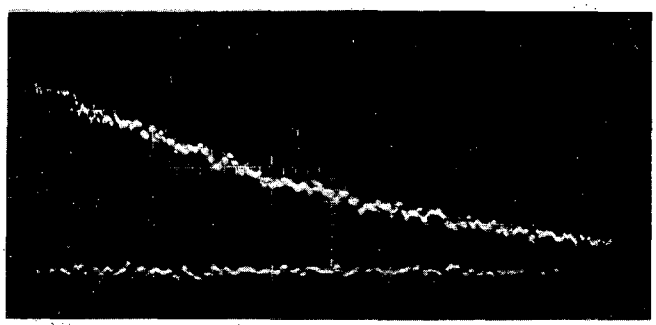

(c) $P(I_2)$ = 156 mtorr
2msec/div.

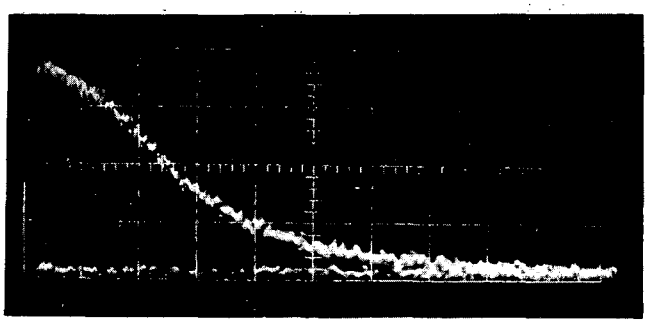

(d) $P(I_2)$ = 129 mtorr
5 msec/div.

XBB 6910-6803

Plate 2. Oscilloscope tracings of fluorescence signals from iodine atoms produced with a mild (~20 Joule) flash discharge.

Further attenuation demonstrated that the systematic error at this level was much smaller than the precision of the data.

The tracings were enlarged with an opaque projector and reproduced on graph paper. Plots of log (Signal) versus time were generally linear, although curves recorded at I_2 pressures below ~25 mtorr seemed to display slight deviation from first-order decay at low iodine-atom concentrations. Figure 35 shows the semi-log plots for (a) and (b) in Plate 2. The deviation from linearity is clear in 35a; this behavior may indicate the onset of second-order I-atom removal as prediced by Eq. (B-3).

The data from the tracings were treated in terms of weighted and unweighted linear logarithmic fits and variable baseline ($y = a + b\, e^{-cx}$) fits. The total dependence

$$-\frac{d[I]}{dt} \approx \Gamma[I] = \frac{k_w[I]}{1 + a\,[I_2]} \qquad (1)$$

was verified for each treatment. Although the results for a single photo varied somewhat for the three methods of analysis, the constants k_w and a were essentially the same in all cases.

The results from the weighted semi-log fits are illustrated in Figure 36, where $1/\Gamma$ is plotted versus $P(I_2)$. These points were recorded on two days a week apart; they are in good agreement with the results from similar experiments carried out six months earlier. Statistically the linear behavior described by (1) is borne out by the data,[1] with $1/k_w = 3.01 \pm 0.13$ and $a/k_w = 0.0486 \pm 0.017$ msec/mtorr. A closer examination of Figure 36 reveals a short "plateau" at low $P(I_2)$ and slight negative deviation from the calculated linear dependence at high $P(I_2)$

1. Application of an F test (Parratt, 1961, p. 134) indicated the first-order fit was superior to a quadratic fit.

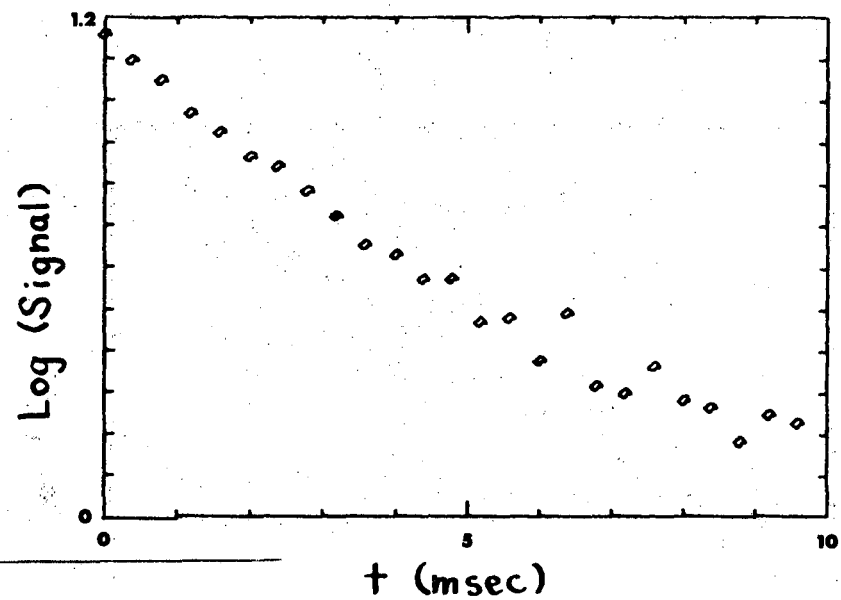

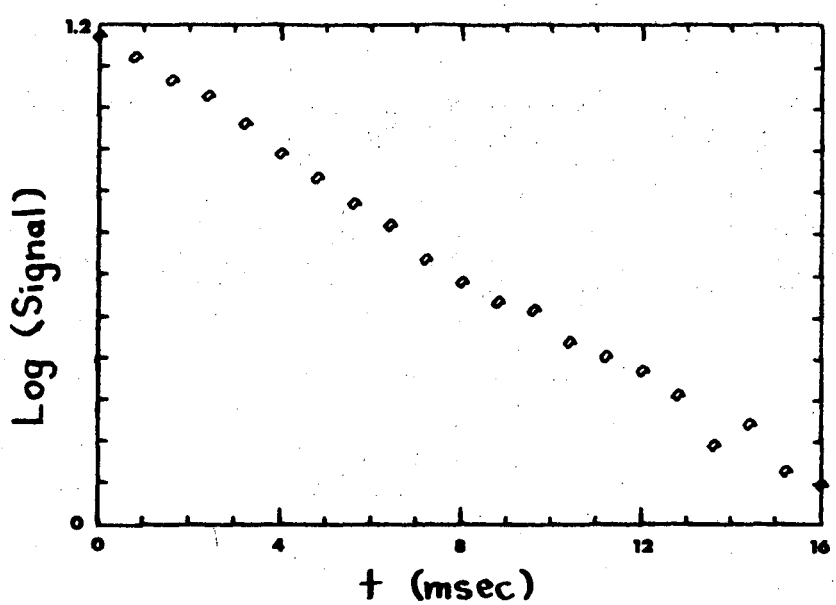

XBL 6910-5813

Fig. 35. Logarithmic plots of data from tracings in Plate 2. Upper plot is for curve (a), $P(I_2)$ = 8.5 mtorr. Lower plot is for curve (b), $P(I_2)$ = 56 mtorr. (Only half the recorded data points are included in these graphs.)

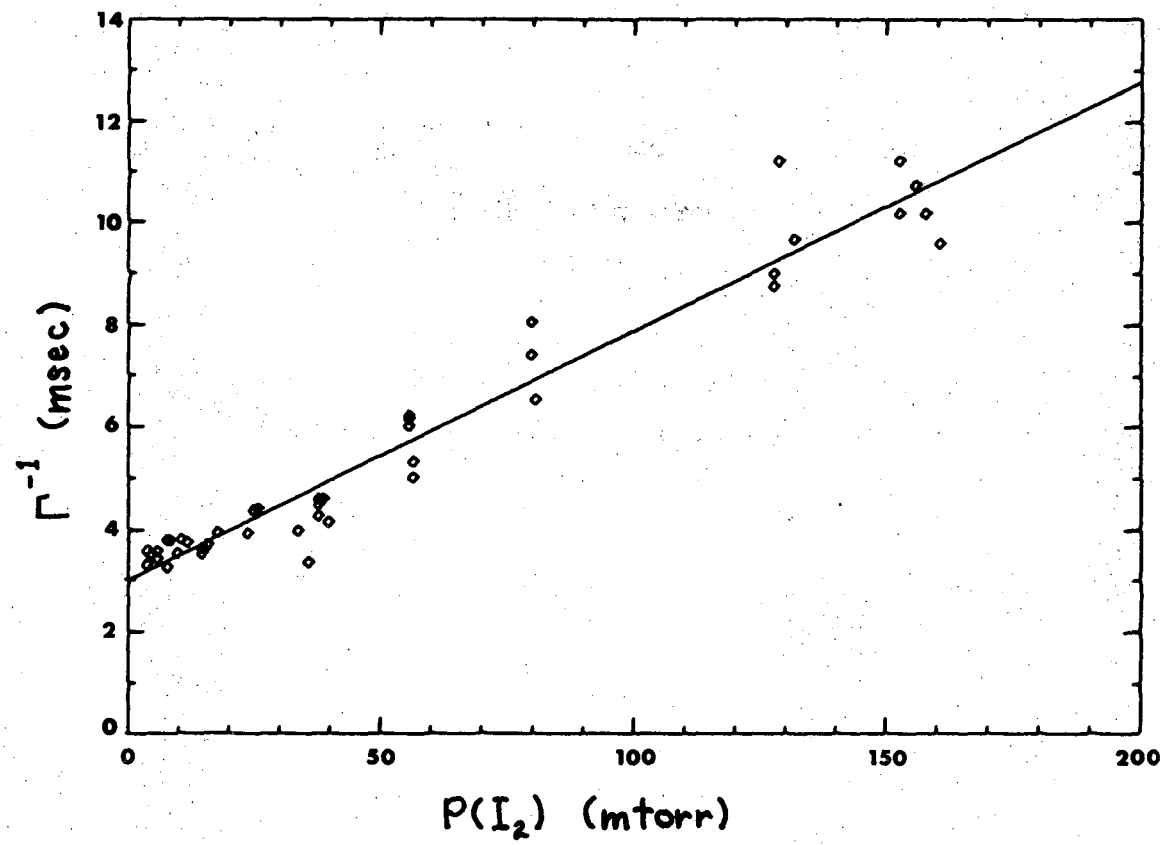

XBL 6910-5839

Fig. 36. Iodine atom removal rate as a function of I_2 pressure.

values. Both of these appear to be real rather than random phenomena. The plateau may be a result of the slight deviation from first-order decay at low [I]; extrapolated slopes from the linear region in the semi-log plots for these points would reduce the intercept to ~ 2 msec. On the other hand this leveling off could indicate that the sticking efficiency is a function of the I_2 vapor pressure; adsorbed I_2 might expedite the removal of I atoms at higher pressures. Similarly the deviation from linearity at high $P(I_2)$ may be due to effects of adsorbed I_2; or it could represent the contribution of homogeneous recombination according to (B-6). On the latter assumption an approximate rate for the formation of I_3 will be calculated below.

Equation (B-13) gives a value of 0.049 for the sticking probability $(1 - \beta)$. If the true intercept is taken as 2 msec, $(1 - \beta)$ increases to 0.075. The relationship between the measured rate Γ and the diffusion constant D in (B-11,12) is not simple. However, it turns out for this case that the dependence of $\frac{x^2}{r_o^2} D$ on pressure is for all practical purposes described by the relationship (C-1) above. A few points calculated with the values $\beta = 0.951$ and $D = 9\ cm^2/(sec\ P_{torr}(I_2))$ gave good agreement with the observed data at low $P(I_2)$, but were ~ 10% below the measured rates Γ at 150 mtorr I_2. With $\beta = 0.925$, the best value of D was 8; in this case the data at 150 mtorr were about 15% low in Fig. 36.

From (B-11) we can estimate that Γ' is ~ 10/sec at 150 mtorr I_2. For simplicity we have assumed that

$$\Gamma' = k_1[I_2] \qquad (2)$$

for the process $I + I_2 \xrightarrow{k_1} I_3$. The collision rate between I and I_2 at this pressure is 6.4×10^5/sec (for a collision diameter of 3.9 A). Therefore only one in 64,000 I - I_2 collisions leads to the formation of

I_3, if this interpretation is valid. If the increase in the measured rate at these I_2 pressures is due to a higher wall sticking probability, the volume removal rate will be even lower, so that the value $k = 2 \times 10^{-15}$ cm^3/sec represents a rough upper limit on the rate constant for this process. This rate, though small, is still several orders of magnitude greater than the estimated three-body removal rate for I atoms in the concentrations encountered here.[1]

As pointed out above, D is relatively insensitive to variations in $(1 - \beta)$. Hence the value

$$D = 9.0\ (\pm\ 25\%)\ \frac{cm^2}{sec \cdot P_{I_2,torr}} \tag{3}$$

should accurately represent the rate for diffusion of $I(^2P_{3/2})$ atoms through I_2. This value of D may be related to a cross section for diffusion through the simple expression

$$D = \bar{v}\ L/3 \tag{4}$$

where $\bar{v}$ and L are the mean velocity and mean free path of the iodine atoms. A rigorous treatment of the diffusion problem gives, for a hard-sphere model (Hirshfelder, et al., 1954, p. 14)

$$D_{12} = \frac{3}{32} \left(\frac{8\ kT}{\pi\ \mu}\right)^{1/2} \frac{1}{Nd^2} \tag{5}$$

where μ is the reduced mass for the collision partners. From (5) the collision cross section is 89 A^2, which is about five times the hard-sphere cross section. Thus we see that the I-I_2 interactions are strong, but not strong enough to produce appreciable concentrations of I_3 for I_2 pressures lower than 1 torr.

---

1. Johnston (1966) quotes a value of 6.5×10^{-30} cm^6/sec for k_r in Eqs. (A-1,2), so the termolecular half-life of the I-atom concentration is more than 100 seconds under these conditions.

The flash-photolysis atomic-fluorescence technique used in this work should be widely applicable in studies of reactions of atoms. The advantage of simplicity is obvious; but more important is the extreme sensitivity of the detection method, which allows one to employ small perturbative flashes instead of cataclysmic ones. To the author's knowledge a technique of this sort has been reported in the literature only once, that being the work by Braun and Lenzi (1967), in which reactions of atomic hydrogen with olefins were followed by measuring absorption and fluorescence of Lyman-α radiation.

APPENDIX I. Absorption and Fluorescence Formulas

To facilitate the use of Eq. (III-B-12)

$$Ab = \frac{\int E_\nu (1-e^{-k_\nu \ell})\, d\nu}{\int E_\nu d\nu} \qquad \text{(III-B-12)}$$

it is desirable to have at hand expressions for the absorption for several commonly occurring forms of E_ν. Perhaps the most frequently encountered situation is one in which k_ν can be approximated as a Doppler-broadened absorption coefficient. We can rewrite (III-B-5) in a simpler way for the purpose of computations:

$$k_\nu = k_0 e^{-\alpha\omega^2} \qquad (1)$$

where

$$\alpha = \frac{4 \ln 2}{(\Delta\nu_D)^2} \qquad (2)$$

$$\omega = \nu - \nu_0$$

Consider first the case where the source line is also Gaussian (corresponding to Eq. (III-B-9)), with the same center frequency ν_0.

$$E_\nu = C\, e^{-\alpha'\omega^2} \qquad (3)$$

(Primes will be used throughout this section to represent source quantities.) Technically the integrals in Eq. (III-B-12) have limits 0 and ∞, but the lower limit may be extended to $-\infty$ without introducing any discernable change. Then the denominator is simply

$$\int E_\nu d\nu = C \sqrt{\frac{\pi}{\alpha'}} \qquad (4)$$

The numerator cannot be evaluated so directly. Fortunately, however, the integrand may be represented as a uniformly convergent power series, suitable for term-by-term integration.

$$E_\nu \left(1-e^{-k_\nu \ell}\right) = C\, e^{-\alpha'\omega^2} \left[-\sum_{n=1}^{\infty} \frac{(k_0\ell)^n}{n!} e^{-n\alpha\omega^2} \right] \tag{5}$$

$$\int E_\nu \left(1-e^{-k_\nu \ell}\right) d\nu = -C \sqrt{\frac{\pi}{\alpha'}} \sum_{n=1}^{\infty} \frac{(-k_0\ell)^n}{n!} (1 + m\gamma)^{-1/2}$$

$$\gamma = \alpha/\alpha' \tag{6}$$

Hence for this case

$$Ab = -\sum_{n=1}^{\infty} \frac{(-k_0\ell)^n}{n!} (1 + m\gamma)^{-1/2} \tag{7}$$

If the source radiation is produced by the same atom or molecule whose absorption is being investigated, γ will be simply the ratio of temperatures in the source and absorption cells, $\gamma = T'/T$.

A second commonly occurring case is that for which E_ν is given by (III-B-8). Here both numerator and denominator must be integrated term by term.

$$Ab = \frac{\int C\left(1-e^{-k'_\nu \ell'}\right)\left(1-e^{-k_\nu \ell}\right) d\nu}{\int C\left(1-e^{-k'_\nu \ell'}\right) d\nu} \tag{8}$$

$$= \frac{-\sum_{m=1}^{\infty} \sum_{n=1}^{\infty} \frac{(-k'_0\ell')^n}{n!} \frac{(-k_0\ell)^m}{m!} (n+m\gamma)^{-1/2}}{\sum_{n=1}^{\infty} \frac{(-k'_0\ell')^n}{n!\sqrt{n}}}$$

Knowing Ab one may solve for $(k_0\ell)$ using (7) or (8). γ and $(k'_0\ell')$ are the adjustable parameters mentioned in Section III-B. Working the

results out by brute manpower is a formidable job best accomplished by calculating a few points $Ab(k_0\ell, \gamma, [k_0'\ell'])$ and interpolating graphically. However, it is a simple matter to solve (7) or (8) with a computer, using Newton's approximation method.[1] Two function routines, ODNEWT and ODNEWT2, have been programmed to calculate the roots for (7) and (8), respectively; the listing are included in Appendix III.

A third interesting case involving Doppler coefficients occurs when the source and absorption lines have slightly different center frequencies ν_0' and ν_0. Setting

$$\begin{aligned} \omega' &= \nu - \nu_0' \\ \Delta\nu &= \nu_0' - \nu_0 \end{aligned} \tag{9}$$

we obtain

$$Ab = -\sum_{n=1}^{\infty} \frac{(-k_0\ell)^n}{n!} (1+m\gamma)^{-1/2} e^{\frac{-m\alpha(\Delta\nu)^2}{1+m\gamma}} \tag{10}$$

A comparison of (7) with (10) shows the two differ by the exponential factor under the summation sign, which is quite strongly dependent on the frequency difference $\Delta\nu$.

Finally the equivalent width (III-B-15) can be taken over directly from the calculation of the expression for the denominator in (8).

$$\begin{aligned} EW &= \int (1-e^{-k_\nu \ell})\, d\nu \\ &= -\sqrt{\frac{\pi}{\alpha}} \sum_{n=1}^{\infty} \frac{(-k_0\ell)^n}{n!\sqrt{n}} \end{aligned} \tag{11}$$

1. See any basic calculus text.

We can apply the techniques and some of the results developed above to produce expressions for the fluorescence function discussed in Section IV-A. Using the Doppler form for E_ν, the integral in (IV-A-2) becomes

$$\int E_\nu \; e^{-k_\nu(\ell + \frac{b}{2})} \; (k_\nu \; b) \; d\nu$$

$$= C\sqrt{\frac{\pi}{\alpha'}} \; (k_0 b) \sum_{n=0}^{\infty} \frac{[-k_0(\ell + b/2)]^n}{n!} \; [1 + (n+1)\gamma]^{-1/2} \tag{12}$$

The more exact expression (IV-A-3) gives, for this E_ν

$$\int E_\nu \; e^{-k_\nu \ell} \; (1 - e^{-k_\nu b}) \; d\nu$$

$$= C\sqrt{\frac{\pi}{\alpha'}} \sum_{n=0}^{\infty} \frac{(-k_0 \ell)^n}{n!} \; (1 + n\gamma)^{-1/2} \; \{1 - (1 + b/\ell)^n\}$$

$$= C\sqrt{\frac{\pi}{\alpha'}} \sum_{m=1}^{\infty} \sum_{n=0}^{\infty} \frac{(-k_0 \ell)^n}{n!} \; \frac{(-k_0 b)^m}{m!} \; [1 + (m+n)\gamma]^{-1/2} \tag{13}$$

If we choose to use the form $C(1 - e^{-k_\nu' \ell'})$ for E_ν, we have

$$(1 - e^{-k_\nu' \ell'}) = -\sum_{i=1}^{\infty} \frac{(-k_0' \ell')^i}{i!} \; e^{-i\alpha'\omega^2} \tag{14}$$

$$(1 - e^{-k_\nu b}) = -\sum_{m=1}^{\infty} \frac{(-k_0 b)^m}{m!} \; e^{-m\alpha\omega^2}$$

$$e^{-k_\nu \ell} = \sum_{n=0}^{\infty} \frac{(-k_0 \ell)^n}{n!} \; e^{-n\alpha\omega^2}$$

so that

$$\int E_\nu \; e^{-k_\nu \ell} \; (1 - e^{-k_\nu b}) \; d\nu$$

$$= C\sqrt{\frac{\pi}{\alpha'}} \sum_{i=1}^{\infty} \sum_{m=1}^{\infty} \sum_{n=0}^{\infty} \left\{ \frac{(-k_0' \ell')^i}{i!} \; \frac{(-k_0 b)^m}{m!} \; \frac{(-k_0 \ell)^n}{n!} \times [i + (m + n)\gamma]^{-1/2} \right\} \tag{15}$$

The correction for scattered light in Eq. (IV-A-4) can be taken from the absorption formulas.

Expressions (12-15) can be evaluated easily with computer routines. Fewer than ten terms in the sums are necessary to evaluate points in the positive-slope region of the curves in Fig. 15. The calculating and plotting of 400 points for each of the three curves required two or three seconds of core processer time on a CDC 6600.

APPENDIX II. Radiation Coefficients

Einstein B coefficients tend to be confusing because of the variety of units used to describe the radiation field. The transition rate is of the form

$$-\frac{d N_b}{dt} = \rho_\nu B N_b \tag{1}$$

as given in Eq. (III-A-3), with ρ_ν representing the radiation field and N_b the concentration of particles in state b. With ρ_ν in units of energy density per unit wave-number interval (erg/cm^2), B is related to A by

$$B = \frac{1}{8\pi hc\nu^3} A \tag{2}$$

considering non-degenerate levels only. For excitation from a beam it might be more practical to take ρ_ν in units of radiance (flux per unit solid angle per unit surface area at normal incidence). This ρ_ν is related to the previous one by a factor of c, so that

$$B = \frac{1}{8\pi hc^2\nu^3} A \tag{3}$$

In photochemical work, quantum density and quantum flux are more directly related to experimental results than energy density and energy flux. In this case (2) and (3) become

$$B = \frac{1}{8\pi\nu^2} A \tag{4a}$$

and

$$B = \frac{1}{8\pi c\nu^2} A \tag{4b}$$

Finally, for isotropic irradiance the B values in (3) and (4) must be multiplied by 4π.

Occasionally ρ_ν may be expressed as a distribution function of the frequency in sec^{-1}. In that case

$$\rho' \left(\frac{\text{erg} \cdot \text{sec}}{\text{cm}^3}\right) = \frac{1}{c}\, \rho \left(\frac{\text{erg}}{\text{cm}^2}\right) \tag{5a}$$

and

$$B' = c\, B \tag{5b}$$

The equation corresponding to (2) is

$$B' = \frac{1}{8\pi h \nu^3} A \tag{6}$$

and analogous to (3) we have

$$B' = \frac{1}{8\pi h c \nu^3} A \tag{7}$$

Thus we see that the transformation from units of energy density per unit frequency interval to energy density per unit wave-number interval ((6) to (2)) is the same in the effect on B as the conversion from density (erg-sec/cm^3) to radiance ((6) to (7)) -- a good example of the confusing aspects of B values.

Strictly speaking, A and B should be treated as functions of frequency so that (1) should be

$$-\frac{dN_b}{dt} = N_b \int B_\nu \rho_\nu \, d\nu \tag{8}$$

but the commonly quoted A and B values are the integrated quantities

$$\begin{aligned} A &= \int A_\nu d\nu \\ B &= \int B_\nu d\nu \end{aligned} \tag{9}$$

The frequency dependence in A is seldom a matter of concern in photochemical work, but the frequency dependence in B may be crucial. This is taken into account in the discussion of the absorption coefficient in Section III-B, where it is stated

$$\int k_\nu \, d\nu = \frac{1}{8\pi c \nu^2} N A \tag{10}$$

Note the similarity between (10) and (4b). Only in the limit of very low absorption is the area of the absorption line equal to the area under the

absorption coefficient, as is clear from the expression for the equivalent width (III-B-15,16); and in that situation the integral B values will give correct results for the absorption. (See the text by Davidson (1962, Chpt. 12) for a treatment of frequency-dependent Einstein coefficients, absorption coefficients, and extinction coefficients.)

APPENDIX III. Computer Programs

A. Main Programs

Here we present the listings for the computer routines used to analyze much of the data obtained in the experiments of Sections III-V. Most of the main programs were designed to use one or more subroutines from a library of general routines for curve fitting, numerical integration, interpolation, etc., written by the author for operation on the CDC 6600 computers at the Lawrence Radiation Laboratory at Berkeley. The program language is CDC's Chippewa Fortran, nearly identical to Fortran IV. Many of the more versatile subroutines are listed below in Subsection B. None of these programs required more than 10 seconds of core processer time.

1. DATFIT

Program DATFIT is a simple procedure representative of those used to obtain least-squares linear fits from various sets of data. The main program merely controls the input and output of information; all the work is performed by Subroutine POWFIT and associated routines, which are listed and described in B. Here the input data are (1) a data set identifier LAMDA, (2) the data points (x_i, y_i), recorded one to a card in columns 11-30, with a non-zero indicator in columns 1-5, (3) a blank data set terminating card, and (4) a continuation card for additional data sets, with the number 33 in columns 4-5. (A blank card is used to terminate the entire input deck.) Included in the output are listings of the input data and the least-squares best values for a and b in the function $y = a + bx$.

```
      PROGRAM DATFIT(INPUT,OUTPUT)
C
C     DATFIT PROVIDES LEAST-SQUARES VALUES FOR A,B IN FUNCTION  Y = A + BX.
C
      DIMENSION  X(100),Y(100),B(10),SDB(10)
    1 FORMAT(5I5)
    2 FORMAT(1H1,///10X,*RESULTS AT*I5,*  ANGSTROMS*////)
    3 FORMAT(I5,5X,2F10.5)
    4 FORMAT(10X,I5,*  POINTS*//)
    5 FORMAT(///*INTERCEPT =*F6.3,5X,*ST. DEV. =*F6.3//*SLOPE = *E12.3,
     1     5X,*ST. DEV. = *E12.3///)
    6 FORMAT(*VARIANCE = *E12.3)
    7 FORMAT(10X,*X VALUE*,12X,*Y VALUE*//)
    8 FORMAT(10X,E12.3,8X,E12.3)
  100 READ 1,  LAMDA
      PRINT 2,  LAMDA
      DO 20  I=1,100
      READ 3,  IND,X(I),Y(I)
        IF (IND.EQ.0)  GO TO 21
   20 CONTINUE
   21     NUM = I - 1
      PRINT 4,  NUM
      PRINT 7
      PRINT 8,  (X(I),Y(I), I=1,NUM)
      CALL POWFIT(NUM,2,0,X,Y,B,SDB,VAR)
      PRINT 5,  B(1),SDB(1),B(2),SDB(2)
      PRINT 6,  VAR
      READ 1,  IGO
        IF (IGO.EQ.33)  GO TO 100
      END
```

2. EXFIT2

This program was used to obtain values for the constants a, b, and p in the variable baseline exponential fit $y = a + be^{-px}$. It was designed for analyzing the oscilloscope tracing data obtained in the I-atom recombination experiments, so the input and output statements are rather specific; otherwise the routine is quite general. The results are obtained from an iterative procedure which was generally observed to converge adequately in 3-5 cycles; the simultaneous equations resulting from the general least-squares equations summarized by Deming (1964) are solved by the method of determinants. Input information includes (1) the number of data sets NSETS, (2) a picture number IDENT and number of points NPOI for each data set, (3) the distance TDEL between evenly spaced x values for the points (x_i, y_i), along with initial guesses for the three unknowns A,B,P, and (4) the y values Y(I) for the NPOI data points. The output includes values for A,B,P resulting from each cycle, along with the final standard deviations.

```
      PROGRAM EXFIT2 (INPUT,OUTPUT)
C     EXFIT DETERMINES THE BEST LEAST-SQUARES FIT OF A SET OF DATA TO THE
C           FUNCTION   Y = A + B*EXP(-P*X)
      DIMENSION  X(50),Y(50)
      DIMENSION  Y1(50)
  100 FORMAT(5I5)
  101 FORMAT(8F10.2)
  102 FORMAT(4E15.4)
  103 FORMAT(5(F6.2,4X,2F6.2,4X))
  110 FORMAT(80H
     1                                        )
  111 FORMAT(///10X,19HINPUT DATA      X(I) //)
  112 FORMAT(///10X,24HINPUT AND CALC. Y VALUES //)
  113 FORMAT(///10X,1HA,14X,1HB,14X,2HDP,13X,1HP//)
  114 FORMAT(///10X,19HSTANDARD DEVIATIONS //)
  115 FORMAT(///10X,2HSY,13X,2HSA,13X,2HSB,13X,2HSP//)
  116 FORMAT(///10X,28HREDUCTION OF PHOTOLYSIS DATA)
  117 FORMAT(/////10X,24HRESULTS FOR PICTURE NO.   ,I5)
  120 FORMAT(16F5.2)
      PRINT 116
      READ 110
      PRINT 110
      READ 100,  NSETS
      DO 6  NIJ = 1,NSETS
      READ  100,  IDENT,NPOI
      READ  101,  TDEL,A,B,P
      READ 120,  (Y(I),I=1,NPOI)
          TN = NPOI
      PRINT 117,  IDENT
      PRINT 113
          IND = 0
    2     S1 = 0.0
          S2 = 0.0
          S3 = 0.
          S4 = 0.
          S5 = 0.
          S6 = 0.
          S7 = 0.
          S8 = 0.
          T = 0.0
      DO 1  I=1,NPOI
          X(I) = T
          FEX = EXP(-P*X(I))
          S1 = S1 + FEX
          S2 = S2 + X(I)*FEX
          S3 = S3 + Y(I)
          S4 = S4 + FEX**2
          S5 = S5 + X(I)*FEX**2
          S6 = S6 + Y(I)*FEX
          S7 = S7 + X(I)**2*FEX**2
          S8 = S8 + X(I)*Y(I)*FEX
    1     T = T + TDEL
          PT = P
          C11 = TN
          C12 = S1
          C13 = -B*S2
          C14 = S3 - P*B*S2
          C21 = S1
```

```
      C22 = S4
      C23 = -B*S5
      C24 = S6 - P*B*S5
      C31 = S2
      C32 = S5
      C33 = -B*S7
      C34 = S8 - P*B*S7
      DEN = C11*C22*C33 + C12*C23*C31 + C13*C21*C32 - C31*C22*C13
 1          - C32*C23*C11 - C33*C21*C12
      A = 1./DEN*(C14*C22*C33 + C12*C23*C34 + C13*C24*C32
 1          - C34*C22*C13 - C32*C23*C14 - C33*C24*C12)
      B = 1./DEN*(C11*C24*C33 + C14*C23*C31 + C13*C21*C34
 1          - C31*C24*C13 - C34*C23*C11 - C33*C21*C14)
      P = 1./DEN*(C11*C22*C34 + C12*C24*C31 + C14*C21*C32
 1          - C31*C22*C14 - C32*C24*C11 - C34*C21*C12)
      DP = P - PT
      IND = IND + 1
    IF (IND.EQ.5)  20,19
19 PRINT 102, A,B,DP,P
    GO TO 2
20 PRINT 102, A,B,DP,P
      SSQY = 0.0
      ST1 = 0.
      ST2 = 0.
      ST3 = 0.
  DO 4  I=1,NPOI
      FEX = EXP(-P*X(I))
      Y1(I) = A + B*FEX
      DYI = Y(I) - Y1(I)
      SSQY = SSQY + DYI**2
      DADYI = C22*C33 + C12*C23*X(I)*FEX + C13*C32*FEX
 1          - X(I)*FEX*C22*C13 - C32*C23 - C33*C12*FEX
      DBDYI = C11*C33*FEX + C23*C31 + C13*C21*X(I)*FEX
 1          - C31*C13*FEX - X(I)*FEX*C23*C11 - C33*C21
      DPDYI = C11*C22*X(I)*FEX + C12*C31*FEX + C21*C32
 1          - C31*C22 - C32*C11*FEX - C21*C12*X(I)*FEX
      ST1 = ST1 + DADYI**2
      ST2 = ST2 + DBDYI**2
      ST3 = ST3 + DPDYI**2
 4 CONTINUE
  PRINT 112
  PRINT 103,  (X(I),Y(I),Y1(I), I=1,NPOI)
  PRINT 114
  PRINT 115
      SY = SQRT(SSQY/TN)
      SA = SY/ABS(DEN)*SQRT(ST1)
      SB = SY/ABS(DEN)*SQRT(ST2)
      SP = SY/ABS(DEN)*SQRT(ST3)
  PRINT 102, SY,SA,SB,SP
 6 CONTINUE
  END
```

3. RATFUN

Program RATFUN provides values for the unknown constants a, b, and c in the function $y = c(1 + ax)/(1 + bx)$, the form used to obtain the high-pressure intercepts in the yield functions of Section IV. The method is again the general least-squares technique; but here the initial values for the desired constants are provided internally, and the simultaneous equations are solved by matrix inversion. The input and output information are essentially the same as for program DATFIT.

```
      PROGRAM RATFUN(INPUT,OUTPUT)
C
C    RATFUN PROVIDES LEAST-SQUARES VALUES FOR A,B,C IN FUNCTION
C              Y = C*(1 + A*X)/(1 + B*X).
C
      DIMENSION X(100),Y(100),XX(10),SD(10),AA(10,10),YY(10),AAIN(10,10)
      FO(X,Y) = Y - CO*(1. + AO*X)/(1. + BO*X)
      FA(X) = -CO*X/(1. + BO*X)
      FB(X) = CO*X*(1. + AO*X)/(1. + BO*X)**2
      FC(X) = -(1. + AO*X)/(1. + BO*X)
    1 FORMAT(10I5)
    2 FORMAT(8F10.5)
    3 FORMAT(I5,5X,2F10.5)
    4 FORMAT(10X,I5,*  POINTS*//)
    5 FORMAT(1H1,///10X,*RESULTS AT*I5,*  ANGSTROMS*////)
    6 FORMAT(*VARIANCE = *E12.3)
    7 FORMAT(10X,*X VALUE*,12X,*Y VALUE*//)
    8 FORMAT(10X,E12.3,8X,E12.3)
    9 FORMAT(////*A = *E12.4,5X,*ST. DEV. = *E12.4//*B = *E12.4,5X,
     1     *ST. DEV. = *E12.4//*C = *E12.4,5X,*ST. DEV. = *E12.4///)
   80 FORMAT(///*CONVERGENCE HAS FAILED.*I5,*  ITERATIONS COMPLETED.*/
     1     *CONTINUE WITH NEW DATA SET.*///)
  100 READ 1,  LAMDA
      PRINT 5,  LAMDA
      DO 10  I=1,100
      READ 3,  IND,X(I),Y(I)
        IF (IND.EQ.0)  GO TO 11
   10 CONTINUE
   11     NP = I - 1
      PRINT 4,  NP
      PRINT 7
      PRINT 8,  (X(I),Y(I),I=1,NP)
          AO = .6  $   BO = 1.0  $   CO = 1.2
   19 DO 18  MI = 1,10
      DO 12  I = 1,3
          YY(I) = 0.0
      DO 12  J=1,3
          AA(I,J) = 0.0
   12 CONTINUE
      DO 20  I=1,NP
          XT = X(I)  $  YT = Y(I)
          AT = FA(XT)  $   BT = FB(XT)
          CT = FC(XT)
          FT = FO(XT,YT)
          AA(1,1) = AA(1,1) + AT**2
          AA(1,2) = AA(1,2) + AT*BT
          AA(1,3) = AA(1,3) + AT*CT
          AA(2,2) = AA(2,2) + BT**2
          AA(2,3) = AA(2,3) + BT*CT
          AA(3,3) = AA(3,3) + CT**2
          AA(2,1) = AA(1,2)
          AA(3,1) = AA(1,3)
          AA(3,2) = AA(2,3)
          YY(1) = YY(1) + AT*FT
          YY(2) = YY(2) + BT*FT
          YY(3) = YY(3) + CT*FT
   20 CONTINUE
      CALL INVERT(3,AA,AAIN,IFAIL)
```

```
      IF (IFAIL.EQ.1)  GO TO 35
   CALL MATVEC(3,AAIN,YY,YY)
        AO = AO - YY(1)
        BO = BO - YY(2)
        CO = CO - YY(3)
      IF (ABS(CO).GT.100.)  17,18
17 PRINT 80,  MI
     GO TO 35
18 CONTINUE
        COMP = ABS(YY(3)/CO)
      IF (COMP.GT..0001)  GO TO 19
        SSQ = 0.0
   DO 21  I=1,NP
        DSQ = FO(X(I),Y(I))**2
        SSQ = SSQ + DSQ
21 CONTINUE
        SVAR = SSQ/(NP-3)
        SDY = SQRT(SVAR)
   DO 31  I=1,3
31      SD(I) = SDY*SQRT(AAIN(I,I))
   PRINT 9,  AO,SD(1),BO,SD(2),CO,SD(3)
   PRINT 6,  SVAR
35 READ 1,  IGO
     IF (IGO.EQ.33)  GO TO 100

   END
```

4. FILTAB

FILTAB was used to compute the (v',v") distributions for the excitation process in the I_2 visible absorption. The frequencies of the R and P lines for each band are calculated by means of function statements for the rotational and vibrational constants, B(v) and G(v). The frequencies are converted to wavelengths by function VACUUM, which uses Edlen's (1953) formula for the refractive index of air. Individual line strengths for each band are multiplied by the Boltzmann factor and the filter transmission function FLTR, and then summed (to J ~ 300) to obtain a total strength for the given band. The latter value is then multiplied by the Franck-Condon factor to obtain the relative contribution of each vibrational band.

The filter function FLTR is defined as Gaussian, with the maximum and the dispersion index fixed by the input values FPOS (wavelength of max. transmittance), FTRAN (max. fractional transmittance), and FWDTH (full width at half max.). The bands to be included in the calculation and their F-C factors are specified by the input variables V1(I), V2(I), and FC(I). The output includes a breakdown of the v' and v" populations into relative contributions, plus the value of the total summed excitation for the particular filter.

```
      PROGRAM FILTAB(INPUT,OUTPUT)
      DIMENSION  V1(100),V2(100),ORIG(100),FC(100),JLIM(100),
     *     BANDSUM(100),BMFV(100),RELSTR(100),AO(100)
      DIMENSION  WLR(500),SLR(500),WLP(500),SLP(500)
      DIMENSION  VPRI(50),BANDEX(50)
      COMMON/BLOW/FPOS,FTRAN,DISP
    1 FORMAT(I5,2F5.1,F12.5)
    2 FORMAT(3F10.5)
    3 FORMAT(1H1,///10X,*CALCULATION OF RELATIVE V1 POPULATIONS EXCITED
     1IN I2*////)
    4 FORMAT(*FILTER CHARACTERISTICS*//10X,*MAX. TRANSMISSION IS *F6.3*  AT*F5.
     1 AT*F5.0*  ANGSTROMS*/10X,*WIDTH AT HALF-PEAK = *F4.0*  ANGSTROMS*
     2   //)
    5 FORMAT(////*CHARACTERISTICS OF CONTRIBUTING ABSORPTION BANDS*//5X,
     1    *V1*5X*V2*10X*JMAX*7X*ORIGIN*8X*INT. PROFILE*5X*BOLT. FACTOR*
     2    7X*FC FACTOR*7X*REL. STRENGTH*//)
    6 FORMAT(4X,F3.0,4X,F3.0,10X,I4,5X,F10.3,5X,E12.3,5X,E12.3,5X,E12.3,
     1     5X,E12.3)
    7 FORMAT(///*SUMMED BAND STRENGTHS = *E12.3//)
    8 FORMAT(////5X*V1*5X*RELATIVE POPULATION*//)
    9 FORMAT(F7.0,12X,F6.3)
   10 FORMAT(///*SUM OF RELATIVE POPULATIONS = *F6.3)
   11 FORMAT(/////5X*V2*5X*RELATIVE CONTRIBUTION TO TOTAL ABSORPTION*//)
   12 FORMAT(///*SUM OF RELATIVE CONTRIBUTIONS = *F6.3)
      G1(V) = 125.531*(V+.5) - .73389*(V+.5)**2 - .004133*(V+.5)**3 +
     *     1.195E-06*(V+.5)**4 + 2.208E-07*(V+.5)**5
      G2(V) = 214.5766*(V+.5) - .65242*(V+.5)**2 + .005974*(V+.5)**3
      B1(V) = .028873 - 1.345E-04*(V+.5) - 1.148E-06*(V+.5)**2 -
     *     2.08E-08*(V+.5)**3
      B2(V) = .03734 - 1.208E-04*(V+.5) + .444E-06*(V+.5)**2 -
     *     1.839E-08*(V+.5)**3 - .057E-10*(V+.5)**4
           VOO = 15769.48
      READ 2,  FPOS,FTRAN,FWDTH
      DO 20  I=1,100
      READ 1,  NOGO,V1(I),V2(I),FC(I)
        IF (NOGO.NE.0)  GO TO 21
   20 CONTINUE
   21      NB = I-1
           DELX = FWDTH/2.
           DISP = ALOG(2.)/DELX**2
      DO 30  I=1,NB
           GV1 = G1(V1(I))
           GV2 = G2(V2(I))
           ORIG(I) = VOO + GV1 - GV2
           AO(I) = VACUUM(ORIG(I))
           BV1 = B1(V1(I))  $  BV2 = B2(V2(I))
           EXF = 1.4387*BV2/300.
           JULT = 2.*SQRT(4./EXF)
           JLIM(I) = JULT
           JULT = JULT + 1
      DO 35  JR = 1,JULT
           J = JR - 1
           BLTZ = EXP(-EXF*J*(J+1.))
           FREQ = ORIG(I) + BV1*(J+1.)*(J+2.) - BV2*J*(J+1.)
           WL = VACUUM(FREQ)
           WLR(JR) = WL
           SLR(JR) = BLTZ*(J+1.)*FLTR(WL)
           FREQ = ORIG(I) + BV1*J*(J-1.) - BV2*J*(J+1.)
```

```
      WL = VACUUM(FREQ)
      WLP(JR) = WL
      SLP(JR) = BLTZ*J*FLTR(WL)
35 CONTINUE
      SUMT = 0.0
   DO 36  JR = 1,JULT
36    SUMT = SUMT + SLR(JR) + SLP(JR)
      BANDSUM(I) = SUMT
      VIBEN = GV2 - G2(0.)
      BMFV(I) = EXP(-1.4387*VIBEN/300.)
      RELSTR(I) = BANDSUM(I)*BMFV(I)*FC(I)
30 CONTINUE
      SUMINT = 0.0
   DO 31  I=1,NB
31    SUMINT = SUMINT + RELSTR(I)
   PRINT 3
   PRINT 4,  FTRAN,FPOS,FWDTH
   PRINT 5
   PRINT 6,  (V1(I),V2(I),JLIM(I),AQ(I),BANDSUM(I),BMFV(I),FC(I),
  1    RELSTR(I), I=1,NB)
   PRINT 7,  SUMINT
      VLOW = FMIN(NB,V1)
      VHI = FMAX(NB,V1)
      MR = VHI - VLOW + 1.1
      VRUN = VLOW
   DO 40  K=1,MR
      SUM = 0.0
   DO 41  I=1,NB
     IF (V1(I).EQ.VRUN)  SUM = SUM + RELSTR(I)
41 CONTINUE
      VPRI(K) = VRUN
      BANDEX(K) = SUM/SUMINT
40    VRUN = VRUN + 1.0
      SUMCHK = 0.0
   DO 45  K=1,MR
45    SUMCHK = SUMCHK + BANDEX(K)
   PRINT 8
   PRINT 9,  (VPRI(K),BANDEX(K), K=1,MR)
   PRINT 10, SUMCHK
      VRUN = 0.0
   DO 50  K=1,6
      SUM = 0.0
   DO 51  I=1,NB
     IF (V2(I).EQ.VRUN)  SUM = SUM + RELSTR(I)
51 CONTINUE
      VPRI(K) = VRUN
      BANDEX(K) = SUM/SUMINT
50    VRUN = VRUN + 1.0
      SUMCHK = 0.0
   DO 55  K=1,6
55    SUMCHK = SUMCHK + BANDEX(K)
   PRINT 11
   PRINT 9,  (VPRI(K),BANDEX(K), K=1,6)
   PRINT 12,  SUMCHK
   END
```

```
      FUNCTION FLTR(X)
      COMMON/BLOW/XO,A,B
          FLTR = A*EXP(-B*(X-XO)**2)
      RETURN
      END
```

```
      FUNCTION VACUUM(VW)
      VW=VW*1.E-4
      P=((6432.8+2949810./(146.-VW**2)+25540./(41.-VW**2))*1.E-8)
     1    + 1.
      VACUUM=1.E4/(VW*P)
      VW=VW*1.E4
      RETURN
      END
```

```
      FUNCTION  FMIN(N,X)
      DIMENSION  X(100)
          A = X(1)
      DO 10  I=1,N
        IF (X(I).LT.A)  A = X(I)
   10 CONTINUE
      FMIN = A
      RETURN
      END
```

```
      FUNCTION  FMAX(N,X)
      DIMENSION  X(100)
          B = X(1)
      DO 11  I=1,N
        IF (X(I).GT.B)  B = X(I)
   11 CONTINUE
      FMAX = B
      RETURN
      END
```

5. FIGPLOT

Program FIGPLOT was used to produce the data plots displayed in this work. The comment cards adequately describe the input and output variables.

```
      PROGRAM FIGPLOT (INPUT,OUTPUT,TAPE98,PLOT,TAPE99=PLOT)
      DIMENSION  X(500),Y(500),FORT(5),XLABEL(3),YLABEL(3)
      COMMON/CCPOOL/XMIN,XMAX,YMIN,YMAX,XDMIN,XDMAX,YDMIN,YDMAX
      COMMON/CCFACT/FINCH
      INTEGER  FORT
    1 FORMAT(10I5)
    2 FORMAT(8F10.5)
    3 FORMAT(2I5,2F10.5)
    4 FORMAT(3A10)
    5 FORMAT(3I5,2X,A3)
    6 FORMAT(5A10)
    7 FORMAT(/////*POINTS FOR PLOT NO.  *I3//6X,*X*,21X,*Y*///)
    8 FORMAT(E12.3,10X,E12.3)
   10 FORMAT(80H
     1                                        )
          FINCH = 100.
  100 READ 10
C
C     THIS CARD IDENTIFIES PLOT.
C
      PRINT 10
      READ 2,  XDMIN,XDMAX,YDMIN,YDMAX
C
C     THESE VARIABLES DEFINE THE PAPER COORDINATES OF THE PLOT.  EXAMPLE,
C     (1.,7.,5.,10.) WOULD DEFINE A 5 BY 6 INCH PLOT POSITIONED NEAR THE TOP OF
C     THE PLOT PAPER.
C
      READ 2,  XMIN,XMAX,YMIN,YMAX
C
C     THESE VARIABLES FIX THE SCALE FOR THE PLOT.
C
      READ 1,  NX1,NX2,NX3,NY1,NY2,NY3
C
C     DETERMINE NO. OF INTERVALS AND SUBINTERVALS MARKED BY GRID LINES(1), MAJOR
C     TICK MARKS(2), AND MINOR TICK MARKS(3) ON AXES.  (ALL QUANTITIES = 1
C     RESULTS IN BARE RECTANGULAR GRID.)
C
      READ 1,  LABX,LABY
C
C     DETERMINES NO. OF LABELED INTERVALS ON PLOT.  (BOTH = 1 RESULTS IN
C     NUMERICAL LABELS AT CORNERS ONLY.)
C     LAB = 0  RESULTS IN NO NUMERICAL LABELS.
C     SUBROUTINE CCLBL DETERMINES SIZE AND FORMAT FOR NUMERICAL LABELS AND MAY BE
C     ALTERED TO SUIT THE USER.
C
      CALL CCGRID (NX1,NX2,NX3,6HNOLBLS,NY1,NY2,NY3)
      CALL CCLBL(LABX,LABY)
      READ 3,  KX,NXCHAR,XLX,XLY
      READ 4,  (XLABEL(I),I=1,3)
      READ 3,  KY,NYCHAR,YLX,YLY
      READ 4,  (YLABEL(I),I=1,3)
C
C     XLX,XLY,YLX,YLY ARE PAPER COORDINATES FOR STARTING THE LETTERING.
C     KX,KY ARE MAGNIFICATION FACTORS.  (K = 10 RESULTS IN CHARACTERS .4*.6 INCH.
C     NXCHAR,NYCHAR ARE NOS. OF CHARACTERS IN X AND Y LABELS.
C     XLABEL, YLABEL ARE ALPHANUMERIC LABELS (MAX 30 CHARACTERS).
C
          NPLT = 0
```

```
        IF (NXCHAR.EQ.0)  GO TO 19
      CALL CCLTR(XLX,XLY,0,KX,XLABEL,NXCHAR)
   19   IF (NYCHAR.EQ.0)  GO TO 20
      CALL CCLTR (YLX,YLY,1,KY,YLABEL,NYCHAR)
   20 READ 6,  (FORT(I),I=1,5)
      READ 5,  NP,NSYM,NTH,PCON
C
C    FORT IS THE FORMAT FOR READING IN THE POINTS (X,Y).
C    NP = NO. OF POINTS.  NSYM DESIGNATES SYMBOL (SEE CC HANDOUT) PLOTTED AT
C    1ST POINT AND EVERY NTH POINT THEREAFTER.  PCON = YES IF POINTS SHOULD BE
C    CONNECTED, NO IF NOT.
C
C
C    IF NP IS GIVEN, POINTS WILL BE READ ACCORDING TO FORMAT FORT IN AN IMPLIED
C    DO LOOP.  ANY NO. OF POINTS PER CARD ALLOWED.
C
C    IF NP = 0 (BLANK) POINTS WILL BE READ IN A PROGRAM DO LOOP.  ONLY ONE
C    POINT (X,Y) PER CARD.
C    PROGRAM EXECUTION IS STOPPED IF NP IS GT. 500.
C
        IF (NP.GT.500)  STOP
        IF (NP.EQ.0)  GO TO 201
      READ FORT,  (X(I),Y(I), I=1,NP)
        GO TO 221
  201 DO 21  I=1,500
      READ FORT,  MUSH,X(I),Y(I)
        IF (MUSH.NE.0)  GO TO 22
   21 CONTINUE
   22     NP = I - 1
C
C    PROGRAM DO LOOP INPUT MODE IS USED WHEN NP = 0.
C    DATA CARDS MUST INCLUDE AN INDICATOR CALLED MUSH, X(I), Y(I).  AFTER LAST
C    POINT INSERT CARD WITH MUSH NON-ZERO.  ALL OTHERS ZERO.
C
  221     NPLT = NPLT + 1
      PRINT 7,  NPLT
      PRINT 8,  (X(I),Y(I),I=1,NP)
        IF (PCON.EQ.3HYES)  23,24
   23 CALL CCPLOT(X,Y,NP,4HJOIN,NSYM,NTH)
        GO TO 25
   24 CALL CCPLOT(X,Y,NP,6HNOJOIN,NSYM,NTH)
   25 READ 1,  ICON
        IF (ICON.EQ.99)  GO TO 20
C
C    ICON = 99 CAUSES RETURN TO 20 TO PICK UP MORE DATA TO BE PLOTTED ON SAME
C    GRID.  FILL IN BLANK CARD OTHERWISE.
C
      READ 1,  MSKP
        IF (MSKP.EQ.22)  GO TO 100
C
C    MSKP = 22 CAUSES RETURN TO 100 FOR NEW GRID AND PLOTS, BUT WITHOUT
C    ADVANCING PAPER.  LEAVE BLANK OTHERWISE.
C
      CALL CCNEXT
      READ 1,  IPLOT
        IF (IPLOT.EQ.22)  GO TO 100
C
C    IPLOT = 22 CAUSES RETURN TO BEGINNING FOR NEW GRID AND PLOTS.
C
      CALL CCEND
      END
```

```
      SUBROUTINE CCLBL(NX1,NY1)                                         CCLBL
      COMMON/CCPOOL/XMIN,XMAX,YMIN,YMAX,CCXMIN,CCXMAX,CCYMIN,CCYMAX
      COMMON/CCFACT/FACTOR
      ISZERO=0
       IF (NX1.EQ.0.AND.NY1.EQ.0)  RETURN
       IF (NX1.EQ.0)  GO TO 10
         XD = XMAX - XMIN
         CCXD = CCXMAX - CCXMIN
         XI = XD/FLOAT(NX1)
      KSIZE=1                $KORIENT=1
C     LABEL FROM RIGHT TO LEFT ALONG THE X-AXIS.
      DO 2 NX=ISZERO,NX1
      CCX=CCXMAX-CCXD*FLOAT(NX)/FLOAT(NX1)
      X=(CCX-CCXMIN)*XD/CCXD+XMIN
C     SET X TO A TRUE ZERO IF X=0. TO WITHIN MACHINE ACCURACY.
      IF(ABS (X/XI).LT.1.0E-6)X=0.
     WRITE(98,28)X
2     CALL CCLTR(CCX+6.*FLOAT(KSIZE)/FACTOR,
     * CCYMIN-70.*FLOAT(KSIZE)/FACTOR,KORIENT,KSIZE)
       IF (NY1.EQ.0)  RETURN
   10    YD = YMAX - YMIN
         CCYD = CCYMAX - CCYMIN
         YI = YD/FLOAT(NY1)
      KSIZE=1                $KORIENT=0
C     LABEL UPWARD ALONG THE Y-AXIS.
      DO 3 NY=ISZERO,NY1
      CCY=CCYMIN+CCYD*FLOAT(NY)/FLOAT(NY1)
      Y=(CCY-CCYMIN)*YD/CCYD+YMIN
C     SET Y TO A TRUE ZERO IF Y=0. TO WITHIN MACHINE ACCURACY.
      IF(ABS (Y/YI).LT.1.0E-6)Y=0.
      WRITE(98,27)Y
3     CALL CCLTR(CCXMIN-70.*FLOAT(KSIZE)/FACTOR,CCY,KORIENT,KSIZE)
   27 FORMAT(F5.2)
   28 FORMAT(F5.1)
      RETURN
      END
```

B. Subroutines and Function Routines

1. The POWFIT Package

Subroutine POWFIT and the associated routines SUMXN, MATVEC, and INVERT are useful for obtaining least-squares power series fits for a set of data. The order and number of terms in the series are specified through the input variables INITPOW and NCON, which are described in sufficient detail in the comment cards. Function SUMXN provides values for the terms of type $\Sigma x_i^m y_i^n$ which appear in the matrix of simultaneous equations which must be solved to obtain the constants C(I). The equations are solved by matrix methods using INVERT and MATVEC: INVERT is a matrix inversion routine that utilizes row operations, and MATVEC is a simple matrix-vector multiplication routine. Output variables produced by POWFIT include the constants C(I) and their standard deviations SDC(I), along with the variance in y, SVAR.

The POWFIT routine has been used successfully to obtain parameters for fits to orders as high as 6, but it is likely that the row operations used in INVERT would lead to round-off problems for matrices much larger than 6 x 6.

```
      SUBROUTINE POWFIT (NV,NCON,INITPOW,X,Y,C,SDC,SVAR)
C     POWFIT FITS A SET OF POINTS TO A LEAST SQUARES BEST POWER SERIES.  NCON IS
C   THE NUMBER OF TERMS IN THE SERIES, INITPOW IS THE LOWEST POWER OF X TO BE
C   INCLUDED.  NV IS THE NUMBER OF POINTS.  THE C(I) ARE THE RESULTING CONSTANTS.
C   NOTE CONSTANT TERM REQUIRES INITPOW = 0.
      DIMENSION  X(100),Y(100),C(10),AA(10,10)
      DIMENSION  AAIN(10,10),SDC(10)
          NCON1 = NCON + 1
          NC2 = NCON*2
      DO 12  NR = 2,NC2
          IPOW = NR - 2 + 2*INITPOW
          F1 = SUMXN(NV,IPOW,X,Y,2)
      DO 13  I=1,NCON
      DO 14  J=1,NCON
        IF ((I+J).EQ.NR) 15,14
   15     AA(I,J) = F1
   14 CONTINUE
   13 CONTINUE
   12 CONTINUE
      DO 16  I=1,NCON
          JPOW = I - 1 + INITPOW
   16     C(I) = SUMXN(NV,JPOW,X,Y,1)
      CALL INVERT(NCON,AA,AAIN)
      CALL MATVEC(NCON,AAIN,C,C)
          SSQ = 0.0
      DO 21  I=1,NV
          SSX = 0.0
      DO 22  J=1,NCON
          JPOW = INITPOW + J - 1
        IF (JPOW.EQ.0)  GO TO 221
          TER = C(J)*X(I)**JPOW
        GO TO 222
  221     TER = C(J)
  222     SSX = SSX + TER
   22 CONTINUE
          SSQ = SSQ + (Y(I)-SSX)**2
   21 CONTINUE
          SVAR = SSQ/(NV-NCON)
          SDY = SQRT(SVAR)
      DO 31  I=1,NCON
   31     SDC(I) = SDY*SQRT(AAIN(I,I))
      RETURN
      END



      FUNCTION SUMXN(NT,N,X,Y,JJ)
      DIMENSION X(200),Y(200)
          S = 0.0
        IF (JJ.EQ.1) 1,3
    1 DO 2  I=1,NT
    2     S = S + Y(I)*X(I)**N
        GO TO 20
    3 DO 4  I=1,NT
    4     S = S + X(I)**N
   20 SUMXN = S
      RETURN
      END
```

```
      SUBROUTINE MATVEC (N,A,X,Y)
      DIMENSION  X(10),Y(10),XT(10),A(10,10)
      DO 9  I=1,N
 9        XT(I) = X(I)
      DO 10  I=1,N
          TEM = 0.0
      DO 11  J=1,N
          TEM = TEM + A(I,J)*XT(J)
11    CONTINUE
          Y(I) = TEM
10    CONTINUE
      RETURN
      END
```

```
      SUBROUTINE INVERT (N,A,AIN)
      DIMENSION  A(10,10),AIN(10,10),STOR(10,10)
      DO 10  I=1,N
      DO 10  J=1,N
10        STOR(I,J) = A(I,J)
      DO 11  I=1,N
      DO 11  J=1,N
11        AIN(I,J) = 0.0
      DO 12  I=1,N
12        AIN(I,I) = 1.0
      DO 21  I=1,N
          ATEM = STOR(I,I)
      DO 22  J=1,N
          STOR(I,J) = STOR(I,J)/ATEM
22        AIN(I,J) = AIN(I,J)/ATEM
      DO 23  K=1,N
        IF ((K-I).EQ.0)  GO TO 23
          BTEM = STOR(K,I)
      DO 24  J=1,N
          STOR(K,J) = STOR(K,J) - BTEM*STOR(I,J)
24        AIN(K,J) = AIN(K,J) - BTEM*AIN(I,J)
23    CONTINUE
21    CONTINUE
      RETURN
      END
```

2. <u>ODNEWT and ODNEWT2</u>

These routines solve for $(k_o l)$ in the expressions (7) and (8) in Appendix I. The input and output variables are explained in the comment cards. Both routines require function FACT, which computes n-factorial.

```
      FUNCTION  ODNEWT(GAM,AB)
C
C     ODNEWT USES NEWTONS APPROXIMATION METHOD TO COMPUTE THE OPTICAL DEPTH
C     FROM THE ABSORPTION (AB) AND THE LINEWIDTH PARAMETER (GAM) FOR AN
C     ASSUMED GAUSSIAN SOURCE LINE.
C
          Y = AB
          X2 = 1.0
C
C     CALCULATE ABSORPTION.
C
          NTIM = 0
    5     SUM = 0.0
          X1 = X2
      DO 10  I=1,100
          TEMP = SUM
          COMP = .0001*ABS(TEMP)
          TERM = (-X1)**I/FACT(I)/SQRT(1.+GAM*I)
          SUM = SUM + TERM
          TEST = ABS(TEMP-SUM)
        IF (TEST.LT.COMP)  GO TO 11
   10 CONTINUE
   11     FX = Y + SUM
C
C     CALCULATE DERIVATIVE.
C
          SUM = 0.0
      DO 12  J=1,100
          TEMP = SUM
          COMP = .0001*ABS(TEMP)
          TERM = (-X1)**(J-1)/FACT(J-1)/SQRT(1.+GAM*J)
          SUM = SUM + TERM
          TEST = ABS(TEMP-SUM)
        IF (TEST.LT.COMP)  GO TO 13
   12 CONTINUE
   13     FPX = -SUM
C
C     COMPUTE NEW VALUE FOR ROOT, X2.
C
          X2 = X1 - FX/FPX
          DX = X2 - X1
          CHK = ABS(DX/X1)
          NTIM = NTIM + 1
        IF (NTIM.EQ.10)  GO TO 30
        IF (CHK.GT..0005)  GO TO 5
          ODNEWT = X2
      RETURN
   30 PRINT 1
    1 FORMAT(//10X,*SOLUTION NOT REACHED IN TEN ITERATIONS*///)
          ODNEWT = X2
      RETURN
      END
```

```
      FUNCTION  ODNEWT2(XP,GAM,AB)
C
C     ODNEWT2 USES NEWTONS APPROXIMATION METHOD TO CALCULATE THE OPTICAL DEPTH
C     FOR A DOPPLER ABSORPTION LINE AND AN IDEAL RESONANCE LAMP SOURCE LINE.
C     THE LATTER IS ASSUMED TO BE DETERMINED BY THE DOPPLER PROFILE AND MUST
C     BE OPTICALLY THIN IF CORRECT RESULTS ARE ARE DESIRED FROM THIS ROUTINE, IE
C     THE SOURCE OPTICAL DEPTH MUST BE LESS THAN 3. OR 4., SINCE ONLY TEN TERMS
C     IN THE EXPANSION ARE CALCULATED.
C
          ODNEWT2 = 0.0
          X2 = 1.0
          NTIM = 0
        IF (XP.EQ.0.)  GO TO 35
    5     X = X2
C
C     CALCULATE ABSORPTION.
C     CALCULATE DERIVATIVE.
C
          SUMDEN = 0.0
          SUMNUM = 0.0
          SUMPR = 0.0
      DO 20  N=1,10
          TP = (-XP)**N/FACT(N)
      DO 21  M=1,20
          T = (-X)**M/FACT(M)
          R1 = N  $  R2 = M
          TD = T*R2/X
          FAC = SQRT(R1 + R2*GAM)
          SUMNUM = SUMNUM + TP*T/FAC
          SUMPR = SUMPR + TP*TD/FAC
   21 CONTINUE
          SUMDEN = SUMDEN + TP/SQRT(R1)
   20 CONTINUE
          DENOM = SUMDEN
          FX = AB + SUMNUM/DENOM
          FPX = SUMPR/DENOM
C
C     COMPUTE NEW VALUE FOR ROOT, X2.
C
          X2 = X - FX/FPX
          X1 = X
          DX = X2 - X1
          CHK = ABS(DX/X1)
          NTIM = NTIM + 1
        IF (NTIM.EQ.10)  GO TO 30
        IF (CHK.GT..0005)  GO TO 5
          ODNEWT2 = X2
      RETURN
   30 PRINT 1
    1 FORMAT(//10X,*SOLUTION NOT REACHED IN TEN ITERATIONS*///)
          ODNEWT2 = X2
      RETURN
   35 PRINT 2
      RETURN
    2 FORMAT(//10X,*SOURCE OPTICAL DEPTH CANNOT BE 0, OR INTENSITY IS 0.
     1   *///)
      END
```

```
      FUNCTION FACT(N)
          FACT = 1.0
        IF (N.EQ.0)  RETURN
          XR = 1.0
      DO 10  J=1,N
          FACT = FACT*XR
10        XR = XR + 1.0
      RETURN
      END
```

3. <u>INTERP1</u>

INTERP1 is a general interpolation routine useful for obtaining y values for input values of x (= S) relative to a set of points (FX,FY). The other variables are explained in the comment cards. Note the restriction that the array (FX,FY) must be ordered according to increasing FX values.

```
      SUBROUTINE  INTERP1(S,NN,FX,FY,F)
C       INTERP1 IS A GENERAL INTERPOLATION ROUTINE USEFUL FOR CALCULATING
C     Y VALUES FOR A GIVEN X VALUE RELATIVE TO AN ARRAY FY(FX).  FX VALUES MUST
C     BE ORDERED IN INCREASING VALUE.  NN IS THE SIZE OF THE INPUT X--Y ARRAY.
C     F IS THE OUTPUT VALUE.
      DIMENSION  FX(100),FY(100),X(4),Y(4)
        IF (FX(1).GE.S)  12,10
   12 DO 13  N=1,4
         X(N) = FX(N)
   13    Y(N) = FY(N)
      GO TO 28
   10 DO 22  K=1,NN
      IF (FX(K).LE.S.AND.FX(K+1).GE.S)  23,22
   23   IF (K.LE.2)  24,25
   24 DO 31  N=1,4
         X(N) = FX(N)
   31    Y(N) = FY(N)
      GO TO 28
   25   IF (K.GE.(NN-1))  26,27
   26 DO 32  N=1,4
         Y(N) = FY(N+NN-4)
   32    X(N) = FX(N+NN-4)
      GO TO 28
   27 DO 33  N=1,4
         Y(N) = FY(K-2+N)
   33    X(N) = FX(K-2+N)
      GO TO 28
   22 CONTINUE
   28 CONTINUE
         DN12 = X(1) - X(2)  $  DN21 = -DN12
         DN13 = X(1) - X(3)  $  DN31 = -DN13
         DN14 = X(1) - X(4)  $  DN41 = -DN14
         DN23 = X(2) - X(3)  $  DN32 = -DN23
         DN24 = X(2) - X(4)  $  DN42 = -DN24
         DN34 = X(3) - X(4)  $  DN43 = -DN34
         X12 = Y(1)/DN12 + Y(2)/DN21
         X123 = Y(1)/(DN12*DN13) + Y(2)/(DN21*DN23) + Y(3)/(DN31*DN32)
         X1234 = Y(1)/(DN12*DN13*DN14) + Y(2)/(DN21*DN23*DN24) +
     1   Y(3)/(DN31*DN32*DN34) + Y(4)/(DN41*DN42*DN43)
      F = Y(1) + (S-X(1))*X12 + (S-X(1))*(S-X(2))*X123 + (S-X(1))*
     1          (S-X(2))*(S-X(3))*X1234
      RETURN
      END
```

4. AREA and GAUSS

Functions AREA and GAUSS are numerical integration routines. AREA uses Simpson's method, with an additional higher order corrective term applied to all intervals except those on each end of the domain of the function Y. N is the number of points and H is the constant interval Δx. AREA is particularly appropriate for obtaining areas under empirical curves or curves for explicitly defined functions of a complex nature.

GAUSS uses the method of Gauss to obtain the area under the curve described by the input function F(X). The indicator IND determines whether a Gauss-Laguerre (IND = 1) or a Gauss-Legendre (IND $\neq$ 1) quadrature will be used to obtain the area. The former is applicable to integrals of the type $\int_A^\infty F(x)dx$, and the latter is appropriate for integrals $\int_A^B F(x)dx$. (A and B here are equivalent to the A and B parameters appearing in the Function identifier card.) The Gauss-Laguerre quadrature is taken over six points, the Gauss-Legendre over ten. Function GAUSS gives exceptionally good results for "well-behaved" functions, since the method of Gauss represents the highest order of accuracy achievable in numerical integration of a function F(x) which is expressable as a polynomial.

```
      FUNCTION AREA(N,H,Y)
      DIMENSION  Y(100)
          A1 = 0.0
          COR = 0.0
        IF (N.LT.3)  GO TO 500
          NM1 = N-1
          NM2 = N-2
      DO 1 I = 2,NM1,2
          A1 = A1 + H/3.*(Y(I-1) + Y(I+1) + 4.*Y(I))
    1 CONTINUE
        IF (N.LT.5)  GO TO 500
      DO 2  I = 3,NM2,2
          COR = COR - H/90.*(Y(I-2) + Y(I+2)) + 2.*H/45.*(Y(I-1) +
     1          Y(I+1)) - H/15.*Y(I)
    2 CONTINUE
  500 AREA = A1 + COR
      RETURN
      END
```

```
      FUNCTION GAUSS(IND,A,B,F)
      DIMENSION  V1(9),V2(10),R1(9),R2(10)
      DATA  (V1(I),I=1,6)/.2228466042,1.1889321017,2.9927363261,
     1     5.7751435691,9.8374674184,15.9828739806/
      DATA  (R1(I),I=1,6)/.45896467395,.4170008308,.1133733821,
     1     .0103991975,.0002610172028,.000000898547906/
      DATA  (V2(I),I=1,10)/.0130467357,.0674683167,.1602952159,
     1     .2833023029,.4255628305,.5744371695,.7166976971,.8397047842,
     2     .9325316833,.9869532642/
      DATA  (R2(I),I=1,10)/.03333567215,.0747256746,.10954318126,
     1     .13463010546,.14776211236,.14776211236,.13463010546,
     2     .10954318126,.0747256746,.03333567215/
          AR = 0.0
        IF (IND.EQ.1)  GO TO 1
      DO 10  I=1,10
   10     AR = AR + R2(I)*F(A+(B-A)*V2(I))
          AR = AR*(B-A)
        GO TO 77
    1 DO 11  I=1,6
   11     AR = AR + R1(I)*EXP(V1(I))*F(V1(I)+A)
   77   GAUSS = AR
      RETURN
      END
```

ACKNOWLEDGMENTS

I would like to express my thanks to Professor Leo Brewer for his guidance throughout the course of this eclectic work. I particularly appreciated his manner of confronting scientific "truth": his n-odd explanations for every observed datum caused me to scratch my head constructively time and time again. He somehow managed to inspire my study without once demanding results.

Many others have contributed significantly to my life and work in Berkeley. In particular the ideas of John Link provided impetus in the initial phases of the predissociation studies. I also enjoyed many discussions of "the iodine problem" (and one or two unrelated topics) with Paul Cunningham. My numerous colleagues and friends in Berkeley have all helped to make my life here more enjoyable and meaningful; in this area I wish to single out Helen Johansen for a special note of gratitude.

The technical assistance of the LRL and Chemistry Department personnel has been a continual aid to my work. I am afraid the efficiency of these people and the convenience of these facilities have spoiled me for any future position I may take up.

Finally I want to thank my parents and my brother for encouragement at a distance.

Most of this work was conducted with the aid of a Graduate Fellowship from the National Science Foundation. Fill-in financial assistance from the AEC was also gratefully accepted.

REFERENCES

C. Arnot and C. A. McDowell, Can. J. Chem. 36, 114 (1958).

N. S. Bayliss and J. V. Sullivan, J. Chem. Phys. 22, 1615 (1954).

W. Berg, Z. Physik 79, 89 (1933).

G. R. Bird, J. Chem. Phys. 38, 2678 (1963).

K. D. Bowers, R. A. Kamper, and C. D. Lustig, Proc. Phys. Soc. B 70, 1176 (1957).

W. Braun and M. Lenzi, Disc. Faraday Soc. 44, 252 (1967).

R. G. Breene, Jr., Rev. Mod. Phys. 29, 94 (1957).

L. Brewer, R. A. Berg, and G. M. Rosenblatt, J. Chem. Phys. 38, 1381 (1963).

R. L. Brown and W. Klemperer, J. Chem. Phys. 41, 3072 (1964).

W. G. Brown, Phys. Rev. 38, 1187 (1931).

D. L. Bunker and N. Davidson, J. Am. Chem. Soc. 80, 5085 (1958).

G. E. Busch, R. T. Mahoney, R. I. Morse, and K. R. Wilson, J. Chem. Phys. 51, 837 (1969).

M. I. Christie, J. Am. Chem. Soc. 84, 4066 (1962).

A. Chutjian, (Ph.D. Thesis), University of California, Berkeley; UCRL-16441 (January, 1966).

A. Chutjian, "Calculation of Predissociation Rates of the B $^3\Pi_{0^+u}$ State of I_2," to be published in J. Chem. Phys., December, 1969.

A. Chutjian and T. C. James, J. Chem. Phys. 51, 1242 (1969).

A. Chutjian, J. K. Link, and L. Brewer, J. Chem. Phys. 46, 2666 (1967).

E. U. Condon and G. H. Shortley, The Theory of Atomic Spectra, (Cambridge University Press, Cambridge, 1951).

P. T. Cunningham, (Ph.D. Thesis), University of California, Berkeley; UCRL-18419 (November, 1968).

N. Davidson, Statistical Mechanics, (McGraw-Hill Book Company, Inc., New York, 1962).

E. O. Degenkolb, J. I. Steinfeld, E. Wassermann, and W. Klemperer, J. Chem. Phys. 51, 615 (1969).

W. E. Deming, Statistical Adjustment of Data, (Dover Publications, Inc., New York, 1964).

R. J. Donovan and D. Husain, Nature 206, 171 (1965).

R. J. Donovan and D. Husain, Nature 209, 609 (1966).

R. J. Donovan and D. Husain, Trans. Faraday Soc. 62, 11, 1050, 2023 (1966).

R. J. Donovan, F. G. M. Hathorn, D. Husain, Trans. Faraday Soc. 64, 1228, 3192 (1968).

V. Dose, Rev. Sci. Instr. 39, 1055 (1968).

L. Dunkelman, J. Quant. Spectrosc. Radiat. Transfer 2, 533 (1962).

L. Dunkelman, W. B. Fowler, and J. Hennes, Appl. Optics 1, 695 (1962).

H. E. Edgerton, J. Opt. Soc. Am. 36, 390 (1946).

B. Edlen, J. Opt. Soc. Am. 43, 339 (1953).

A. Einstein, Phys. Zeits. 18, 121 (1917).

M. Eliashevitch, Physik. Z. d. Sowjetunion 1, 510 (1932).

S. Ezekiel and R. Weiss, Phys. Rev. Letters 20, 91 (1968).

W. E. Falconer and E. Wassermann, J. Chem. Phys. 45, 1843 (1966).

J. Franck and R. W. Wood, Phil. Mag. (6) 21, 314 (1911).

S. Gabelnick, (Ph.D Thesis), University of California, Berkeley; UCRL-18623 (January, 1969).

M. Gee and J. Tellinghuisen, unpublished work.

C. A. Goy and H. O. Pritchard, J. Mol. Spectry. 12, 38 (1964).

D. Grimes and S. P. Davis, unpublished lifetime results by the direct-decay method.

M. Halmann, J. Chem. Phys. 44, 2406 (1966).

M. Halmann and I. Laulicht, J. Chem. Phys. 44, 2398 (1966).

J. Ham, J. Am. Chem. Soc. 76, 3386 (1954).

R. A. Harris, J. Chem. Phys. 39, 978 (1963).

R. Harris, M. Blackledge, and J. Generosa, J. Mol. Spectry. 30, 506 (1969).

P. Harteck, R. R. Reeves, Jr. and B. A. Thompson, Z. Naturforschg. 19a, 2 (1964).

G. Herzberg, Atomic Spectra and Atomic Structure, (Dover Publications, Inc., New York, 1944).

G. Herzberg, Spectra of Diatomic Molecules, (D. Van Nostrand Company, Inc., Princeton, 1950).

T. L. Hill, An Introduction to Statistical Thermodynamics, (Addison-Wesley Publishing Company, Inc., Reading, Mass., 1960).

J. O. Hirshfelder, C. F. Curtiss, and R. B. Bird, Molecular Theory of Gases and Liquids, (John Wiley and Sons, Inc., New York, 1954).

L. Holland, The Properties of Glass Surfaces, (Chapman and Hall, London, 1964).

B. J. Huebert and R. M. Martin, J. Phys. Chem. 72, 3046 (1968).

D. Husain and J. R. Wiesenfeld, Nature 213, 1227 (1967).

D. Husain and J. R. Wiesenfeld, Trans. Faraday Soc. 63, 1349 (1967).

V. Jaccarino, J. G. King, R. A. Satten, and H. H. Stroke, Phys. Rev. 94, 1798 (1954).

JANAF Thermochemical Tables, The Dow Chemical Company, Midland, Michigan, 1961.

H. S. Johnston, Gas Phase Reaction Rate Theory, (The Ronald Press Company, New York, 1966).

L. M. Julien and W. B. Person, J. Phys. Chem. 72, 3059 (1968).

M. Kimura and K. Tonomura, Pieter Zeeman, (Martinus Nijhoff, The Hague, Netherlands, 1935), p. 241.

V. Kondratjew and L. Polak, Physik. Z. d. Sowjetunion 4, 764 (1933).

M. Kovacs, D. R. Rao, and A. Javan, J. Chem. Phys. 48, 3339 (1968).

R. Kronig, Z. Physik 50, 347 (1928).

R. H. Kummler and M. McCarty, Jr., J. Phys. Chem. 71, 2456 (1967).

G. M. Lawrence, Astrophys. J. 148, 261 (1967).

F. W. Loomis and H. O. Fuller, Phys. Rev. 39, 180 (1932).

L. Mathieson and A. L. G. Rees, J. Chem. Phys. 25, 753 (1956).

J. W. Mayo, (Ph.D. Thesis), Massachusetts Institute of Technology (June, 1964).

R. T. Meyer, J. Phys. Chem. 72, 1583 (1968).

A. C. G. Mitchell and M. W. Zemansky, Resonance Radiation and Excited Atoms, (Cambridge University Press, Cambridge, 1934).

C. E. Moore, Atomic Energy Levels, Vol. III, Nat. Bur. Stand. Circ. 567 (1958).

C. E. Moore, An Ultraviolet Multiplet Table, Nat. Bur. Stand. Circ. 488, Section 3 (1962).

R. S. Mulliken, Phys. Rev. 46, 549 (1934).

R. S. Mulliken, Phys. Rev. 57, 500 (1940).

A. Nobs and K. Wieland, Helv. Phys. Acta 39, 564 (1966).

R. G. W. Norrish and G. Porter, Nature 164, 658 (1949).

E. A. Ogryzlo, Can. J. Chem. 39, 2556 (1961).

E. A. Ogryzlo and G. E. Thomas, J. Mol. Spectry. 17, 198 (1965).

O. Oldenberg, Z. Physik 18, 1 (1923).

S. S. Penner, Quantitative Molecular Spectroscopy and Gas Emissivities, (Addison-Wesley Publishing Company, Inc., Reading, Mass., 1959).

L. G. Parratt, Probability and Experimental Errors in Science, (John Wiley and Sons, Inc., New York, 1961).

J. C. Polanyi, Can. J. Chem. 36, 121 (1958).

E. Rabinowitch and W. C. Wood, Trans. Faraday Soc. 32, 540 (1936a).

E. Rabinowitch and W. C. Wood, J. Chem. Phys. 4, 358 (1936b).

E. Rabinowitch and W. C. Wood, J. Chem. Phys. 4, 497 (1936c).

F. Rössler, Z. Physik 96, 251 (1935).

G. A. W. Rutgers and J. C. De Vos, Physica 20, 715 (1954).

J. A. R. Samson, Techniques of Vacuum Ultraviolet Spectroscopy, (John Wiley and Sons, Inc., New York, 1967).

Th. Schmidt, Z. Physik 112, 199 (1939).

D. A. Shirley and W. F. Giauque, J. Am. Chem. Soc. 81, 4778 (1959).

J. I. Steinfeld, J. Chem. Phys. 44, 2740 (1966).

J. I. Steinfeld, J. D. Campbell, and N. A. Weiss, J. Mol. Spectry. 29, 204 (1969).

J. I. Steinfeld and W. Klemperer, J. Chem. Phys. 42, 3475 (1965).

J. I. Steinfeld, R. N. Zare, L. Jones, M. Lesk, and W. Klemperer, J. Chem. Phys. 42, 25 (1965).

P. Sulzer and K. Wieland, Helv. Phys. Acta 25, 653 (1952).

S. Tolansky, Proc. Roy. Soc. London (A) 152, 663 (1935).

F. K. Truby, Phys. Rev. 172, 24 (1968).

L. A. Turner, Phys. Rev. 31, 983 (1928).

L. A. Turner, Phys. Rev. 38, 574 (1931).

L. A. Turner, Phys. Rev. 41, 627 (1932).

R. D. Verma, J. Chem. Phys. 32, 738 (1960).

K. Vogt and J. Koenigsberger, Z. Physik 13, 300 (1923).

E. Wassermann, W. E. Falconer, and W. A. Yager, Berichte der Bunsengesellschaft 72, 248 (1968a).

E. Wassermann, W. E. Falconer, and W. A. Yager, J. Chem. Phys. 49, 1971 (1968b).

K. Wieland and J. Tellinghuisen, incomplete results from an isotope-shift study of the emission of I_2 in the presence of Ar.

J. D. Winefordner and T. J. Vickers, Anal. Chem. 36, 161 (1964).

R. J. Wolff, (Ph.D. Thesis), University of California, Berkeley (August, 1967).

R. W. Wood and M. Kimura, Astrophys. J. 46, 181, 197 (1917).

R. N. Zare, "Programs for Calculating Relative Intensities in the Vibrational Structure of Electronic Band Systems," Lawrence Radiation Laboratory Report UCRL-10925 (1963).

LEGAL NOTICE

This report was prepared as an account of Government sponsored work. Neither the United States, nor the Commission, nor any person acting on behalf of the Commission:

A. Makes any warranty or representation, expressed or implied, with respect to the accuracy, completeness, or usefulness of the information contained in this report, or that the use of any information, apparatus, method, or process disclosed in this report may not infringe privately owned rights; or

B. Assumes any liabilities with respect to the use of, or for damages resulting from the use of any information, apparatus, method, or process disclosed in this report.

As used in the above, "person acting on behalf of the Commission" includes any employee or contractor of the Commission, or employee of such contractor, to the extent that such employee or contractor of the Commission, or employee of such contractor prepares, disseminates, or provides access to, any information pursuant to his employment or contract with the Commission, or his employment with such contractor.

TECHNICAL INFORMATION DIVISION
LAWRENCE RADIATION LABORATORY
UNIVERSITY OF CALIFORNIA
BERKELEY, CALIFORNIA 94720